OPEN ACCESS

African Journal of **Biotechnology**

May 2021
ISSN 1684-5315
DOI: 10.5897/AJB
www.academicjournals.org

ACADEMIC JOURNALS
expand your knowledge

About AJB

The African Journal of Biotechnology (AJB) is a peer reviewed journal which commenced publication in 2002. AJB publishes articles from all areas of biotechnology including medical and pharmaceutical biotechnology, molecular diagnostics, applied biochemistry, industrial microbiology, molecular biology, bioinformatics, genomics and proteomics, transcriptomics and genome editing, food and agricultural technologies, and metabolic engineering. Manuscripts on economic and ethical issues relating to biotechnology research are also considered.

Indexing

CAB Abstracts, CABI's Global Health Database, Chemical Abstracts (CAS Source Index) Dimensions Database, Google Scholar, Matrix of Information for The Analysis of Journals (MIAR), Microsoft Academic, Research Gate

Open Access Policy

Open Access is a publication model that enables the dissemination of research articles to the global community without restriction through the internet. All articles published under open access can be accessed by anyone with internet connection.

The African Journals of Biotechnology is an Open Access journal. Abstracts and full texts of all articles published in this journal are freely accessible to everyone immediately after publication without any form of restriction.

Article License

All articles published by African Journal of Biotechnology are licensed under the Creative Commons Attribution 4.0 International License. This permits anyone to copy, redistribute, remix, transmit and adapt the work provided the original work and source is appropriately cited. Citation should include the article DOI. The article license is displayed on the abstract page the following statement:

This article is published under the terms of the Creative Commons Attribution License 4.0
Please refer to https://creativecommons.org/licenses/by/4.0/legalcode for details
about Creative Commons Attribution License 4.0

Memberships and Standards

Academic Journals strongly supports the Open Access initiative. Abstracts and full texts of all articles published by Academic Journals are freely accessible to everyone immediately after publication.

All articles published by Academic Journals are licensed under the Creative Commons Attribution 4.0 International License (CC BY 4.0). This permits anyone to copy, redistribute, remix, transmit and adapt the work provided the original work and source is appropriately cited.

Crossref is an association of scholarly publishers that developed Digital Object Identification (DOI) system for the unique identification published materials. Academic Journals is a member of Crossref and uses the DOI system. All articles published by Academic Journals are issued DOI.

Similarity Check powered by iThenticate is an initiative started by CrossRef to help its members actively engage in efforts to prevent scholarly and professional plagiarism. Academic Journals is a member of Similarity Check.

CrossRef Cited-by Linking (formerly Forward Linking) is a service that allows you to discover how your publications are being cited and to incorporate that information into your online publication platform. Academic Journals is a member of CrossRef Cited-by.

Academic Journals is a member of the International Digital Publishing Forum (IDPF). The IDPF is the global trade and standards organization dedicated to the development and promotion of electronic publishing and content consumption.

Contact

Editorial Office: ajb@academicjournals.org

Help Desk: helpdesk@academicjournals.org

Website: http://www.academicjournals.org/journal/AJB

Submit manuscript online http://ms.academicjournals.org

Academic Journals
73023 Victoria Island, Lagos, Nigeria
ICEA Building, 17th Floor,
Kenyatta Avenue, Nairobi, Kenya.

Editor-in-Chief

Editorial Board Members

Table of Content

Vol. 20(5), pp.169-174, May, 2021
DOI: 10.5897/AJB2021.17324
Article Number: BB0FBAD66718
ISSN: 1684-5315

http://www.academicjournals.org/AJB

ACADEMIC JOURNALS
expand your knowledge

African Journal of Biotechnology

Full Length Research Paper

Precise assessment of angular leaf spot severity using the Leaf Doctor app for common beans

Caléo Panhoca de Almeida[1*], Gabriel Francesco Janini Bonfante[1], Jean Fausto de Carvalho Paulino[1], Bianca Cristina de Deus[2], Flávia Rodrigues Alves Patrício[2], Sérgio Augusto Morais Carbonell[3], Alisson Fernando Chiorato[3] and Luciana Lasry Benchimol-Reis[1]

[1]Centro de Pesquisa em Recursos Genéticos Vegetais, Instituto Agronômico (IAC), Campinas (SP), Brazil.
[2]Centro Experimental Central, Instituto Biológico (IB), Campinas (SP), Brazil.
[3]Centro de Análises e Pesquisa Tecnológica do Agronegócio dos Grãos e Fibras, Instituto Agronômico (IAC), Campinas (SP), Brazil.

Received 4 February 2021; Accepted 28 April, 2021

Angular leaf spot (ALS) is one of the most severe diseases of common bean. However, there is as yet no standardization of the phenological stage, inoculum concentration, diagrammatic scale (DS), and day of assessment for screening ALS resistance in bean lines. The present study aimed to evaluate the potential for assessment of ALS severity in common beans using the Leaf Doctor app and inoculation at the V2 phenological stage under two inoculation concentrations. The experiment was carried out in a completely randomized design in a 3 × 2 × 2 factorial arrangement with three cultivars (AND 277, IAC-Milênio, and IAC-Carioca), two monosporic isolates (31-31 and 10-59), and two inoculum concentrations (2×10^4 and 4×10^4 conidia/mL). Disease severity was evaluated from 11 to 15 days after inoculation (d.a.i) using a diagrammatic scale and the Leaf Doctor. The results showed that 15 d.a.i., the concentration of the inoculum was no longer significant and that the isolates showed no significant difference in terms of pathogenicity. Moreover, in 15 d.a.i. it was possible to separate the cultivars into three phenotypic classes: resistant (AND-277), moderately susceptible (IAC-Milênio) and susceptible (IAC-Carioca). Considering the diagrammatic scale of notes, the cultivar AND 277 had a score of 2.3, while for the image evaluation, it was observed that only 0.65% of the total leaf area was affected by the disease. For this reason, 15 d.a.i. was recommended as the better day for evaluation, and the concentration of 2×10^4 conidia/mL may be adopted in order to reduce the amount of inoculum needed for the experiment. In addition, the evaluation with the Leaf Doctor app increases accuracy and improves discrimination between resistant and susceptible cultivars.

Key words: *Pseudocercospora griseola, Phaseolus vulgaris*, digital analysis, disease resistance.

INTRODUCTION

Common bean (*Phaseolus vulgaris* L.) is one of the grains most consumed by humans throughout the world (Assefa et al., 2019). Regarding the consumption of beans, Brazil stands out as the largest consumer of this

*Corresponding author. E-mail: caleoalmeida@hotmail.com.

grain (FAOSTAT, 2021), with an average of 18 kg year^{-1} per capita (Carneiro et al., 2015). The nutritional value of this grain and the potential health benefits explain the relevance that this legume has in the human diet, being a source of carbohydrates, fibers, vitamins and minerals (Pires et al., 2006), as well as a source of polyphenolic compounds with antioxidant properties (Polya, 2003). In addition to being the largest consumer, Brazil is the third largest producer of beans in the world (FAOSTAT, 2021). The estimated production of the last bean crop in Brazil was about 3.1 million tons, with an average yield of 1.074 kg/ha (CONAB, 2021). Bean yield is affected by several factors, and in Brazil, disease is one of the main problems. Angular leaf spot, caused by the fungus *Pseudocercospora griseola* (Sacc.) Crous and U. Braun, is one of the most serious diseases in common beans; it may cause yield losses of up to 80% (Nay et al., 2019a; Librelon et al., 2020).

In bean breeding programs, evaluation of the level of disease resistance is based on disease severity, which is defined as the area of plant tissue affected by the disease-causing organisms and expressed as a percentage of the total amount of plant tissue (Schoonhove and Pastor-Corrales, 1987; Forrest et al., 1991). In evaluation of ALS severity, breeders routinely adopt the V3 (first expanded trifoliate leaf) phenological stage (Pastor Corrales and Jara, 1995; Pereira et al., 2015; Bassi et al., 2017; Vidigal Filho et al., 2020; Almeida et al., 2020). However, when assessing the disease at the initial stages of plant development, Pereira et al. (2011) proposed the use of the V2 phenological stage (expanded primary leaves), making it possible to reduce the amount of inoculum used and the amount of time to perform the analyses.

All the diagrammatic scales (DS) developed to assess ALS resistance were proposed for the V3 stage (Moreno, 1977; Schoonhove and Pastor-Corrales, 1987; Inglis, 1988; Godoy et al., 1997), and they are not appropriate for the V2 stage. Librelon et al. (2015) proposed a specific DS for the V2 stage, which has been successfully used for evaluation and selection of ALS resistant bean lines (Pereira et al. 2019a, b, Librelon et al., 2020; Almeida et al., 2021a). DSs are contingent on the subjectivity of each evaluator, and Librelon et al. (2015) reported that the majority of 14 evaluators tested underestimated ALS severity using a DS.

An alternative to the DS for assessment of disease severity is quantification of infected tissue by digital image analysis, with advantages such as high precision, accuracy, reliability, and the possibility of non-destructive sampling, allowing data to be collected from the same individual at the experimental site over a period of time (Bock et al., 2008; Arnal Barbedo, 2013; Mutka and Bart, 2015). Several programs have been developed to quantify plant diseases, such as “Quant”, “Assess 2.0”, “ImageJ”, “Scion Image”, and “CompuEye” (Vale et al., 2001; Lobet et al., 2013; Mutka and Bart, 2015; Mahlein, 2016). However, some of these programs do not have friendly interfaces and are rather expensive, and require a Windows operating system interface, meaning that image processing must occur on a desktop and/or laptop only after capturing the images by another device (that is, photo camera or scanner).

With the advance of technology, an app for smartphones, named Leaf Doctor (https://www.quantitative-plant.org/software/leaf-doctor), was developed to perform image quantification on a portable mobile device in a fast and simpler way (Pethybridge and Nelson, 2015). The app has an extremely friendly interface, and it only requires the user to take photos with the device in the app itself, indicating the color of healthy and infected leaf tissues. After a few seconds of processing, the app shows the percentage of leaf area affected by the pathogen (Pethybridge and Nelson, 2015). This is advantageous in bean breeding programs, considering that generally many plants need to be evaluated with high accuracy in a short period of time. The purpose of the present study was to test the efficiency of using the Leaf Doctor app to perform assessment of the severity of ALS in common bean at the V2 phenological stage and compare with the evaluation carried out by a DS proposed for the V2 stage. In addition, two different inoculum concentrations were adopted (2×10^4 and 4×10^4 conidia/mL) in order to identify possible interaction and recommendation of better one.

MATERIALS AND METHODS

Three common bean cultivars (that is, AND 277, IAC-Milênio, and IAC-Carioca) with different levels of resistance to ALS were selected from the Germplasm Bank of the Instituto Agronômico - IAC (Campinas, São Paulo, Brazil). The AND 277 cultivar (Andean) is highly resistant and widely used as a source of resistance to angular leaf spot (Gonçalves-Vidigal et al., 2011; Oblessuc et al., 2012; Bassi et al., 2017; Almeida et al., 2020). The IAC-Carioca and IAC-Milênio cultivars (Mesoamerican) are susceptible, though they have different levels of susceptibility; the IAC-Carioca has been used as a check cultivar for susceptibility in some studies (Oblessuc et al., 2012; Bassi et al., 2017). The experiment was carried out in a completely randomized design in a 3 × 2 × 2 factorial arrangement, consisting of three cultivars, two monosporic isolates of *P. griseola* characterized as physiological races 31-31 and 10-59, and two inoculum concentrations (that is, 2×10^4 and 4×10^4 conidia/mL), with three replicates. A plot consisted of a pot with one plant.

Seeds of each cultivar were pre-germinated, aiming at selection of seedlings with the same size and vigor. Plants were inoculated according to the method proposed by Pereira et al., (2011). Plants were kept in a greenhouse for 10 days. When they reached the V2 stage, they were placed in an inoculation chamber, where they remained under controlled temperature (24°C) and moisture (95-100%) conditions in the absence of light for 24 h. The inoculum suspensions of both isolates were prepared as described by Almeida et al. (2020), and the inoculum concentrations were adjusted to those described earlier. Inoculation was performed on the adaxial and abaxial surfaces of the primary leaves using an air compressor (*De Vilbiss*). Twenty-four hours after inoculation, the

Table 1. Analysis of variance and the Tukey mean test for angular leaf spot severity for the following factors: isolate, inoculum concentration, and cultivar and the interactions between the factors, estimated by the diagrammatic scale (1-9) and the Leaf Doctor app at different days of evaluation (from 11 to 15 d.a.i.).

Factor	Number of days after inoculation					Leaf Doctor	AUDPC
	11	12	13	14	15		
Isolate							
31-31	2.05[a]	2.44[a]	2.88[a]	3.44[a]	4.11[a]	9.24[a]	24.38[a]
10-59	2.16[a]	2.33[a]	2.77[a]	3.72[a]	4.22[a]	7.53[a]	25.38[a]
Concentration							
2×10^4 conidia mL^{-1}	1.88[b]	2.27[b]	2.55[b]	3.38[b]	4.00[a]	7.26[a]	24.84[a]
4×10^4 conidia mL^{-1}	2.33[a]	2.50[a]	3.11[a]	3.77[a]	4.33[a]	9.51[a]	24.92[a]
Cultivar							
IAC-Carioca	2.66[a]	3.00[a]	3.58[a]	4.75[a]	5.41[a]	14.66[a]	31.95[a]
IAC-Milênio	2.41[a]	2.83[a]	3.16[b]	3.75[b]	4.75[b]	9.84[b]	28.20[b]
AND 277	1.25[b]	1.25[b]	1.75[c]	2.25[c]	2.33[c]	0.65[c]	14.51[c]
Interaction							
Iso. × Cult.	0.007	<0.001	0.006	0.679	0.123	0.502	0.006
Iso. × Con.	0.061	1.000	0.006	0.123	0.558	0.927	0.815
Con. × Cult.	0.821	0.002	0.193	0.679	0.105	0.146	0.623

The mean values with the same letter in the same column do not differ significantly by the Tukey test ($p < 0.05$).

chamber was adjusted to 80% humidity, with controlled photoperiod (12 h/12 h) (Monda et al., 2001; Sartorato, 2004), until the end of the evaluation. In addition, two plants of each cultivar were treated with only distilled water and Tween® (mock).

Assessment of angular leaf spot severity was performed at 11, 12, 13, 14, and 15 days after inoculation (d.a.i.) with the aid of the diagrammatic scales (DS) developed by Librelon et al. (2015). The scale has nine levels of severity: 1 to 3 correspond to resistant plants, 4 to 6 to moderately resistant plants, and 7 to 9 to susceptible plants. At 15 d.a.i., ALS severity was also estimated with the Leaf Doctor app on a smartphone with an iPhone Operating System (that is, iPhone 7 model) after the primary leaves of each cultivar were individually photographed against a black background. Statistical analysis of variance (ANOVA) was performed on each evaluation and the mean values were compared by the Tukey test at 5% significance ($p < 0.05$). The area under the disease progress curve (AUDPC) was estimated from each evaluation using the following formula:

$$\text{AUDPC} = \sum_{i=1}^{n_i-1}(y_i + y_{i+1}/2)(t_{i+1} - t_i)$$

where n is the number of evaluations, y is the severity of the disease, and $(t_{i+1} - t_i)$ is the time interval between two consecutive evaluations (Campbell and Madden, 1990). All data were analyzed using the SANEST software (Zonta and Machado, 1980).

RESULTS AND DISCUSSION

The results were significant for the cultivar factor for all the days of evaluation and approaches used (that is, diagrammatic scale and Leaf Doctor app) due to differences in the degree of resistance of the cultivars. The Tukey mean test showed there was a significant difference between susceptible cultivars (that is, IAC-Milênio and IAC-Carioca) only from 13 to 15 d.a.i., and all cultivars were considered resistant (that is, level < 3) until 12 d.a.i. (Table 1). The ANOVA showed no significance for the isolate factor, showing that the pathogenicity of both isolates (31-31 and 10-59) was similar for the set of cultivars tested. Nevertheless, a significant interaction was observed between isolate and cultivar from 11 to 14 d.a.i., and significance was also found for the isolate × concentration interaction at 12 d.a.i.

Regarding the concentration factor, there was significance only until 14 d.a.i., and a higher degree of severity was found for the 4×10^4 conidia mL^{-1} concentration. The AUDPC showed significance only for cultivar, allowing separation of the three cultivars into three distinct groups, with significance for the isolate × cultivar interaction. The IAC-Carioca cultivar was most susceptible to ALS for both *P. griseola* isolates; IAC-Milênio had an intermediate reaction; and AND 277 was the most resistant cultivar (Figure 1).

Although ALS is a highly significant disease for common bean worldwide, there is no consensus in the literature regarding the best day for assessment after inoculation under controlled conditions of infection. In the V3 stage, there are reports of assessment of degree of

Figure 1. The severity of angular leaf spot disease in primary leaves of AND 277, IAC-Milênio, and IAC-Carioca common bean cultivars at 15 days after inoculation in the V2 phenological stage.

resistance at 7 d.a.i. (Vidigal Filho et al., 2020), 9 d.a.i. (Gonçalves-Vidigal et al., 2011), 12 d.a.i. (Guzman et al., 1995), 15 d.a.i. (Oliveira et al., 2004; Bassi et al., 2017; Almeida et al., 2020, 2021b), 18 d.a.i. (Almeida et al., 2021a), 21 d.a.i. (Nay et al., 2019b), and 28 d.a.i. (Carvalho et al., 1998). However, one of the advantages of considering the V2 stage for this assessment is reduction in the number of days necessary to complete the experiment. Pereira et al. (2011) proposed the use of the V2 stage and evaluated plants at 14 d.a.i. Librelon et al. (2015) evaluated 15 d.a.i. for validation of the V2 DS, while other authors used the same number of days for ALS assessment at the V2 stage (Pereira et al., 2019a, b, Librelon et al. 2020). Our results showed that, in the case of the V2 stage, at least 15 days after inoculation is necessary for reliable evaluation, since only on the last day of evaluation (day 15), could the cultivars be well discriminated. Before that, IAC-Milênio showed ALS severity similar to IAC-Carioca.

Another reason to use 15 d.a.i. for assessment of resistance to ALS is that from that day on, the inoculum concentration used was no longer significant, so the difference between the concentrations did not affect the degree of severity in the cultivars tested, and there was no significant interaction among the factors (that is, cultivar, concentration, and isolate). Just as for number of days for assessment, there is no consensus regarding the inoculum concentration to be used for inoculation 1×10^4 conidia mL^{-1} (Oblessuc et al., 2012; Perseguini et al., 2016), 1.2×10^4 conidia mL^{-1} (Gonçalves-Vidigal et al., 2020; Vidigal Filho et al., 2020), 2×10^4 conidia mL^{-1} (Carvalho et al., 1998; Guzman et al., 1995; Keller et al., 2015; Pastor-Corrales and Jara, 1995), and 4×10^4 conidia mL^{-1} (Pereira et al., 2011; Almeida et al., 2020) are most used. Pereira et al. (2011) reported that the concentration of 2×10^4 conidia mL^{-1} did not discriminate resistant bean lines from susceptible ones, and that the 4×10^4 conidia mL^{-1} generated a greater degree of severity. However, the authors evaluated the inoculated plants at 14 d.a.i., and the results also showed significance regarding the concentration used for 14 d.a.i. Librelon et al. (2015) used the concentration of 2×10^4 conidia mL^{-1} for development of the V2 DS, and Pereira et al. (2019a, b) and Librelon et al. (2020) used the same concentration for evaluation of resistance in advanced bean lines.

The main problem with the DSs proposed for evaluation of ALS severity is not only the subjectivity of the evaluators, but also the difference between the number of scores and the specific range of score variation in terms of leaf area affected by the disease. Schoonhove and Pastor-Corrales (1987) proposed a DS ranging from 1 to 9, with score 3 representing plants with up to 2% of leaf area affected. Godoy et al. (1997) also proposed a DS ranging from 1 to 9, but score 3 represented plants with up to 0.9% of leaf area affected. Moreno (1977) proposed another DS, ranging from 1 to 5, with score 3 representing up to 25% of leaf area affected; and Inglis et al. (1988) adapted the same DS, and score 3 was now understood as plants with up to 50% of leaf area affected.

A more reproducible and accurate way to assess resistance to ALS is through digital image analysis. However, in a study carried out by Rezende et al. (2014) under field conditions for evaluation of ALS using DS (Schoonhove and Pastor-Corrales, 1987) and the image analysis software Quant (Vale et al., 2001), the authors reported that the use of the DS was the most practical way to discriminate the bean lines. Software like Quant proposes a considerable problem in that it is not practical at all; leaves need to be detached and scanned one by one and images must be transferred to the computer for processing and quantification. In contrast, Leaf Doctor is

a smartphone app, and digital image quantification of leaf area affected by the disease can be performed in the field and/or greenhouse through simple capture of images and fast processing, without the need to detach leaves or scan them, and/or even transfer the images to computers. The Leaf Doctor approach is quantitatively more sensitive, precise and accurate than the DS, as observed in the present study, allowing the definition of greater differences among the genotypes through the app. This enhancement in precision of assessment could improve the initial steps of bean breeding programs.

CONFLICT OF INTERESTS

The authors have not declared any conflict of interests.

ACKNOWLEDGEMENTS

The authors are very thankful to Dr. Elaine Aparecida de Souza from the Genetics and Plant Breeding Department (UFLA, MG, Brazil) who kindly provided the *P. griseola* isolates for development of this study. They are also grateful to the Fundação de Amparo à Pesquisa do Estado de São Paulo (FAPESP) for granting fund for the research project (FAPESP Number 2014/11145-2) and scholarships (FAPESP Numbers 2017/01753-3, 2014/19967-1, 2019/19670-2), which enabled this study to be carried out.

REFERENCES

Almeida CP, Paulino JFC, Santos IL, Bajay MM, Gonçalves JGR, Carvalho CRL, Carbonell SAM, Chiorato AF, Benchimol-Reis LL (2021b). Marker-assisted backcrossing for disease resistance and agronomic traits in carioca beans. Crop Science csc2.20528.

Almeida CP, Arruda N, Paulino JF de C, Freitas GM de, Bonfante GFJ, Bajay MM, de Deus BC, Patrício FRA, Carbonell SAM, Chiorato AF, Benchimol-Reis LL (2020). Genetic diversity of *Pseudocercospora griseola* resistance loci in common beans. Tropical Plant Pathology 1-10.

Almeida CP, Carvalho Paulino JF, Bonfante GFJ, Perseguini JMKC, Santos IL, Gonçalves JGR, Patrício FRA, Taniguti CH, Gesteira G de S, Garcia AAF, Song Q, Carbonell SAM, Chiorato AF, Benchimol-Reis LL (2021a). Angular leaf spot resistance *loci* associated with different plant growth stages in common bean. Frontiers in Plant Science 12:650.

Arnal Barbedo JG (2013). Digital image processing techniques for detecting, quantifying and classifying plant diseases. SpringerPlus 2:1-12.

Assefa T, Assibi Mahama A, Brown AV, Cannon EKS, Rubyogo JC, Rao IM, Blair MW, Cannon SB (2019). A review of breeding objectives, genomic resources, and marker-assisted methods in common bean (*Phaseolus vulgaris* L.). Molecular Breeding 39(2). doi:10.1007/s11032-018-0920-0.

Bassi D, Briñez B, Rosa JS, Oblessuc PR, Almeida CP, Nucci SM, da Silva LCD, Chiorato AF, Vianello RP, Camargo LEA, Blair MW, Benchimol-Reis LL (2017). Linkage and mapping of quantitative trait *loci* associated with angular leaf spot and powdery mildew resistance in common beans. Genetics and Molecular Biology 40:109-122.

Bock CH, Parker PE, Cook AZ, Gottwald TR (2008). Visual rating and the use of image analysis for assessing different symptoms of citrus canker on grapefruit leaves. Plant Disease 92:530-541.

Campbell CL, Madden LV (1990). Introduction to plant disease epidemiology. Wiley, New York, 532p.

Carneiro JE de S, Paula Junior TJ, Borém A (2015). Feijão: do plantio à colheita. 384 p.p.

Carvalho G, Paula TJ, Alzate-Marin AL, Nietsche S, Barros EG, Moreira MA (1998). Herança da resistência da linhagem and-277 de feijoeiro-comum à raça 63-23 de *Phaeoisaropsis griseola* e identificaçao de marcador RAPD ligado ao gene de resistência. Fitopatologia Brasileira 23:482–485.

CONAB (2021). Acompanhamento da safra brasileira de grãos: Safra 2020/21 - Quarto levantamento. Companhia Nacional de Abastecimento. Available at <https://www.conab.gov.br/info-agro/safras/graos/boletim-da-safra-de-graos/> Accessed on January 21, 2021.

FAOSTAT (2021) Food and agriculture organization of the united nations (FAO). Statistical database, Food and Agriculture. Available at <http://www.fao.org/faostat/en/#data/QC/visualize> Accessed on January 12, 2021.

Forrest W, Nutter J, Teng P, Shokes F (1991). Disease assessment terms and concepts. Plant Disease 75:1187-1188.

Godoy CV, Carneiro SMTPG, Iamauti M, Dalla Pria M, Amorim L, Berger RD, Bergamin Filho A (1997). Diagrammatic scales for bean diseases: Development and vali-dation. Zeitschrift fur Pflanzenkrankheiten und Pflanzenschutz 104:336-345.

Gonçalves-Vidigal MC, Cruz AS, Garcia A, Kami J, Filho PSV, Sousa LL, McClean P, Gepts P, Pastor-Corrales MA (2011). Linkage mapping of the *Phg-1* and *Co-1*^{4} genes for resistance to angular leaf spot and anthracnose in the common bean cultivar AND 277. Theoretical and Applied Genetics 122:893-903.

Gonçalves-Vidigal MC, Gilio TAS, Valentini G, Vaz-Bisneta M, Vidigal Filho PS, Song Q, Oblessuc PR, Melotto M (2020). New andean source of resistance to anthracnose and angular leaf spot: fine-mapping of disease-resistance genes in california dark red kidney common bean cultivar. PloS One 15:e0235215.

Guzman P, Gilbertson RL, Nodari R, Johnson WC, Temple SR, Mandala D, Mkandawire AB, Gepts P (1995). Characterization of variability in the fungus *Phaeoisariopsis griseola* suggests coevolution with the common bean (*Phaseolus vulgaris*). Phytopathology 85:600-607.

Inglis DA (1988). Use of dry inoculum to evaluate beans for resistance to anthracnose and angular leaf spot. Plant Disease 72:771.

Keller B, Manzanares C, Jara C, Lobaton JD, Studer B, Raatz B (2015). Fine-mapping of a major QTL controlling angular leaf spot resistance in common bean (*Phaseolus vulgaris* L.). Theoretical and Applied Genetics 128:813-826.

Librelon SS, Pádua PF de, Abreu Â de FB, Ramalho MAP, Souza EA de (2020). Increasing the efficiency of recurrent selection for angular leaf spot resistance in common bean. Crop Science 60:751-758.

Librelon SS, Souza EA, Pereira R, Pozza EA, Abreu AFB (2015). Diagrammatic scale to evaluate angular leaf spot severity in primary leaves of common bean. Australasian Plant Pathology 44:385-395.

Lobet G, Draye X, Périlleux C (2013). An online database for plant image analysis software tools. Plant methods 9(1):1-8.

Mahlein AK (2016). Plant disease detection by imaging sensors–Parallels and specific demands for precision agriculture and plant phenotyping. Plant Disease 100:241-254.

Monda EO, Sanders FE, Hick A (2001). Infection and colonization of bean leaf by *Phaeoisariopsis griseola*. Plant Pathology 50:103-110.

Moreno RA (1977). Effect of different cropping systems on the severity of bean angular spot (*Phaseolus vulgaris* L), caused by *Isariopsis griseola* Sacc. Agronomia Costarricense 1:39-42.

Mutka AM, Bart RS (2015). Image-based phenotyping of plant disease symptoms. Frontiers in Plant Science 5:734.

Nay MM, Mukankusi CM, Studer B, Raatz B (2019b). Haplotypes at the phg-2 locus are determining pathotype-specificity of angular leaf spot resistance in common bean. Frontiers in Plant Science 10:1-11.

Nay MM, Souza TLPO, Raatz B, Mukankusi CM, Pastor-Corrales MA, Abreu AFB, Melo LC (2019a). A review of angular leaf spot resistance in common bean. Crop Science 59:1376-1391.

Oblessuc PR, Baroni RM, Garcia AAF, Chioratto AF, Carbonell SAM, Camargo LEA, Benchimol-Reis LL (2012). Mapping of angular leaf

spot resistance QTL in common bean (*Phaseolus vulgaris* L.) under different environments. BMC Genetics 13(1):1-9.
Oliveira EJ, Alzate-Marin AL, Borém A, Melo CLP, Barros EG de, Moreira MA (2004). Reação de cultivares de feijoeiro comum a quatro raças de *Phaeoisariopsis griseola*. Fitopatologia Brasileira 29(2):220-223.
Pastor-Corrales MA, Jara CE (1995). The evolution of *Phaeoisariopsis griseola* with the common bean in Latin America, pp. 15-24.
Pereira LA, Costa LC, de Pádua PF, Ramalho MAP (2019b). Variability for angular leaf spot and anthracnose resistance among common bean progenies with different levels of endogamy. Tropical Plant Pathology 44(3):275-283.
Pereira R, Abreu Â de FB, Nalin RS, de Souza EA (2019a). Phenotyping for angular leaf spot severity and its implication in breeding common bean for resistance. Scientia Agricola 76(5):415-423.
Pereira R, Abreu MJ, Souza EA (2011). Alternative method to assess the reaction of common bean lines to *Pseudocercospora griseola*. Annual Report of the Bean Improvement Cooperative 54:104-105.
Pereira R, Souza EA, Barcelos QL, Abreu AFB, Librelon SS (2015). Aggressiveness of *Pseudocercospora griseola* strains in common bean genotypes and implications for genetic improvement. Genetics and Molecular Research 14(2):5044-5053.
Perseguini JMKC, Oblessuc PR, Rosa JRBF, Gomes KA, Chiorato AF, Carbonell SAM, Garcia AAF, Vianello RP, Benchimol-Reis LL (2016). Genome-wide association studies of anthracnose and angular leaf spot resistance in common bean (*Phaseolus vulgaris* L.). PLoS One 11(3):e0150506
Pethybridge SJ, Nelson SC (2015). Leaf doctor: A new portable application for quantifying plant disease severity. Plant Disease 99(10):1310-1316.
Pires CV, Oliveira MG, Rosa JC, Costa NM (2006). Nutritional quality and chemical score of amino acids from different protein sources. Food Science and Technology 26(1):179-187.
Polya G (2003). Biochemical targets of plant bioactive compounds: a pharmacological reference guide to sites of action and biological effects. CRC press.
Rezende BA, Abreu Â de FB, Ramalho MAP, de Souza EA (2014). Severity evaluation methods in common bean recurrent selection programme for resistance to angular leaf spot. Journal of Phytopathology 162(10):643-649.
Sartorato A (2004). Pathogenic variability and genetic diversity of *Phaeoisariopsis griseola* isolates from two counties in the State of Goias, Brazil. Journal of Phytopathology 152:385-390.
Schoonhove A, Pastor-Corrales M (1987). Standard System for the Evaluation of Bean Germplasm. CIAT, CALI, 56 p.
Vale FXR, Fernandes Filho EI, Liberato JR, Zambolim L (2001). Quant - A software to quantify plant disease severity. International Workshop on Plant Disease Epidemiology 8:160.
Vidigal Filho PS, Gonçalves-Vidigal MC, Bisneta MV, Souza VB, Gilio TAS, Calvi AA, Lima LRL, Pastor-Corrales MA, Melotto M (2020). Genome-wide association study of resistance to the anthracnose and angular leaf spot diseases in Brazilian Mesoamerican and Andean common bean cultivars. Crop Science 60(6):2931-2950.
Zonta E, Machado A (1980). SANEST-Sistema de análise estatística. São Paulo, Escola Superior de Agricultura Luiz de Queiro.

Vol. 20(5), pp.175-185, May, 2021
DOI: 10.5897/AJB2020.17291
Article Number: 3AC792B66728
ISSN: 1684-5315

http://www.academicjournals.org/AJB

ACADEMIC JOURNALS
expand your knowledge

African Journal of Biotechnology

Full Length Research Paper

Synthesis, physicochemical and antimicrobial properties of rhenium (I) tricarbonyl complexes of isatin Schiff bases

Adebomi A. Ikotun[1*], Abimbola A. Owoseni[2] and Gabriel O. Egharevba[3]

[1]Industrial Chemistry Programme, College of Agriculture, Engineering and Sciences, Bowen University, Iwo, Nigeria.
[2]Microbiology Programme, College of Agriculture, Engineering and Sciences, Bowen University, Iwo, Nigeria.
[3]Department of Chemistry, Obafemi Awolowo University, Ile-Ife, Nigeria.

Received 1 December, 2020; Accepted 31 March, 2021

The Schiff base of isatin and sulphanilamide (L1; $C_{14}H_{11}N_3O_3S$) was prepared and reacted with $Re(CO)_5X$ (X = Cl and Br) in toluene to give $[Re(C_{14}H_{10}N_2O)(CO)_3X]$ (X = Cl, 1 and X = Br, 2). The prepared Schiff base of isatin and 4-methoxyaniline (L2; $C_{15}H_{12}N_2O_2$) was reacted with $Re(CO)_5X$ in toluene to give $[Re(C_{14}H_{10}N_2O)(CO)_3X]$, where X = Cl, 3 and X = Br, 4. L2 and $Re(CO)_5Br$ were refluxed in dry toluene under nitrogen and recrystallized to give $[Re(C_{15}H_{12}N_2O_2)(CO)_3Br].^1/_2C_2H_5OH$ (5). Spectroscopic characterization of compounds was done using FTIR, UV-Visible, NMR and Mass spectra analyses. Magnetic susceptibility measurements and melting points were also determined. Elemental analysis of 5 revealed it was a solvate molecule of 4. The *in-vitro* antimicrobial activities of compounds were evaluated against *Staphylococcus aureus, Bacillus subtilis,* Haemolytic *Staphylococcus aureus*, *Pseudomonas aeruginosa, Escherichia coli, Klebsiella* sp., *Aspergillus niger*, *Trichoderma viride* and *Penicillium citrinum*. Spectroscopic analyses revealed new terminal carbonyl bands formed between 1900 and 2030 cm^{-1}, as L1 and L2 coordinated through their azomethine nitrogen and keto oxygen donor atoms towards Re(I). Results of the antimicrobial studies revealed immerse improved activities upon coordination against tested microorganisms especially gram-negative bacteria, therefore they are recommended for further studies in cell imaging.

Key words: Isatin Schiff bases, rhenium (I) tricarbonyl complexes, antimicrobial, antifungal.

INTRODUCTION

Indole-2,3-dione (isatin) is a versatile starting material in syntheses. Its Schiff bases and complexes have been found to possess several pharmacological effects including anticonvulsant, antimicrobial and antiviral activities, inhibition of monoamine oxidase (Sridhar et. al., 2002; Adetoye et al., 2009), behavioural effects (Chohan et al., 2006) and activities against human immune-deficiency virus (Sriam et al., 2005). Isatin is an endogenous compound found in the brains and some tissues of mammals (Sridhar et al., 2002). It was first

*Corresponding author. E-mail: ikotunadebomi@gmail.com or adebomi.ikotun@bowen.edu.ng. Tel: +234 803 585 6562.

isolated from the fruits and flowers of the Cannon ball tree (*Couroupita gueanensis*), thereafter its good antioxidant, antibacterial and anticancer properties have also been established (Premanathan et al., 2012; Guo, 2019; Ding et al., 2020). Coogan et al. (2009) and Azzarelli et al. (2019) have also shown that heavy metals are not just "poisonous", but also possess great biological importance through the synthesis of several novel d^6 transition organometallic based agents, which were also used to target specific biological entities. Therefore, the coordination of Re(I) to isatin Schiff bases is promising with prospective biological activities which could even target biological entities of cancerous cells and could also possess some therapeutic anticancer effects. Presently, there is little or no report on Re(I) complexes of isatin derivatives. All these primarily motivated this research, which aimed at preparing new biologically active Re(I) tricarbonyl complexes of isatin derivatives. Previously, the Re(I) tricarbonyl complexes of the Schiff base of isatin and aniline with good antimicrobial activities were reported (Ikotun et al., 2019a). In this paper, the successful preparations of Re(I) tricarbonyl complexes of the Schiff bases of isatin with sulfanilamide and isatin with 4-methoxyaniline as well as its antimicrobial activities were reported.

EXPERIMENTAL

Chemicals

Isatin, 4-methoxyaniline, sulphanilamide, $Re(CO)_5Cl$ and $Re_2(CO)_{10}$ were obtained from Aldrich. $Re(CO)_5Br$ was prepared from $Re_2(CO)_{10}$ according to literature (Angelici, 1990). The solvents methanol, ethanol, chloroform and *N,N*-dimethylformamide (DMF) were all purchased from Sigma-Aldrich and SAARChem.

Instrumentation

The Infrared spectra were recorded on a Shimadzu IRAffinity-1 spectrometer with a pike MIRacle ATR system (diamond crystal) in the range of 4000 to 400 cm^{-1}. The ^1H NMR and ^{13}C NMR (400 MHz) spectra were recorded at room temperature on Bruker Spectrometer. The UV-Visible spectra were recorded on a Shimadzu UV-1800 spectrometer. Mass spectra were determined using a Fisons VG Quattro Spectrometer, a MicromassZabspec instrument (FAB) or an Applied Biosystem STR Voyager (MALDI-TOFMS) instrument, equipped with a nitrogen laser (337 nm, 3 ns pulse, 20 Hz maximum firing rate). Room temperature magnetic susceptibility measurements were measured using Johnson Matthey Magnetic Susceptibility balance. The monitoring of the reactions and the purity of the compounds were checked by Thin-Layer Chromatography (TLC) carried out on Silica Gel 60 F254 alumina plates (E Merk) using appropriate solvent mixtures of chloroform: diethyl ether (either 5:5 or 6:4) and visualized in UV chamber (365 nm). The melting points of compounds were determined using a Gallenkemp variable heater apparatus or an OptiMelt MPA 100 apparatus, which possesses a digital image processing technology. Microanalysis of compounds was carried out at University of Notre Dame, Notre Dame, Indiana, United States.

Syntheses

Preparation of the ligands

The ligands were prepared according to literature (Adetoye et al., 2009). L1 ($C_{14}H_{11}N_3O_3S$) was prepared by completely dissolving isatin (5 g; 339.8 mmol) in 200 ml methanol. Sulphanilamide (5.85 g; 339.8 mmol) was added while stirring at room temperature with the addition of 8 drops of concentrated H_2SO_4. Stirring was done at room temperature for $1^1/_2$ h. The precipitated yellow solid was filtered out and recrystallized in ethanol: chloroform (70: 30). The yield was 9.43 g (92%). Likewise, L2 ($C_{15}H_{12}N_2O_2$) was prepared by completely dissolving isatin (3 g; 20.40 mmol) in 120 ml methanol, 4-methoxyaniline (2.51 g; 20.40 mmol) was added and it was stirred at room temperature with the addition of 6 drops of concentrated H_2SO_4 for $2^1/_2$ h. The light yellow solid was filtered and recrystallized in ethanol: chloroform (7:3). The yield was 4.53 g (88%).

Preparations of rhenium complexes

The rhenium (I) tricarbonyl complexes were prepared according to literature (Ikotun et al., 2019a,b). Complex 1, $[Re(C_{14}H_{11}N_3O_3S)(CO)_3Cl]$ was prepared with 0.04 g (0.14 mmol) of L1 and 0.05 g (0.14 mmol) of $Re(CO)_5Cl$ stirred in 20 ml toluene at 100°C for $4^1/_2$ h. The light purple solids were filtered out under suction after cooling in the oil and this weighed 0.07 g (87%). Likewise, $[Re(C_{14}H_{11}N_3O_3S)(CO)_3Br]$ (2) was prepared by stirring $Re(CO)_5Br$ (0.2 g; 0.4931 mmol) and 0.14 g (0.4931 mmol) of L1 in 20 ml of hot toluene at 100°C for 20 h. The purple precipitate was filtered out under vacuum after cooling. This weighed 0.2797 g (92% yield). Also, $[Re(C_{15}H_{12}O_2N_2)(CO)_3Cl]$ (3) was prepared by stirring L2 (0.037 g; 0.14 mmol) and $Re(CO)_5Cl$ (0.05 g; 0.14 mmol) in 20 ml of toluene 3 h at 100°C. The solution was allowed to cool in oil, the light purple precipitate was filtered under vacuum and it weighed 0.04 g (49%). Similarly, $[Re(C_{15}H_{12}O_2N_2)(CO)_3Br]$ (4) was prepared by stirring L2 (0.0621 g; 0.2465 mmol) to complete dissolution in 10 ml toluene at 100°C and then adding $Re(CO)_5Br$ (0.1 g; 0.2465 mmol) to the solution. Stirring was done for 29 h in the hot solvent, the solvent was then removed under vacuum to yield purple amorphous solids (0.1461 g; 98%). The preparation of $[Re(C_{15}H_{12}O_2N_2)(CO)_3Br].^1/_2\ C_2H_5OH$ (5) was done by refluxing L2 (0.062 g; 0.2465 mmol) and $Re(CO)_5Br$ (0.1 g; 0.2465 mmol) in 15 ml dry toluene under nitrogen for 1 h. Cooling was done outside the oil bath and the pale purple amorphous solids formed were filtered under vacuum. Recrystallization was done in ethanol: chloroform (5:5) solution and the weight was 0.1078 g (70% yield). Suitable x-ray crystals could not be obtained for the complexes. All reactions were monitored by TLC.

Antimicrobial activity

Mueller-Hinton agar (MHA) and Potato dextrose agar (PDA) were the media used during the *in vitro* antibacterial and antifungal studies. Antibacterial activities were evaluated against three Gram-positive bacteria (*Staphylococcus aureus, Bacillus subtilis* and Haemolytic *Staphylococcus aureus*) and three Gram-negative bacteria (*Pseudomonas aeruginosa, Escherichia coli* and *Klebsiella* species). Antifungal activities of the compounds were evaluated against three fungi (*Trichoderma viride, Aspergillus niger* and *Penicillium citrinum*). Preliminary identification of the bacteria was done at Bowen University, Iwo, Nigeria, using the methods by Cheesbrough (2002). Tetracycline (30 µg; antibiotic test kit) was used as a standard drug for the bacteria, while dimethylformamide (DMF) was used as control.

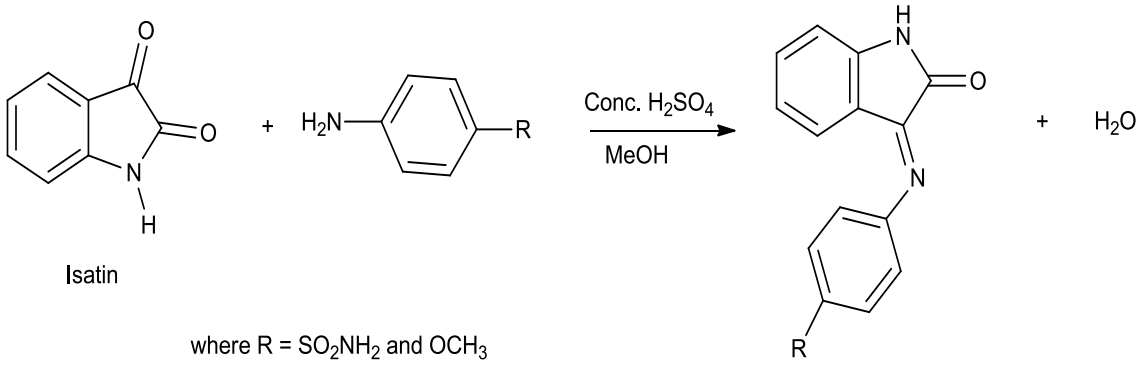

Scheme 1. Scheme of reaction for preparations of L1 and L2.

Antibacterial test

Each test bacterium was prepared according to the methods by CLSI (2016). Also, the antibacterial susceptibility test was carried out according to CLSI (2016) procedures. Disc diffusion method (Emeruwa, 1982) was used to evaluate the antimicrobial activities of the compounds using filter paper discs of diameter 8 mm and synthesized compounds at a concentration of 100 µg/mL dissolved in dimethylformamide (DMF). Antibacterial activities were evaluated by measuring the diameters of zones of growth inhibition in triplicates and the mean of three results of each data set was taken (Owoseni and Sangoyomi, 2014; Mostafa et al., 2018).

Minimum inhibitory concentration (MIC)

The MIC was carried out for only the compound with the highest zone of inhibition for each of the tested bacteria. This was determined by adding 10, 5.0, 2.5, 1.25, 0.625, and 0.3125 µg/ml of each complex into test tubes containing sterile nutrient broth. The organisms that showed susceptibility to the complex initially were then introduced into the broths containing different concentrations of the complex. The tubes were then incubated for 24 h at 37°C. The MIC was taken as the lowest concentration of the compounds that did not permit any visible growth (CLSI, 2016; Mogana et al., 2020).

Antifungal test

The fungal isolates were allowed to grow on Potato dextrose agar (PDA) (LabM) at 25°C for 5 to 7 days to sporulate. After sporulation, the fungal spores were harvested by pouring a mixture of sterile glycerol and distilled water onto the surface of the plate. A sterile glass rod was used to scrape the spores. Standardization of the harvested fungal spores was done to 10^6 spores/ml. One millilitre of the standardized spore suspension was evenly spread on solidified PDA (LabM) plates using a glass spreader. The plates were left for 1 h for the spore suspension to diffuse into the agar. The sterile discs were impregnated with the test compounds and placed aseptically using sterile forceps on the surface of the agar plates. The plates were then allowed to stand on the laboratory bench for 1 h to allow for proper diffusion of the compounds into the media. Plates were incubated at 25°C for 96 h and observed for zones of inhibition. Activity was evaluated by measuring the diameters of zones of growth inhibition in triplicates and the mean of three results were taken.

RESULTS AND DISCUSSION

Isatin was separately condensed with sulfanilamide (L1) and 4-methoxyaniline (L2) at room temperature (Adetoye et al., 2009; Ikotun et al., 2019 b). The scheme of preparation is presented as Scheme 1 (Adetoye et al., 2009).

New rhenium (I) complexes of L1 and L2 were also prepared similar to our previous report (Ikotun et al., 2019a) with slight modifications. The general equation for their preparations is presented as Scheme 2.

The physical properties of these complexes and their ligands are presented as Table 1.

Infra-red spectra

The comparison of the distinctive vibrational frequencies of the prepared complexes with those of the isatin ligands L1 and L2 (Chohan et al., 2006; Ikotun et al., 2019a) have been presented in Table 2. The new and diagnostic υ(CO) bands appeared as terminal carbonyl bands ascertaining the formation of these complexes (Angelici, 1990). In spectrum 1, $[Re(C_{14}H_{11}N_3O_3S)(CO)_3Cl]$, the new υ(CO) bands appeared as a strong band at 1906 cm^{-1}, a shoulder band at 1932 cm^{-1} and a medium band at 2021 cm^{-1}. In spectrum 2, $[Re(C_{14}H_{11}N_3O_3S)(CO)_3Br]$, they were observed as a strong band at 1906 cm^{-1}, a shoulder band at 1929 cm^{-1} and a medium band at 2014 cm^{-1}. In spectrum of complex 3, $[Re(C_{15}H_{12}O_2N_2)(CO)_3Cl]$, they appeared as a strong band at 1899 cm^{-1} and two medium bands at 1924 and 2029 cm^{-1}. In spectrum 4, $[Re(C_{15}H_{12}O_2N_2)(CO)_3Br]$, they appeared as two new strong bands at 1906 and 2029 cm^{-1}, as well as a new shoulder band at 1924 cm^{-1}. In spectrum 5, $[Re(C_{15}H_{12}O_2N_2)(CO)_3Br].^1/_2C_2H_5OH$, they appeared as a new strong band at 1899 cm^{-1} and two medium bands at 1921 and 2029 cm^{-1}. These confirm the formation of these rhenium (I) tricarbonyl complexes of these isatin derivatives. The spectrum of L1 ($C_{14}H_{11}N_3O_3S$) showed a medium band at 3325 cm^{-1} attributable to O-H stretching

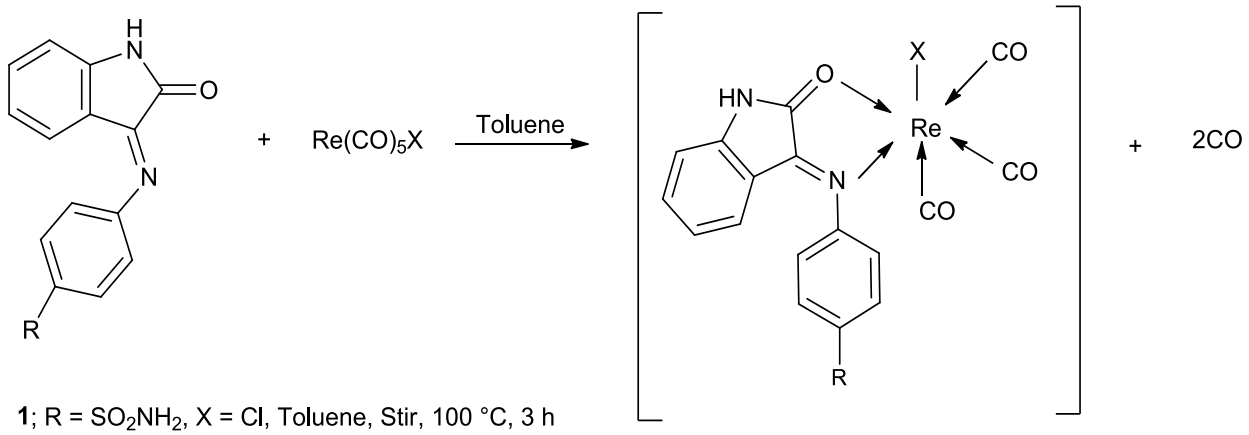

1; R = SO_2NH_2, X = Cl, Toluene, Stir, 100 °C, 3 h

2; R = SO_2NH_2, X = Br, Toluene, Stir, 100 °C, 20 h

3; R = OCH_3, X = Cl, Toluene, Stir, 100 °C, 3 h

4; R = OCH_3, X = Br, Toluene, Stir, 100 °C, 29 h

$[Re(C_{15}H_{12}O_2N_2)(CO)_3Br].^1/_2C_2H_5OH$ (**5**); R = OCH_3, X = Br, Toluene, Reflux, 1 h, N_2, Recrystallized in Ethanol: Chloroform (50: 50)

Scheme 2. Scheme of reaction for preparation of rhenium(I) tricarbonyl complexes.

Table 1. Physical Properties of L1, L2 and their rhenium(I) tricarbonyl complexes.

Compound	Formula (g/mol)	Colour	Melting point (°C)	% Yield
L1 ($C_{14}H_{11}N_3O_3S$)	301	Light Yellow	267 - 268	92
$[Re(C_{14}H_{11}N_3O_3S)(CO)_3Cl]$ (1)	607	Light Purple	298*	87
$[Re(C_{14}H_{11}N_3O_3S)(CO)_3Br]$ (2)	651	Purple	202 - 204	92
L2 ($C_{15}H_{12}N_2O_2$)	252	Light Yellow	229*	88
$[Re(C_{15}H_{12}N_2O_2)(CO)_3Cl]$ (3)	558	Light Purple	300*	49
$[Re(C_{15}H_{12}N_2O_2)(CO)_3Br].^1/_2C_2H_5OH$ (5)	625	Pale purple	301 - 302	70

*To decomposition.

band. This band moved to higher wavenumbers of 3447 and 3395 cm^{-1} in complexes 1 and 2, respectively. This band was absent in the spectra of L2 and its complexes. The medium band at 3233 cm^{-1} in the spectrum of L1 has been assigned to $\upsilon(NH_2)$ stretching vibration of the sulphonamide and it shifted to higher wavenumbers of 3279 and 3287 cm^{-1} in complexes 1 and 2, respectively. This signifies the involvement of the sulphonamide moiety of the ligand in coordination (Adetoye et al., 2009). The medium band at 3102 cm^{-1} in the spectrum of L1 and at 3156 cm^{-1} in the spectrum of L2 is attributable to the N-H stretching vibration of the amido group. This band has moved to higher wavenumbers of 3256 and 3171 cm^{-1} in the spectra of 1 and 2, respectively, while shifting to lower frequencies of 3102, 3132 and 3125 cm^{-1} in 3, 4 and 5, respectively. The strong band appearing at 1744 cm^{-1} in the spectrum of L1, while appearing at 1736 cm^{-1} in the spectrum of L2 appeared as a weak band at 1750 cm^{-1} in the spectrum of 1 and disappeared in 2, 3, 4 and 5. This has been assigned as the $\upsilon(C=O)$ frequency of the amido group. It signifies the involvement of the oxygen of the $\upsilon(C=O)$ bond in coordination. The uncoordinated C=N and C=C stretching vibrations appeared as overlapping bands at 1659 and 1528 cm^{-1} (Chohan et al., 2006) in L1, while appearing as a strong band at 1605 cm^{-1} and a weak band at 1643 cm^{-1} in L2. These bands have moved to higher frequencies of 1682 and 1612 cm^{-1} in the spectra of both complexes 1 and 2, appearing at 1674 and 1614 cm^{-1} in complex 3, at 1674 and 1713 cm^{-1} in complex 4 and at 1674 and 1605 cm^{-1} in

Table 2. Relevant infrared spectral data of L1, L2 and their rhenium(I) tricarbonyl complexes.

Compound	υ(OH) (cm^{-1})	υ(NH_2) (cm^{-1})	υ(NH) (cm^{-1})	υ(CO) (cm^{-1})	υ(C=O) (cm^{-1})	υ(C=N+C=C) (cm^{-1})	υ(SO_2)^{as} (cm^{-1})	υ(SO_2)^{s} (cm^{-1})	υ(C-N+C-C) (cm^{-1})	υ(S-N) (cm^{-1})	υ(C-S) (cm^{-1})	υ(M-N) (cm^{-1})	δ(M-C-O) (cm^{-1})
L 1 ($C_{14}H_{11}N_3O_3S$)	3325m	3233m	3102m	-	1744s	1659m, 1528s	1319s	1142s	1096s	910s	841s	-	-
Complex1; [Re($C_{14}H_{11}N_3O_3S$)$(CO)_3$Cl]	3447m	3279w	3156m	1906s, 1932sh, 2021m	1750w	1682m, 1612m	1337s	1157s	1096m	902m	837m	640s	544m
Complex 2; [Re($C_{14}H_{11}N_3O_3S$)$(CO)_3$Br]	3395m	3287m	3171m	1906s, 1929sh, 2014s	-	1682m, 1612m	1335s	1157s	1103m	-	895m	640s	540s
L2 ($C_{15}H_{12}N_3O_2$)	-	-	3156m	-	1736s	1643m, 1605s	-	-	1034s	-	-	-	-
Complex 3; [Re($C_{15}H_{12}N_3O_2$)$(CO)_3$Cl]	-	-	3102w	1899s, 1924m, 2029m	-	1674w, 1614w	-	-	1099w	-	-	641m	546m
Complex 4; [Re($C_{15}H_{12}N_3O_2$)$(CO)_3$Br]	-	-	3132w	1906s, 1924sh, 2029s	1713w	1674s	-	-	1096m	-	-	679m	548w
Complex 5; [Re($C_{15}H_{12}N_3O_2$)$(CO)_3$Br].$^1/_2C_2H_5OH$	-	-	3125w	1899s, 1921m, 2029m	1682s	1675m, 1605m	-	-	1103w	-	-	679s	548w

υ, Stretching; δ, deformation; m, medium; w, weak; b, broad; s, shoulder, and s, strong.

complex 5 on coordination to the Re(I) ion. The $\upsilon_{assymm}(SO_2)$ band appeared as a strong band at 1319 cm^{-1} in the spectrum of L1. This underwent a shift to higher frequencies of 1337 cm^{-1} and 1335 cm^{-1} in the spectra of 1 and 2 respectively. Likewise, the $\upsilon_{assymm}(SO_2)$ band appeared as a strong band at 1142 cm^{-1} and this underwent a shift to a higher frequency of 1157 cm^{-1} in both complexes 1 and 2. The uncoordinated C-N and C-C stretching vibrations appeared as overlapping strong, medium or weak bands at 1096 cm^{-1} in both L1 and 1, 1103 cm^{-1} in both complexes 2 and 5, 1034 cm^{-1} in L2, 1099 cm^{-1} in 3 and 1096 cm^{-1} in 4. The υ(S-N) band appeared as a strong band at 910 cm^{-1} in the spectrum of L1 and it underwent a shift to a lower frequency of 902 cm^{-1} in complex 1, while it disappeared in the spectrum of complex 2. The υ(C-S) band appeared as a strong band at 841 cm^{-1} in the spectrum of L1 and it underwent a shift to a lower frequency of 837 cm^{-1} in 1, while it moved to a higher frequency of 895 cm^{-1} in the spectrum of complex 2. The new strong or medium bands at 640 cm^{-1} in complexes 1 and 2, 641 cm^{-1} in complex 3, and 679 cm^{-1} in complexes 4 and 5 are attributable to the υ(M-N) bands. Also, the new medium or strong band that appeared at 544, 540, and 546 cm^{-1} in complexes 1, 2, and 3, respectively, also appeared at 548 cm^{-1} in complexes 4 and 5.

These have been assigned to δ(M-C-O) bending mode. All these confirm the formation of these new rhenium (I) tricarbonyl complexes of L1 and L2.

Table 3. Electronic spectra data of L1 and its Re(I) tricarbonyl complexes.

Compound	Band position (nm)	Molar Absorptivity (E; M^{-1}, cm^{-1})	Band position (cm^{-1})	Band Assignment
L1 ($C_{14}H_{11}N_3O_3S$)	406	2,720	24,631	n-π*
	298	6,887	33,557	π-π*
	249	28,550	40,161	π-π*
Complex 1 $[Re(C_{14}H_{11}N_3O_3S)(CO)_3Cl]$	461	9,874	21,692	MLCT
	261	16,194	38,314	π-π*
Complex 2 $[Re(C_{14}H_{11}N_3O_3S)(CO)_3Br]$	478	6,332	20,921	MLCT
	332	8,668	30,120	π-π*
	252	31,739	39,683	π-π*

Electronic spectra

The electronic spectra data of L1 and its rhenium(I) tricarbonyl complexes 1 and 3 as determined in methanol are presented in Table 3. The maximum absorption bands (λ_{max}) for these compounds have also been determined in methanol. The λ_{max} for L1 is 24,631 cm^{-1} (406 nm) with a molar absorptivity value (E) of 2,720 $M^{-1}cm^{-1}$. This is expected due to the extended conjugation which could also include the C=N after deprotonating nitrogen in the indole ring of isatin, thus also presenting the tautomeric enol form of L1 in solution (Adetoye et al., 2009; Ikotun et al., 2019a). The λ_{max} for complex 1 is 21,692 (461 nm) with the molar absorptivity value of 9,874 $M^{-1}cm^{-1}$. The λ_{max} for complex 2 is 20,931 cm^{-1} (478 nm) with the molar absorptivity value of 6,332 $M^{-1}cm^{-1}$.

The ultraviolet spectrum of L1 showed absorption bands at 33,557 and 40,161 cm^{-1} which have been assigned to π – π* transition (Sutton, 1968). The band at 24,631 cm^{-1} is attributable to n – π* transition. The interpretations of ultraviolet spectra of metal complexes of isatin derived Schiff bases revealed that charge – transfer bands occur in the same region with π – π* transitions (Chohan et al., 2006). The ultraviolet spectra of the rhenium carbonyl complex 1; $[Re(C_{14}H_{11}N_3O_3S)(CO)_3Cl]$ was therefore characterized by the absorption band at 38,314 cm^{-1} assigned to ligand π – π* transitions (Sutton, 1968). The absorption band at 21,692 cm^{-1} has been assigned to MLCT {dπ(Re) – π*} transition. Complex 2 $[Re(C_{14}H_{11}N_3O_3S)(CO)_3Br]$ was also characterized by absorption bands at 30, 120 and 39,683 cm^{-1} assigned to ligand π – π* transitions (Scherer, 2009). The absorption band at 20,921 cm^{-1} has been assigned to MLCT {dπ(Re) – π*} transition. All these are consistent with the magnetic moment of 0 as determined for these complexes and a low spin octahedral configuration.

Molecular weight determinations

The exact mass spectrum of L1 showed a relative abundant peak at 302.059, which corresponds to the (M+1) peak. These prepared complexes of L1 and L2 are halides, thus their mass spectra are expected to display peaks such as $(M+2)^+$, $(M+4)^+$, $(M+6)^+$, etc (Adetoye et al., 2009). The spectrum of complex 1; $[Re(C_{14}H_{11}N_3O_3S)(CO)_3Cl]$ showed the highest peak at $^m/_z$ (ESI) 613 (45%), which corresponds to the $[M+6]^+$ peak. This also signifies that the ratio of the reaction for the formation of compound 1, that is, metal: ligand is 1:1 as expected. This ion at $^m/_z$ 613 fragments via two routes is as follows:

(i) The ion at $^m/_z$ 613 fragments by the loss of 3CO (84 mass units), CH_3CN (41 mass units), SO_2NH_2 (80 mass units) and H (1 mass unit) to give the ion at peak $^m/_z$ 407 (3 %) corresponding to $[M\text{-}Cl\text{-}3CO\text{-}SO_2NH_2\text{-}H]^+$. This ion fragments by loss of C (12 mass units) and H (1 mass unit) to give the ion at the base peak $^m/_z$ 394 (100%) corresponding to $[M\text{-}Cl\text{-}3CO\text{-}SO_2NH_2\text{-}H\text{-}C\text{-}H]^+$. This ion equally corresponds to $[M\text{-}Cl\text{-}2CO\text{-}C_6H_5SO_2NH_2]^+$.
(ii) The ion at $^m/_z$ 613 fragments by the loss of CH_3CN (41 mass units), 3CO (84 mass units) and Re^+ ion (186 mass units) to give the ion at the peak $^m/_z$ 302 (4%) corresponding to $[M\text{-}Cl\text{-}3CO\text{-}Re+H]^+$. This peak also corresponds to the ligand peak ($C_{14}H_{11}N_3O_3$; L1). The spectra data analyses for complex 1 are presented in Table 4, while the fragmentation pattern is shown in Scheme 3.

In the mass spectrum of L2 ($C_{15}H_{12}N_2O_2$), the expected molecular ion appeared at $^m/_z$ (ESI) 253 (22 %) corresponding to $[M+H]^+$. The mass spectrum of Compound 4, $[Re(C_{15}H_{12}N_2O_2)(CO)_3Br]$ revealed that the expected molecular ion, $[M[^+$ appeared at $^m/_z$ (MALDI) 602 (25%). This also confirms the formation of the complex, thus the complexation is 1:1. The $[M+2]^+$ also appeared at 604. The molecular ion fragments via two routes as follows:

(i) The molecular fragments by loss of $Br^·$ radical (80 mass units), Re (186 mass unit) and H_2 (2 mass units) to

Table 4. Mass spectral data of complex 1; $[Re(C_{14}H_{11}N_3O_3S)(CO)_3Cl]$.

$^{M}/_{Z}$	Fragment
613	$[M+6]^+$
407	$[M\text{-}Cl\text{-}3CO\text{-}SO_2NH_2\text{-}H]^+$
394	$[M\text{-}Cl\text{-}3CO\text{-}SO_2NH_2\text{-}H\text{-}C\text{-}H]^+$ OR $[M\text{-}2CO\text{-}C_6H_5SO_2NH_2]^+$
302	$[M\text{-}Cl\text{-}3CO\text{-}Re+H]^+$

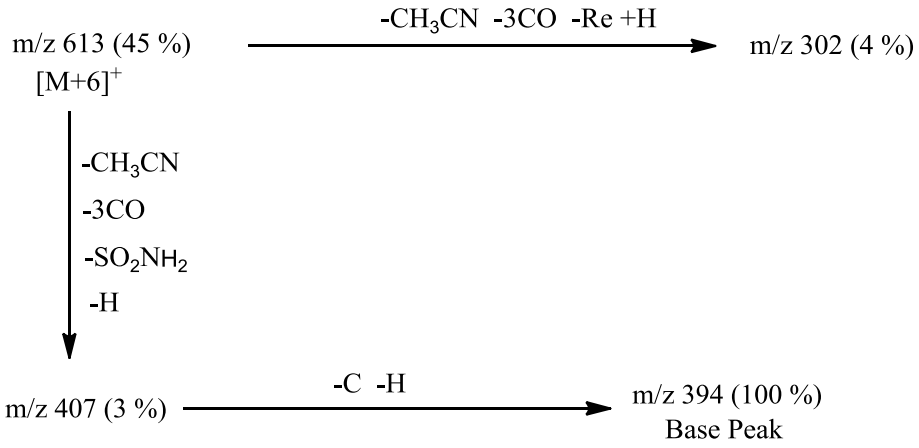

Scheme 3. Fragmentation Pattern of Complex 1; $[Re(C_{14}H_{11}N_3O_3S)(CO)_3Cl]$.

Table 5. Mass spectral data of complex 4; $[Re(C_{15}H_{12}N_2O_2)(CO)_3Br]$

$^{M}/_{Z}$	Fragment
602	$[M]^+$
518	$[M\text{-}3CO]^+$
334	$[M\text{-}Br\text{-}Re\text{-}H_2]^+$
290	$[M\text{-}Br\text{-}Re\text{-}H_2\text{-}CO_2]^+$
252	$[M\text{-}3CO\text{-}Br\text{-}Re]^+$
194	$[M\text{-}3CO\text{-}Br\text{-}Re\text{-}C_4H_{10}]^+$
182	$[M\text{-}Br\text{-}Re\text{-}H_2\text{-}CO_2\text{-}C_6H_5OCH_3]^+$
168	$[M\text{-}Br\text{-}Re\text{-}H_2\text{-}CO_2\text{-}C_6H_5OCH_3\text{-}C\text{-}H]^+$

give the ion at the base peak $^{m}/_{z}$ 334 (100 %), corresponding to $[M\text{-}Br^{\cdot}\text{-}Re\text{-}H_2]^+$. This ion fragments by loss of CO_2 (44 mass units) to yield another ion at $^{m}/_{z}$ 290 (55%) corresponding to $[M\text{-}Br^{\cdot}\text{-}Re\text{-}H_2\text{-}CO_2]^+$. This ion fragments by loss of $C_6H_5OCH_3$ (108 mass units) to yield another ion at peak $^{m}/_{z}$ 182 (62%) corresponding to $[M\text{-}Br^{\cdot}\text{-}Re\text{-}H_2\text{-}CO_2\text{-}C_6H_5OCH_3]^+$. The ion at $^{m}/_{z}$ 182 then loses C (12 mass units) and H (1 mass unit) concomitantly to yield the ion at $^{m}/_{z}$ 168 (95%) corresponding to $[M\text{-}Br^{\cdot}\text{-}Re\text{-}H_2\text{-}CO_2\text{-}C_6H_5OCH_3\text{-}C\text{-}H]^+$.

(ii) The molecular ion fragments by loss of 3CO (84 mass units) to yield the ion at $^{m}/_{z}$ 518 (5%) corresponding to $[M\text{-}3CO]^+$. This ion then loses $Br^{\cdot}$ Radical (80 mass units) and also Re (186 mass units) to give the ion at $^{m}/_{z}$ 252 (20%) corresponding to $[M\text{-}3CO\text{-}Br^{\cdot}\text{-}Re]^+$. This ion also corresponds to the ligand ion (L2). This ion further loses C_4H_{10} (58 mass units) to give the ion at $^{m}/_{z}$ 194 (28%) corresponding to $[M\text{-}3CO\text{-}Br^{\cdot}\text{-}Re\text{-}C_4H_{10}]^+$. The spectral data are collected in Table 5, while the fragmentation pattern is shown in Scheme 4.

Magnetic susceptibility measurement

The magnetic moments for the prepared complexes were measured at room temperature. The value was 0 B.M for the rhenium carbonyl adducts. This value signifies the following:

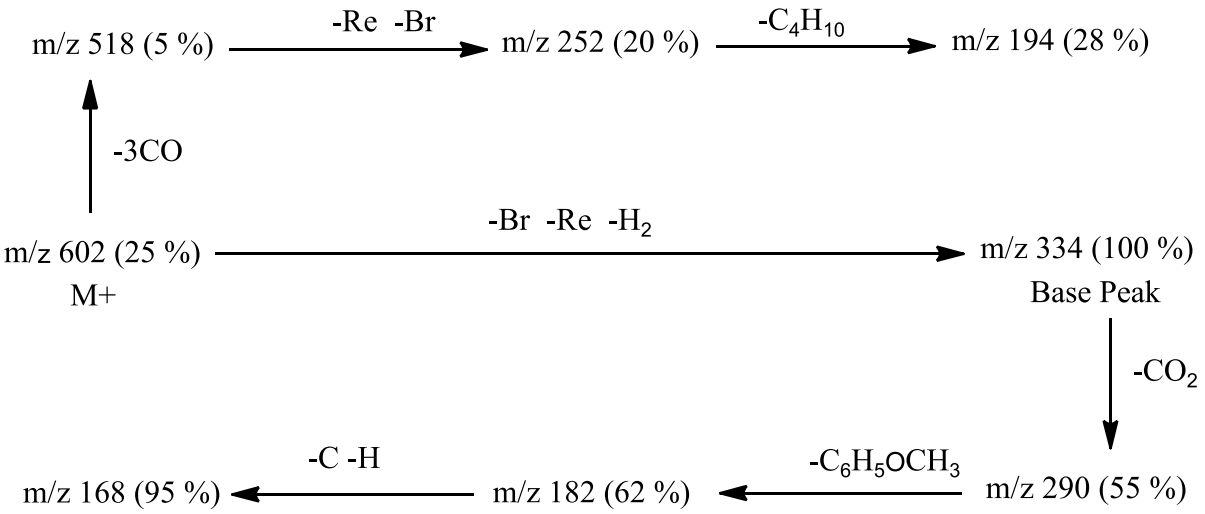

Scheme 4. Fragmentation pattern of compound 4; $[Re(C_{15}H_{12}N_2O_2)(CO)_3Br]$.

(a) these complexes are diamagnetic;
(b) since Re(I) is in the d^6 electronic state, the complexes will assume an octahedral shape;
(c) L1 and L2 are strong field ligands; and
(d) these rhenium carbonyl adducts are low spin.

Elemental analyses

The results of the elemental analyses carried out for complex 5 are presented subsequently. These results revealed that this compound recrystallized as a solvate compound (Egharevba et al., 1982).

Compound 5: $[Re(C_{15}H_{12}O_2N_2)(CO)_3Br\ ].^1/_2\ C_2H_5OH$
Calculated values: C, 36.5; H, 2.42; N, 4.48; O, 14.1%
Found: C, 36.9; H, 4.76; N, 4.79; O, 13.49

^{1}H- and ^{13}C-NMR spectra

The spectrum of L1 showed two resonance signals due to indole-NH at δ 10.95 and 11.06 ppm in a ratio 1:3, indicating that the isatin Schiff base (ligand) exists in DMSO as two stereoisomers (E and Z). The ^{1}H-NMR signals of the two isomers appear as shown in Figure 1. The numbering system for the ligand is presented in Figure 1.

The major stereoisomer showed the following signals (δ, ppm): 7.90 (2H, d, J = 8.4 Hz, H-13 and H-15), 7.41 (4H, m, H-5, H-6 and $SONH_2$), 7.19 (2H, d, J = 8.8 Hz, H-12 and H-16), 6.75 (1H, t, 7.6 Hz, H-7) and 6.35 (1H, d, J = 7.6 Hz, H-8). 10 signals were observed as expected. The minor stereoisomer showed the following signals (δ, ppm): 7.61 (1H, d, J = 7.6 Hz), 7.74 (2H, d, J = 8.8 Hz), 7.48 (1H, t, J = 0.8 Hz), 7.10 (3H, m) and 6.93 (4H, m). This is in agreement with published work (Adetoye et al., 2009). The ^{1}H-NMR spectrum of complex 1, $[Re(C_{14}H_{11}N_3O_3S)(CO)_3Cl]$ is completely different from that of its ligand, L1, thus providing evidence of metal chelation with significant changes in the chemical shifts. The ^{1}H-NMR spectrum of $[Re(C_{14}H_{10}N_2O)(CO)_3Cl]$ showed the following 11 signals as expected (δ, ppm): 11.05 (1H, s, CONH), 7.60 (1H, t, J = 7.6 Hz), 7.46 (1H, d, J = 7.6 Hz), 7.44 (2H, d, J = 8.8 Hz), 7.07 (1H, t, J = 7.6 Hz), 6.90 (3H, d, J = 8.0 Hz), 6.60 (2H, d, J = 8.8 Hz). In the ^{13}C-NMR spectrum of L1, 25 signals were observed as follows (δ, ppm): 163.6 (C =O), 158.9 (C = O), 155.7 (C = N), 154.1 (C =N), 153.7 (Cq), 152.9 (Cq), 147.7 (Cq), 146.5 (Cq), 140.7 (Cq), 139.7 (CH), 135.7 (CH), 135.1 (CH), 127.9 (CH), 126.6 (CH), 125.8 (CH), 123.6 (CH), 122.8 (CH), 122.8 (CH), 121.2 (CH), 119.0 (CH), 118.0 (CH), 115.9 (CH), 112.8 (CH), 112.1 (CH) and 111.3 (CH). 25 signals mean that the carbon atoms of both the E and Z stereoisomers have produced these signals, with the overlap of 3 carbon atoms. The 3 overlapping atoms are most likely quaternary carbons, since 12 signals are expected within the region, but only 9 appeared. This is not too surprising given the antecedent of the peculiar nature of isatin Schiff bases (Adetoye, 2010; Ikotun et al., 2019a). In the ^{13}C-NMR spectrum of 1, the new carbonyl signals appeared as follows (δ, ppm): 196.7 (C ≡ O), 193.0 (C ≡ O), 184.8 (C ≡ O). These new carbonyl bands support the formation of this complex. All other carbon signals from the ligand appear as follows (δ, ppm): 159.8 (C = O), 151.4 (Cq), 151.0 (Cq), 138.7 (Cq), 131.1 (CH), 127.8 (CH), 123.1 (CH), 125.1 (CH), 118.2 (CH), 113.4 (CH), and 112.6 (CH). This collapses to 11 carbon signals from the ligand instead of 15, thus 4 carbon atoms are overlapping. This is quite similar to previously reported Re(I) complexes of the Schiff base of isatin and aniline (Ikotun et al., 2019a).

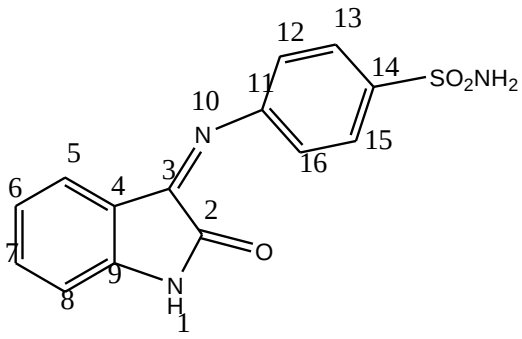

Figure 1. Numbering of atoms in $C_{14}H_{10}N_3O_3S$ (L1).

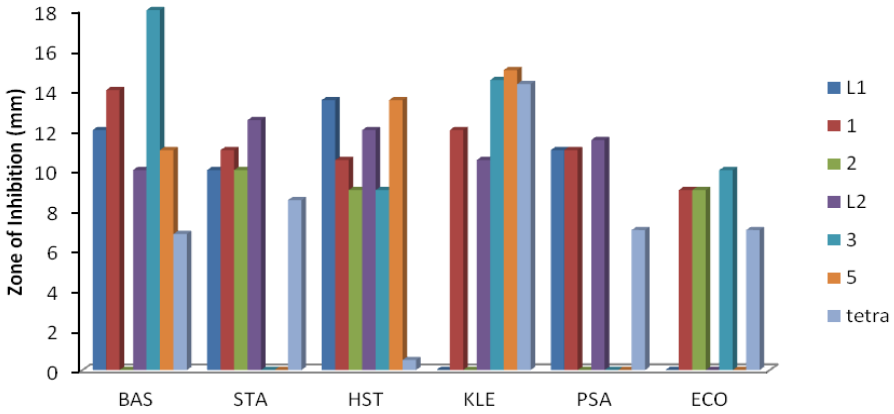

Figure 2. Antibacterial activities of L1, L2 and their rhenium(I) tricarbonyl complexes. BAS = *Bacillus subtilis,* STA= *Staphylococcus aureus,* HST = Haemolytic *Staphylococcus aureus,* KLE = *Klebsiella* spp., PSA = *Pseudomonas aeruginosa,* ECO = *Escherichia coli.* L1 = $C_{14}H_{10}N_2O$, 1 = $[Re(C_{14}H_{11}N_3O_3S)(CO)_3Cl$, L2 = $C_{15}H_{12}O_2N_2$, 2 = $[Re(C_{14}H_{11}N_3O_3S)(CO)_3Br]$, 3 = $[Re(C_{15}H_{12}O_2N_2)(CO)_3Cl]$, 5 = $[Re(C_{15}H_{12}O_2N_2)(CO)_3Br].{}^1/_2C_2H_5OH$.

Antibacterial studies

The results from the antibacterial activities of ligands and the rhenium tricarbonyl complexes are presented in Figure 2.

Complex 1 had a broad spectrum and therefore can be developed as a broad spectrum antibiotic with better activities than the ligand, L1 and tetracycline. L1 was active against all tested Gram positive bacteria with better activities than tetracycline, suggesting that it would be a good grAm positive drug. Compound 2 was active against both *Staphylococcus* bacteria and *E. coli* with a higher zone of inhibition than tetracycline, thus it could be a potential anti-staphylococcal drug. L2 can be developed as a strong anti-enteric bacteria drug due to its high zones of inhibition against *Klebsiella* spp. and *E. coli*. Compound 3 can also be a target anti-enteric bacteria drug. This compound also has the highest zone of inhibition against *S. aureus* (much higher than that of tetracycline). It is also active against *B. subtilis.* Complex 5 had the highest active against Haemolytic *S. aureus*, which even tetracycline was only weakly active against. This compound was also active against *B. subtilis* (better than tetracycline). It had the greatest activity against *Klebsiella* spp. out of all these tested compounds (and also tetracycline), thus it could be a potential drug against *Klebsiella* spp. These results are consistent with previous studies, involving the Schiff base of isatin and aniline with $Re(CO)_5X$ (where X = Cl and Br) (Ikotun et al., 2019a).

Minimum inhibitory concentration (MIC)

The MIC was carried out for only the compound with the highest zone of inhibition for each of the tested bacteria. Complex 5 had the MIC value of 10 µg/ml against *Klebsiella* spp. and compound L2 had the MIC value of 10 µg/ml against *E. coli.*

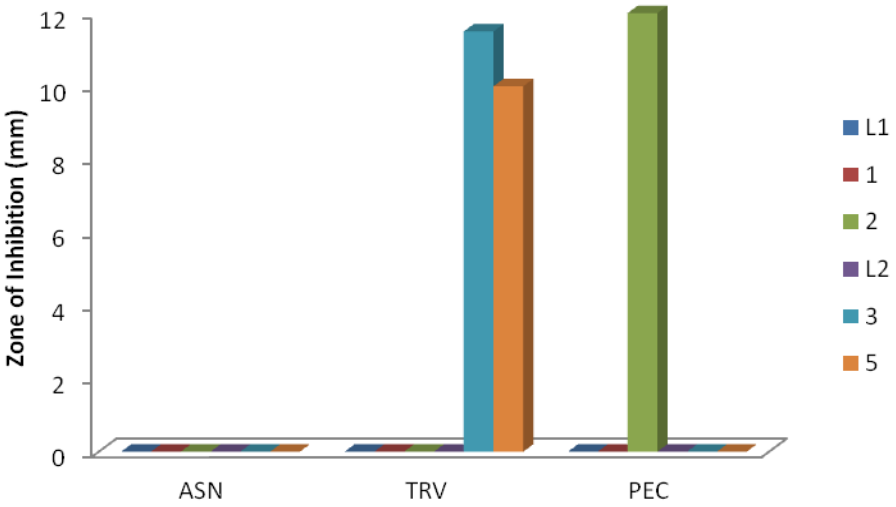

Figure 3. Antifungal activities of L1, L2 and their rhenium(I) tricarbonyl complexes. ASN = *Aspergillus niger,* TRV = *Trichoderma viride,* PEC = *Penicillium citrinum,* L1 = $C_{14}H_{11}N_3O_3S$, 1 = $[Re(C_{14}H_{11}N_3O_3S)(CO)_3Cl]$, 2 = $[Re(C_{14}H_{11}N_3O_3S)(CO)_3Br]$, L2 = $(C_{15}H_{12}O_2N_2)$, 3 = $[Re(C_{15}H_{12}O_2N_2)(CO)_3Cl]$, 5 = $[Re(C_{15}H_{12}O_2N_2)(CO)_3Br].^1/_2C_2H_5OH$.

Antifungal studies

The results from the antifungal activities of ligands and their rhenium(I) tricarbonyl complexes are presented in Figure 3.

Antifungal studies revealed that compound 2 was active against *P. citrinum* while compounds 3 and 5 were active against *T. viride*. All other tested compounds were not active against the tested fungi.

Conclusion

The rhenium (I) tricarbonyl complexes $[Re(C_{14}H_{11}N_3O_3S)(CO)_3Cl]$ (1), $[Re(C_{14}H_{11}N_3O_3S)(CO)_3Br]$ (2), $[Re(C_{15}H_{11}N_2O_2)(CO)_3Cl]$ (3), $[Re(C_{15}H_{11}N_2O_2)(CO)_3Cl]$ (4) and $[Re(C_{15}H_{12}O_2N_2)(CO)_3Br].^1/_2\ C_2H_5OH$ (5) of the prepared isatin Schiff bases, 4-((2-oxoindolin-3-ylidene) amino)benzenesulfonamide (L1) and 3-((4-methoxyphenyl)imino)indolin-2-one (L2) were successfully prepared in good yields. Physicochemical properties of the prepared complexes were determined by spectroscopic means, as well as by magnetic susceptibility and melting point determinations. The spectral data confirmed the complexation of L1 and L2 in ratio metal: ligand = 1:1. The IR spectra of these complexes showed new carbonyl bands identified as terminal carbonyl bands. L1 and L2 have acted in a bidentate manner towards Re(I) coordinating through the azomethine nitrogen and keto oxygen. The prepared complexes were found to be diamagnetic, thus revealing that the ligands are strong field ligands. Results of the antimicrobial studies showed significant inhibitory activities against the growth of tested Gram negative bacteria in the decreasing order 1>3>5>2, therefore they can be recommended for further applications in cell imaging in consistence with literature (Varma et al., 2020).

CONFLICT OF INTERESTS

The authors have not declared any conflict of interests.

ACKNOWLEDGEMENTS

The authors are grateful to Dr. Micheal P. Coogan for his helpful discussions during the course of this research. They also thank Prof. John A. Gladysz for providing facilities for a portion of these studies, and helpful discussions, while AAI visited his group at Texas A & M University, United States. They are grateful to late Professor Gabriel O. Egharevba, a profound Inorganic/Organometallic Chemist, who encouraged collaborative research, provided a ladder for many to climb up strongly. The US National Science Foundation (NSF, CHE 1153085) is thanked for supporting the portion of the research carried out at Texas A & M University.

REFERENCES

Adetoye AA, Egharevba GO, Obafemi CA, Kelly DR (2009). Synthesis and physicochemical properties of Co(II), Cu(II), Fe(III), Mn(II) and Ni(II) complexes of the isatin derivative of sulphanilamide. Toxicological & Environmental Chemistry 91(5):837-846.

Angelici RJ (1990). Inorganic Syntheses: Reagents for Transition Metal Complexes and Organometallic Syntheses. John Wiley &Sons, Inc. 28:160-163, (online version 2007).

Azzarelli N, Ponnala S, Aguirre A, Dampf S, Davis M, Ruggiero M, Lopez Diaz V, Babich J, Coogan M, Korter T, Doyle R, Zubieta J (2019). Defining the origins of multiple emission/excitation in rhenium-bisthiazole complexes. Inorganica Chimica Acta 489:301-309.

Cheesbrough M (2002). Biochemical tests to identify bacteria. In: Laboratory practice in tropical countries. Cheesbrough M (ed.). Cambridge Edition 2:63-87.

Chohan ZH, Shaikh AU, Naseer MM (2006). Metal-based isatin-bearing Sulfonamides: their synthesis, characterization and biological properties. Applied Organometallic Chemistry 20(11):729-739.

Clinical and Laboratory Standards Institute (CLSI) (2016). Methods for antimicrobial dilution and disk susceptibility testing of infrequently isolated or fastidious bacteria. 3rd Ed. CLSI guideline M45-A3. Clinical and Laboratory Standards Institute. Wayne, Pennslvania.

Coogan MP, Fernandez-Moreira V, Hess JB, Pope SJA, Williams C (2009). Rhenium fac-tricarbonyl bisimine complexes: luminescence modulation by hdrophobically driven intermolecular interactions. New Journal of Chemistry 33(5):1094-1099.

Ding Z, Zhou M, Zeng C (2020). Recent advances in isatin hybrids as potential anticancer agents. Archiv der Pharmazie 353(3):e1900367.

Egharevba GO, Megnamisi-Belombe M, Endres H, Rossato E (1982). Hexaaquacobalt(II)Bis[dibromobis(ethanedialdioxamato)cobaltate(III)] Acetone solvate. Acta Crystallographica B38(11):2901-2903.

Emeruwa KC (1982). Antimicrobial substances from Cacaya papaya fruit extracts. Journal of Natural Products 45(2):123-127.

Guo H (2019). Isatin derivatives and their anti-bacterial activities. European Journal of Medicinal Chemistry 15(164):678-688.

Ikotun AA, Coogan MP, Owoseni AA, Egharevba GO (2019a). Design, synthesis, physicochemical and antimicrobial properties of rhenium(I) tricarbonyl complexes of 3-(phenylimino)indole-2-one. Journal of Chemical Society of Nigeria 44(5):948-958.

Ikotun AA, Oladimeji AO, Oluranti OO (2019b). Synthesis, Physicochemical and Antimicrobial Properties of Co(II) and Ni(II) metal complexes of the Schiff base of isatin and 4-methylaniline. Journal of Applied Sciences and Environmental Management 23(11):1957-1962.

Mogana R, Adhikari A, Tzar MN, Ramliza R, Wiart C (2020). Antibacterial activities of the extracts, fractions and isolated compounds from *Canarium patentinervium* Miq. against bacterial clinical isolates. BMC Complimentary Medicine and Therapies 20(1):55-65.

Mostafa AA, Al-Askar, AA, Almaary, KS, Dawoud TM, Sholkamy EN, Bakri MM (2018). Antimicrobial activity of some plant extracts against bacteria strains causing food poisoning diseases. Saudi Journal of Biological Sciences 25(2):361-366.

Owoseni AA, Sangoyomi TE (2014). Effect of solvent extracts of some plants on *Ralstonia solanacearum*. British Microbiology Research Journal 4(1):85-92.

Premanathan M, Radhakrishnan S, Kulangiappar K, Singaravelu G, Thirumalaiarasu V, Sivakumar T, Kathiresan K (2012). Antioxidant & anticancer activities of isatin (1H-indole-2,3-dione), isolated from the flowers of Couroupita guianensis Aubl. Indian Journal of Medical Research 136(5):822-826.

Scherer A (2009). Ph.D Thesis, Friedrich-Alexander Universität, Erlangen-Nürnberg, Germany.

Sriam D, Bal TR, Yogeeswari P (2005). Newer aminopyrimidimino isatin abalogues as non-nucleoside HIV-1 reverse transcriptase inhibitors for HIV and other opportunistic infections of AIDS: design, synthesis and biological evaluation. Il Farmaco 60(5):377-384.

Sridhar SK, Pandeya SN, Stables JP, Ramesh A (2002). Anticonvulsant activity of hydrazones, Schiff and Mannich bases of isatin derivatives. European Journal of Pharmaceutical Sciences 16(3):129-132.

Sutton D (1968). Electronic Spectra of Transition Metal Complexes, McGRAW-HILL, London.

Varma RR, Pursuwani BH, Suresh E, Bhatt BS, Patel MN (2020). Single crystal, DNA interraction and cytotoxicity studies of rhenium (I) organometallic compounds. Journal of Molecular Structure 1200:127068.

Vol. 20(5), pp.186-193, May, 2021
DOI: 10.5897/AJB2020.17282
Article Number: 3C8C9D966746
ISSN: 1684-5315

http://www.academicjournals.org/AJB

ACADEMIC JOURNALS
expand your knowledge

African Journal of Biotechnology

Full Length Research Paper

Production of truncated peptide (cellobiohydrolase Cel6A) by *Trichoderma reesei* expressed in *Escherichia coli*

Miriam Shirley Tellez Calzada, Juan Antonio Rojas Contreras, Jesus Bernardo Paez Lerma, Nicolas Oscar Soto Cruz and Javier López Miranda*

Chemical and Biochemical Engineering Departament, Tecnológico Nacional de México (TecNM), Instituto Tecnológico de Durango (ITD), C.P. 34080, Durango, Dgo., Mexico.

Received 23 November 2020; Accepted 23 April 2021

Enzymatic cellulose hydrolysis is an important step for the production of second-generation biofuels. The filamentous fungus *Trichoderma reesei* is among the most important organisms for obtaining cellulolytic enzymes. The Cel6A (CBH II) cellulase from *T. ressei* plays an important role in cellulose hydrolysis and acts on the non-reducing end of cellulose, in contrast to Cel7B (CBH I), which acts on the reducing end of cellulose thus releasing cellobiose. Therefore, Cel6A deficiency becomes a limiting factor in cellulose saccharification. This work attempted to use codon optimization to enhance Cel6A expression in *Escherichia coli*. A plasmid expression vector, pUCITD04, was designed; this vector contains: the *cel6a* gene, regulatory regions (the promoter and terminator T7 sequences), the OmpT signal peptide that allows the secretion of proteins into the culture medium, and a 6His tail to allow purification of the protein by affinity chromatography. The protein expression experiment using a strain of *E. coli* transformed with pUCITD04 resulted in a 31 kDa polypeptide being secreted into the culture medium that did not possess enzymatic activity, meanwhile, the control strain transformed with the empty plasmid did not secrete any protein fragments, indicating that a truncated Cel6A was being produced by the experimental strain. This phenomenon has been reported during the production of recombinant cellulases in *E. coli.* In this research, we discuss probable causes of this phenomenon, as well as the drawbacks in the production of cellulases by *E. coli,* directing efforts to elucidate the causes of the production of truncated cellulases by this bacterial factory.

Key words: Gene construct, recombinant cellobiohydrolase, *Escherichia coli*.

INTRODUCTION

Lignocellulose materials are mainly composed of cellulose, hemicellulose, and lignin. Cellulose and hemicellulose are sugar-rich fractions of interest for use in fermentation processes, as many microorganisms can

*Corresponding author. E-mail: jlopez@itdurango.edu.mx. Tel: +526181174768.

use these sugars for growth and the production of various compounds, such as ethanol, food additives, organic acids, enzymes, pigments, and drugs (Robak and Balcerek, 2020). Cellulose is the most important glucose reservoir in the world; however, its industrial utilization is limited by its polymerization degree and crystallinity index, as well as its association with hemicellulose and lignin polymers. Particularly, the recalcitrant lignin compound can reduce the efficacy of lignocellulosic feedstocks. To resolve these limit, it is necessary to subject these materials to pre-treatment procedures (Zoghlami and Paës, 2019; Meneses et al., 2020).

The hydrolysis of cellulose may be achieved via chemical or enzymatic procedures. Specifically, the enzymatic procedure requires a consortium of cellulolytic enzymes, including endoglucanases, cellobiohydrolases, and ß-glucosidases (Østby et al., 2020). This consortium is produced by numerous microbial groups, with *Trichoderma reesei* highlighted as a principal producer of cellulolytic enzymes (Runajak et al., 2020). These enzymes are key to developing a viable biorefinery process, which requires the cost-effective production of fermentable sugars from lignocellulosic biomass. Supplementing these various enzymes to optimize the ratio of cellulase components in the enzyme cocktail is an important strategy to obtaining an efficient cellulose hydrolysis; however, implementing this strategy, requires obtaining sufficient amounts of individual cellulase proteins (Fubao et al., 2016). Due to this requirement, research efforts have been oriented towards the development of recombinant procedures such as recombinant enzyme production, particularly recombinant enzymes expressed on prokaryotic systems, such as *Escherichia coli*, as this is the most widely used host and presents rapid and elevated expression levels (Parisutham and Sung, 2012; Rosano and Ceccarelli, 2014; Demain and Vaishnav, 2016). This recombinant system has been widely demonstrated to be useful for expressing non-glycosylated proteins; additionally, the machinery that performs the transcription, translation, and protein folding of this system is known (Wruck et al., 2017). Moreover, the genome can be easily modified, the promoter control is not complex, and the number of plasmids copies can easily be altered (Virolle et al., 2020). This system is able to accumulate up to 80% of its dry weight in recombinant proteins and survive at various environmental conditions (Demain and Vaishnav, 2016; Kent and Dixon, 2019). However, heterologous proteins, which are frequently expressed intracellularly in *Escherichia coli*, require an expensive separation process that includes cell lysis and target protein purification (Zhou et al., 2018). On the other hand, overexpressed proteins often form inclusion bodies or aggregates in the cytoplasmic space, thus requiring complicated and costly pretreating processes to obtain biologically active proteins and resulting in low active protein yields (Choi et al., 2006; Cui et al., 2016; King-Batsios et al., 2018). The likelihood of incorrect folding increases with the routine uses of strong promoters and elevated inducer concentrations, which can result in product yields that exceed 50% of the total cell proteins (Sandomenico et al., 2020). One solution to this problem may be the extracellular production of heterologous proteins, which, in most cases, facilitates further processing as well as provides *in vivo* folding and stability, thus allowing the production of soluble and biologically active proteins at a reduced cost (Mergulhao et al., 2005; Clark and Pazdernik, 2016). Although transfer of proteins to the periplasm is an approach used to facilitate the recovery of recombinant proteins, this method can also increase the rate of protein degradation and the accumulation of secretion precursors, which induces the heat-shock stress response and leads to increased proteolysis (Sandomenico et al., 2020). Full knowledge of the target protein enables the choice of an appropriate method of protein production and facilitates the design of the signal peptide needed to transfer the protein to the periplasmic space (Kleiner-Grote et al., 2018). Given the aforementioned, the aim of this work was to demonstrate that the expression of an optimized gene codifying the production of cellobiohydrolase Cel6A recombinant enzyme results in protein production and transfer to the periplasm.

MATERIALS AND METHODS

Bacterial strains, plasmids, and growing conditions

The *E. coli* strains Top10F´ and BL21 (DE3) were acquired from Invitrogen and Novagen, respectively, while the pUCITD04 expression vector was derived from a pUCIDT cloning plasmid engineered to express the codon optimized *cel6a* gene from *T. ressei*, AmpR (Table 1). Luria-Bertani culture medium was used to spread the strains, while M9 culture medium was used in the recombinant protein production assays (Miller, 1972). The cells were cultured in a liquid medium with vigorous agitation at a temperature of 37°C while cell growth was monitored via measurements of the absorbance at 600 nm. The recombinant strains were selected via the addition of 50 mg/mL kanamycin, sold by SIGMA-ALDRICH.

Design of the gene encoding the synthesis of β-cellobiohydrolase Cel6A

The gene used to encode the synthesis of the recombinant Cel6A was designed using the sequence encoding the synthesis of *T. reesei* Cel6A (XM 006962518.1) as a target; this sequence was obtained from the NCBI database and was optimized for its recognition by *E. coli*. The designed synthetic construct contains the T7 promoter, a lac operating region, a ribosome binding site, an OmpT signal peptide, the optimized coding sequence of *T. reesei* Cel6A, six codons for 6His tail synthesis, and the T7 transcriptional terminator. This construct was synthetized by Integrated DNA Technologies (IDT) Inc.

Table 1. Relevant strains and plasmids utilized in the current study.

Strain/plasmid	Genotype: Relevant characteristics	Source
***E. coli* Strains**		
E. coli Top10F'	F'[lacIq Tn10(tetR)] mcrA Δ(mrr-hsdRMS-mcrBC) φ80lacZΔM15 ΔlacX74 deoR nupG recA1 araD139 Δ(ara-leu)7697 galU galK rpsL(StrR) endA1 λ-	Invitrogen
E. coli BL21 (DE3)	*E. coli* str. B F– ompT gal dcm lon hsdSB(rB–mB–) λ(DE3 [lacI lacUV5-T7p07 ind1 sam7 nin5]) [malB+]K-12(λS)	Novagen
Plasmid		
pUCITD04	Expression vector derivative of pUCIDT cloning plasmid, expressing the codon optimized Cel6A gene from *T. ressei*, AmpR.	This study

Native and synthetic β-cellobiohydrolase Cel6A structure

Three-dimensional structures of the native and synthetic Cel6A enzymes were constructed using Raptor X structures tool (Morten et al., 2012) and visualized with Discovery Studio software (Dassault, 2017).

Cloning of synthetic cellobiohydrolase cel6a gene and transformation of E. coli

The construct was cloned in the pUCIDT KanR plasmid by the Integrated DNA Technologies company (IDT). This plasmid was named pUCITD04. The synthetic plasmid contains the *Bam*HI and *Hind*III restriction sites for gene subcloning. This sequence was verified by the Synthesis and Sequencing Unit of the Biotechnology Institute of Autonomous National University of Mexico (UNAM). Insertion of the *cel6a* gene in the pUCITD04 plasmid was verified by restriction analysis using *Bam*HI and *Hin*dIII endonucleases and electrophoresis on agarose gel stained with EtBr.

Molecular biology techniques

Preparation of $CaCl_2$ competent cells, transformation tests, and plasmidic DNA extraction from *E. coli* were performed using the Sambrook techniques (Sambrook and Green, 2012). The *E. coli* BL21 (DE3) strain transformed with the pUCITD04 plasmid was used to produce the recombinant protein. Insertion of the plasmid with the synthetic *cel6a* gene in the *E. coli* BL21DE3 strain was verified by extraction of plasmidic DNA from the transformed strain and subsequent restriction analysis with *Bam*HI and *Hind*III enzymes. The transformed strain was inoculated on 50 mL of M9 culture medium supplemented with kanamycin and incubated at 37°C for the time necessary to reach an optical density (OD600) of 0.5.

SDS-PAGE analysis

The production of recombinant Cel6A enzyme was induced via the addition of 0.2 mM isopropyl-β-D-thiogalactopyranoside (IPTG) and the samples were incubated for 4 h at 37°C. During the incubation, a 1 mL sample was taken every 30 min and centrifuged, after which the supernatant was used to obtain protein via precipitation with a methanol:chloroform:water solution in a 4:1:3 V/V ratio. The precipitated proteins were resuspended in 100 µL of phosphate-buffer solution and 10 µL of the sample was analyzed by SDS-PAGE, applying a voltage of 100 V for 90 min.

Enzymatic activity determination

To determine enzymatic activity, 250 µL of enzyme extract was incubated with 750 µL of 0.1 M acetate buffer (pH 4.8) and 1% microgranular cellulose (as a substrate) for 1 h at 50°C (Montoya et al., 2015). Next, the samples were centrifuged for 5 min at 13,000 RPM, after which 500 µL of the supernatant was taken and the reducing sugars were determined via the DNS method (Miller, 1959).

RESULTS AND DISCUSSION

Design of cel6a gene

The sequence encoding synthesis of the enzyme Cel6A (XM 006962518.1) that is produced by *T. reesei* was obtained from the NCBI database and then optimized to be recognized and synthesized by *E. coli*. This protein (Figure 1) has a length of 471 amino acids, a homology of 100% with respect to the Cel6A protein, and a homology of 74% with respect to the gene sequence encoding the synthesis of Cel6A that is produced by *T. reseei*.

Modeling of native and synthetic structures of β-cellobiohydrolase Cel6A

According to Raptor X portal, the protein structures of the cellulose-binding domains (Figure 2) demonstrate minor differences due to the signal peptide added to the *cel6a* synthetic gene (Figure 2A) being slightly longer than the signal peptide of native Cel6A (Figure 2B). The catalytic domains of the native and synthetic Cel6A (Figures 3A and 3B) do not show any visual differences between their tertiary structures. The cellulose-binding domain is located between amino acids Methionine-1 and Glycine-

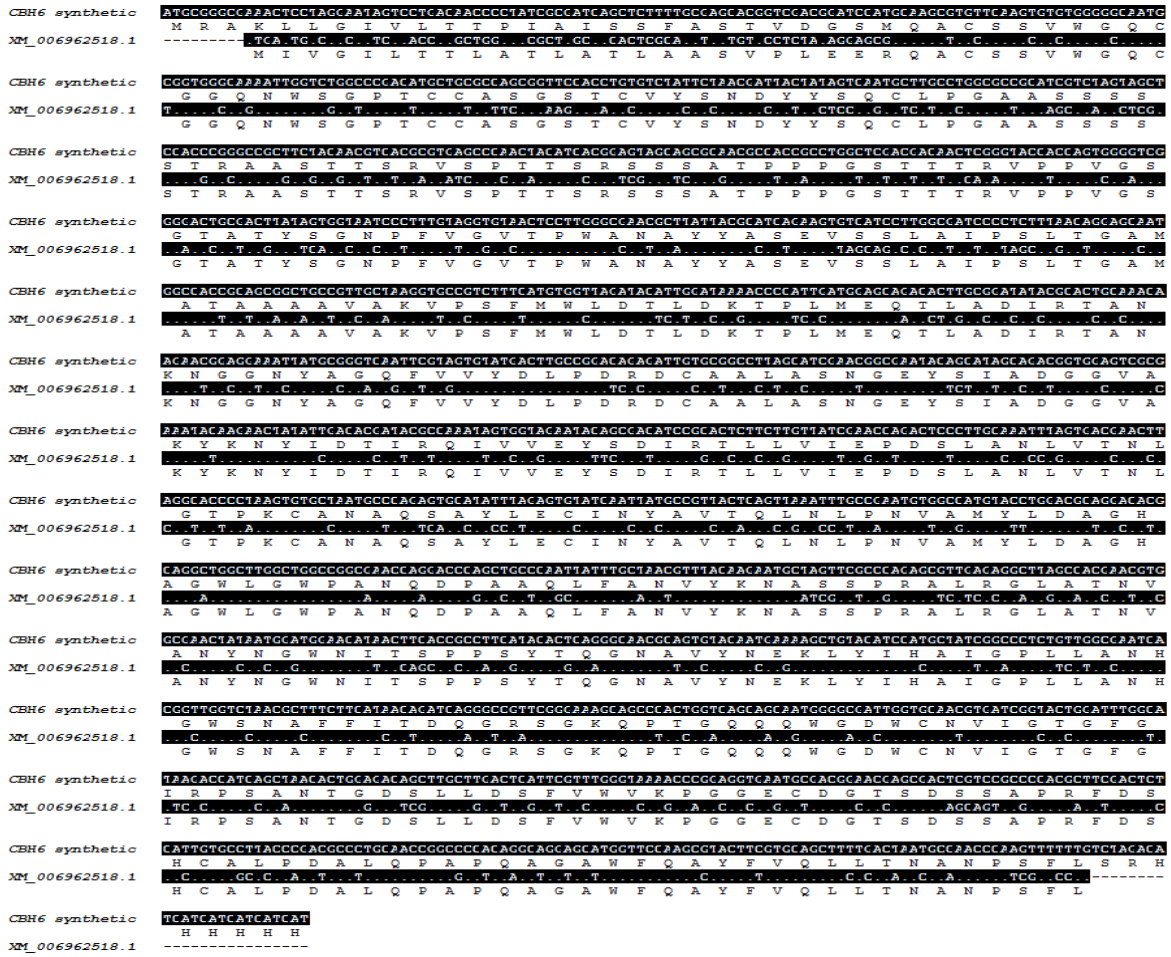

Figure 1. Alignment of the synthetic Cel6A sequence and the XM_006962518.1 sequence corresponding to the *Trichoderma ressei* native Cel6A. The nucleotides of both sequences are highlighted by a black shadow, identical nucleotides between both sequences are shown with dots, the OmpT signal peptide added to the synthetic sequence is framed with a solid line box, and the signal peptide of the native Cel6A from *T. ressei* is framed with a discontinuous line box, while the gaps (dashed lines) present at the beginning and ends of the amino acid sequences represent non-aligned sequences

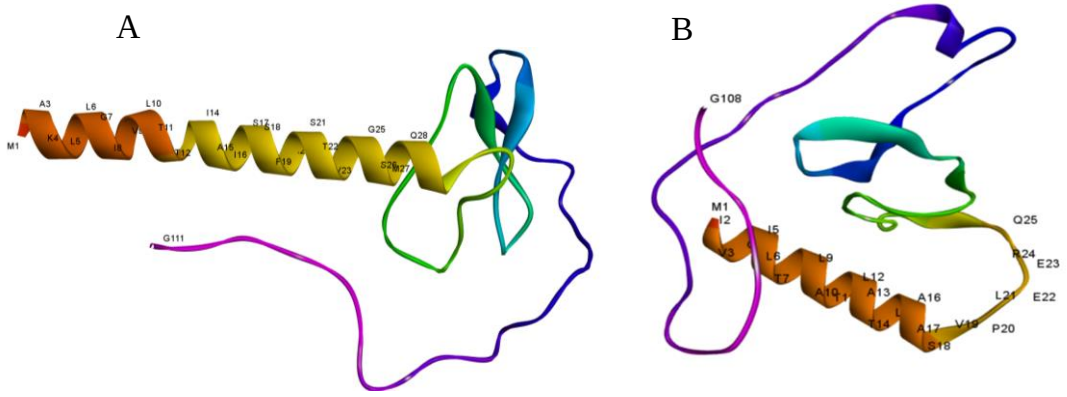

Figure 2. Comparison of the cellulose binding domain (CBD) of the native (A) and synthetic (B) Cel6A enzymes. The CBDs of both enzymes are between the amino acids Methionine-1 and Glycine-108.

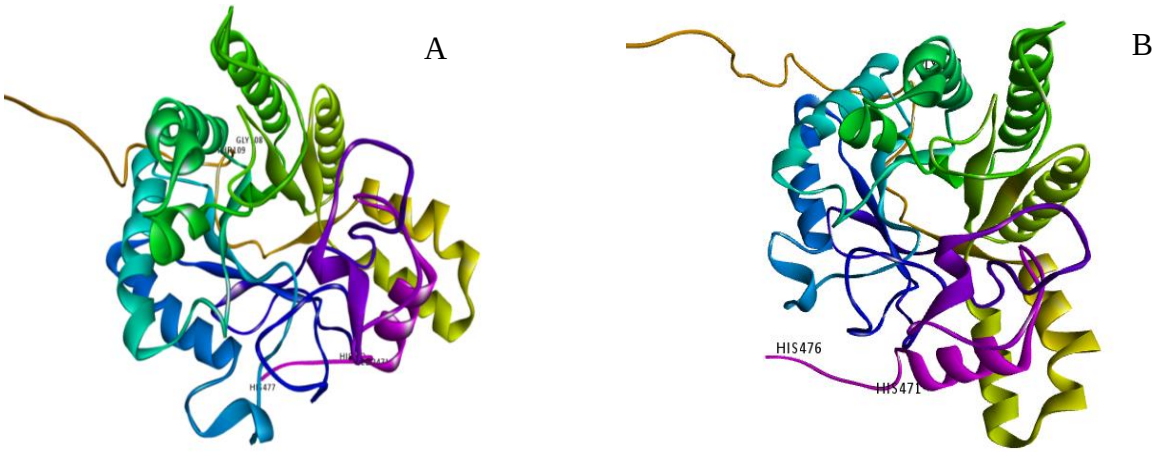

Figure 3. Comparison of the catalytic domain (CD) of the native (A) and synthetic (B) Cel6A enzymes. The CDs of the native and synthetic Cel6A enzymes are between the amino acids Threonine-109 and Leucine-471.

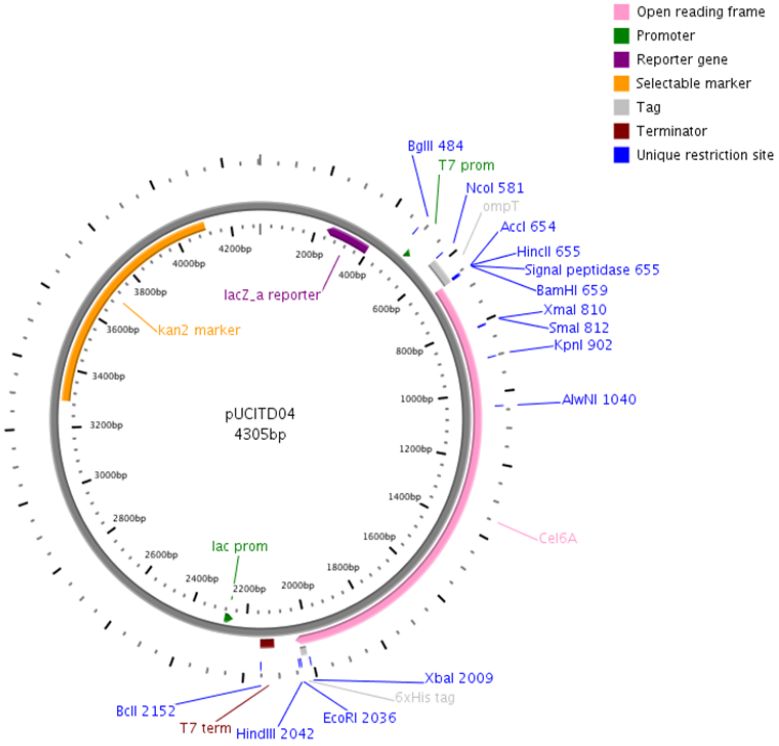

Figure 4. pUCITD04 plasmid map, showing the positions of the *cel6a* gene, the T7 promoter and T7 terminator regulatory zones, the OmpT signal peptide, the 6His tag, and the kanamycin marker.

108, while the catalytic domain is located between Threonine-109 and Leucine-471. The native protein has a molecular weight of approximately 50 kDa and is composed of 471 amino acids, while the synthetic protein has a molecular weight of 50.5 kDa and is composed of 477 amino acids.

The differences between native and recombinant enzymes are attributed to the addition of the six-histidine tail. The designed plasmid, pUCITD04, was utilized as a vector for the production of Cel6A recombinant enzyme in the *E. coli* BL21 (DE3) strain (Figure 4). Plasmid DNA extracted from transformed *E. coli* BL21 (DE3) cells

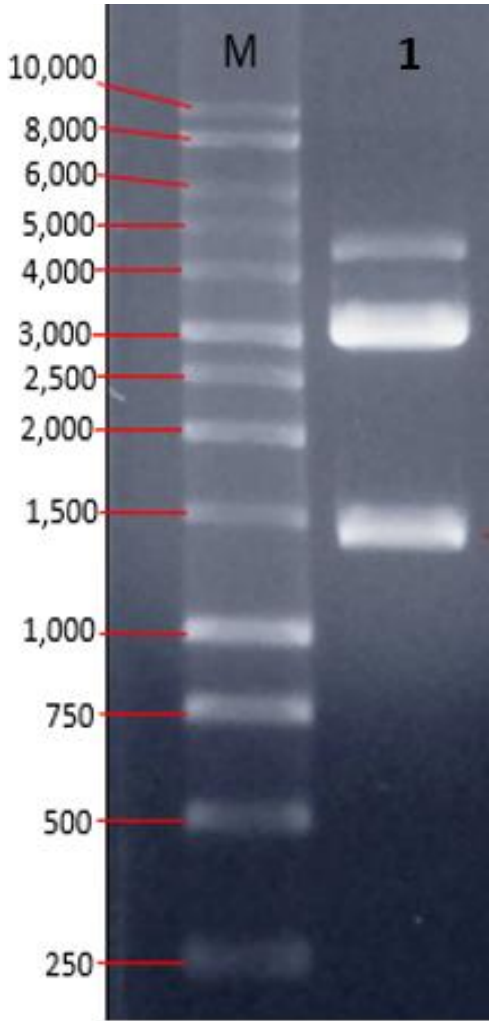

Figure 5. Restriction assay of the pUCITD04 plasmid. Lane M: DNA ladder (1Kb); Lane 1: restriction products from pUCITD04 hydrolysis with *Bam*HI and *Hind*III enzymes. The restriction mixture samples were electrophoresed on a 1% agarose gel and stained with ethidium bromide.

resistant to kanamycin was subjected to a restriction analysis using hydrolysis with *Bam*HI and *Hin*dIII enzymes. Results of the restriction analysis showed that the 2705 bp pUCITD04 plasmid contained a 1446 bp fragment, which corresponds to the cel6a synthetic gene (Figure 5), indicating that the synthesized gene and plasmid were adequately constructed.

The designed and constructed plasmid contains the *cel6a* gene flanked by *Bam*HI and *Hind*III restriction enzyme sites, T7 promoter and T7 terminator regulatory regions, the OmpT signal peptide necessary for protein secretion into the culture medium, and a 6His Tag introduced to favour the purification of the enzyme via affinity chromatography (Freudl, 2018).

Expression and secretion of synthetic CBH Cel6A enzymes

Results from the expression and secretion of the natural and synthetic Cel6A enzymes show that synthetic Cel6A protein was not found in the cell extract. However, when using M9 culture medium with isopropyl-β-D-1-thiogalactopyranoside (IPTG) added as an inducer, results showed that the transformed BL21DE3 strain produced a 31 kDa peptide (Figure 6) that the native strain did not produce. The phenomenon of expression of truncated cellulases has been reported during protein production by recombinant *E. coli* cells (Liu et al., 2018), with prior observations indicating that periplasmic Cel6A is prone to proteolytic truncation in LK111 and K514 *E. coli* strains. The fractions obtained in ion-exchange columns were analyzed by zymogram analysis resulting in two carboxymethyl cellulase (CMScase) bands at 57 and 47 kDa. The larger of these bands corresponds to the full portion of the Cel6A protein, while the smaller band corresponds with proteolytic cleavage near the linker. In other research, an additional truncated CD with higher specific activity on soluble substrates was discovered, however, this enzyme was also found to be prone to proteolytic cleavage (Nakamura et al., 2020). *E. coli* BL21 (DE3) lacks the OmpT signal peptide and Lon proteases and produces large quantities of biomass with important effects on the production of recombinant proteins. While *E. coli* BL21 (DE3) is a genetically modified strain laking the Lon and OmpT proteases (Table 1), it may nonetheless contain low quantities of other proteases, such as DegP, Plp, HtrA, and ClpB, which degraded aggregated protein and, consequently, may impede Cel6A production (Gottesman, 1996; Laskowska et al., 1996; Langen et al., 2001; Jiang et al., 2002).

Protein expression using *E. coli* is the procedure most frequently used in bacterial expression as it is a well characterized procedure that is easy to genetically manipulate. However, the expression of cellulases in *E. coli* has encountered numerous problems, such as degradation of linker sequences in multi-domain cellulases, the formation of inclusion bodies, incorrect transportation across the outer membrane, and decreased specific activity of the cellulases (Choi et al., 2006). In contrast, the protein over-production system in *E. coli*, which is attributed to the RNA polymerase expression system of bacteriophage T7, is limited or incorrectly expressed in the BL21 (DE3) strain. The incorrect expression of Cel6A may be attributed to a toxicity problem caused by the pUCITD04 plasmid (Miroux and Walker, 1996). In our laboratory, the ß-glucosidase, endoglucanase, and xylose reductase

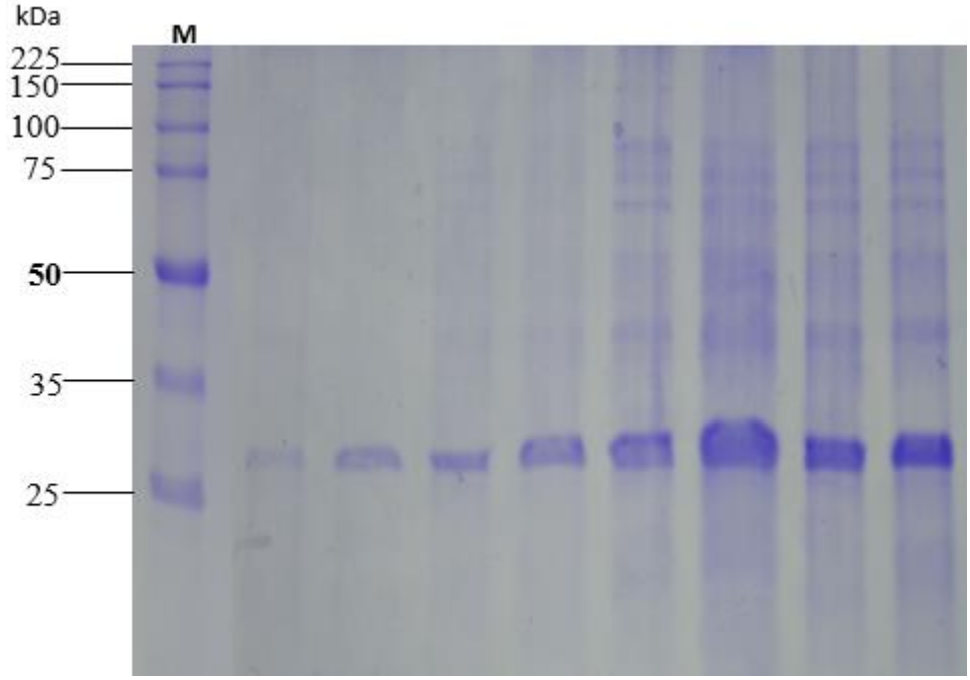

Figure 6. SDS-PAGE analysis of protein secreted into the culture medium by E. coli BL21 (DE3) transformed with the pUCITD04 plasmid. Lane M: molecular marker; lanes 1 to 8: secreted protein in samples taken at 30 min intervals. The secreted proteins were precipitated.

enzymes were expressed using similar conditions that the used for Cel6A recombinant enzyme, however, this protein is structurally more complex, and probably this is the reason that makes it difficult to produce. However, it has been observed that proteolytic cleavage between catalytic and cellulose-binding domains of some ß-glucanases occurs near the linker, and many modular-type-ß-glucanases contain two conserved cysteine residues near their cellulose-binding domains (Kont et al., 2016; Nakamura et al., 2020). The results observed suggest the possibility of exploring several alternatives, including the use of different carbon sources and galactose inducers to produce recombinant Cel6A, experimenting with new microbial vectors to achieve production of Cel6A recombinant enzyme, or production in a cell-free system to reduce complications relating to plasmid toxicity (Kigawa et al., 2004; Robak and Balcerek, 2020).

Conclusion

The vector pUCITD04 does not allow the production of Cel6A enzyme in the BL21 (DE3) *E. coli* strain; however, it does produce a 31 kDa periplasmic polypeptide that must belong to a fraction of Cel6A, although it lacks catalytic and cellulose-binding domains. Results demonstrate the necessity of exploring the use of new microbial vectors. Additionally, to prevent possible plasmid toxicity, it is important to investigate the use of cell-free systems to bypass potential residual proteolytic activity and the complications related to it.

CONFLICT OF INTERESTS

The authors have not declared any conflict of interests.

ACKNOWLEDGEMENT

This research work was performed utilizing the funding of Science and Technology Council of Durango Mexico State (COCYTED) by the project entitled “Design, expression and biochemical characterization of Cellobiohydrolase Cel6A recombinant enzyme”.

REFERENCES

Choi J, Chang KK, Lee S (2006). Production of recombinant proteins by high cell density culture of *Escherichia coli*. Chemical Engineering Science 61(3):876-885.

Clark PD, Nanette JP (2016). Chapter 10 - Recombinant Proteins, Editor(s): David P. Clark, Nanette J. Pazdernik, Biotechnology

(Second Edition), Academic Cell pp. 335-363, ISBN 9780123850157, https://doi.org/10.1016/B978-0-12-385015-7.00010-7.
Cui Y, Meng Y, Zhang J, Cheng B, Yin H, Gao C, Xu P, Yang C (2016). Efficient secretory expression of recombinant proteins in *Escherichia coli* with a novel actinomycete signal peptide. Protein Expression and Purification 129:69-74.
Dassault S (2017). BIOVIA, Discovery Studio**.** Modeling Environment, Release 2017. San Diego: Dassault Systèmes 2016.
Demain A, Vaishnav P (2016). Production of Recombinant Enzymes. Reference Module in Food Science, Elsevier: Doi.org/10.1016/B978-0-08-100596-5.03023-7.
Freudl R (2018). Signal peptides for recombinant protein secretion in bacterial expression systems. Microbial Cell Factories 17(1):52. https://doi.org/10.1186/s12934-018-0901-3
Fubao FS, Xiaoqin Z, Jiapeng H, Yanjun T, Liang W, Haiyan S, Xiang L, Jinguang H (2016). Industrially relevant hydrolyzability and fermentability of sugarcane bagasse improved effectively by glycerol organosolv pretreatment. Biotechnology for Biofuels 9:59 DOI 10.1186/s13068-016-0472-7.
Gottesman S (1996). Proteases and their targets in Escherichia coli. Annual Review of Genetics 30:465-506. https://doi.org/10.1146/annurev.genet.30.1.465
Jiang X, Oohira K, Iwasaki Y, Nakano H, Ichihara S, Yamane T (2002). Reduction of protein degradation by use of protease-deficient mutants in cell-free protein synthesis system of *Escherichia coli*. Journal of Bioscience and Bioengineering 93(2):151-156. doi: 10.1263/jbb.93.151. PMID: 16233180
Kent R, Dixon N (2019). Contemporary Tools for Regulating Gene Expression in Bacteria. Trends in Biotechnology 38(3):316-333. doi.org/10.1016/j.tibtech.2019.09.007
Kigawa T, Yakubi T, Matsuda N, Nakajima R, Tanaka A and Yokoyama S (2004). Preparation of *Escherichia coli* cell extract for highly productive cell-free protein expression. Journal of Structural and Functional Genomics 5:63-68. doi: 10.1023/B:JSFG.0000029204.57846.7d
King-Batsios E, Pujol-García A, Tamargo-Santos B, Marrero-Trujillo G, Fontanies-Hernández M, Blain-Torres K and Sierra-González V (2018). Influencia del medio de cultivo sobre la cinética de crecimiento y expresión de la proteína recombinante Rv2626c de Mycobacterium tuberculosis H37Rv expresada en Streptomyces lividans TK24. Vaccimonitor 27(3):84-92.
Kleiner-Grote GRM, Risse JM, Friehs K (2018). Secretion of recombinant proteins from *E. coli*. Engineering in Life Sciences 18:532-550.
Kont R, Kari J, Borch K, Westh P, Väljamäe P (2016). Inter-domain Synergism Is Required for Efficient Feeding of Cellulose Chain into Active Site of Cellobiohydrolase Cel7A. Journal of Biological Chemistry 291(50):26013-26023.
Langen GR, Harper JR, Silhavy TJ, Howard SP (2001). Absence of the outer membrane phospholipase A suppresses the temperature-sensitive phenotype of Escherichia coli degP mutants and induces the Cpx and sigma(E) extracytoplasmic stress responses. Journal of Bacteriology 183(18):5230-5238. doi:10.1128/jb.183.18.5230-5238.2001
Liu Y, Liu S, Dong S, Li R, Feng, Cui Q (2018). Determination of the native features of the exoglucanase Cel48S from *Clostridium thermocellum*. Biotechnology for Biofuels 11(6).
Meneses D, Montes de Oca-VG, Vega BJ, Rojas-Álvarez M, Corrales-Castillo J, Murillo-Araya L (2020). Pretreatment methods of lignocellulosic wastes into value-added products: recent advances and possibilities. Biomass Conversion and Biorefinery. Doi.org/10.1007/s13399-020-00722-0
Mergulhao F, Summers D, Monteiro G (2005). Recombinant protein secretion in Escherichia coli. Biotechnology Advances 23(3):177-202. https://doi.org/10.1016/j.biotechadv.2004.11.003
Miller GL (1959). Use of Dinitrosalicylic acid reagent for determination of reducing sugar. Analytical Chemistry 31(3):426-428.
Miller JH (1972). Experiments in molecular genetics. Cold Spring Harbor Laboratory Press, Cold Spring Harbor, NY.
Miroux B, Walker J (1996). Over-production of proteins in Escherichia coli: mutant hosts that allow synthesis of some membrane proteins and globular proteins at high levels. Journal of Molecular Biology 260(3):289-298.
Montoya S, Sánchez J, Levin L (2015). Production of lignocellulolytic enzymes from three white-rot fungi by solid-state fermentation and mathematical modeling. African Journal of Biotechnology 14(15):1304-1317.
Morten K, Haipeng W, Sheng, Jian P, Zhiyong W, Hui L, Jinbo X (2012) Template-based protein structure modeling using the RaptorX web server. Nature Protocols 7(8):1511-1522. doi: 10.1038/nprot.2012.085.
Nakamura A, Ishiwata D, Visootsat A, Uchiyama T, Mizutani K, Kaneko S, Murata T, Igarashi K, Iino R (2020). Domain architecture divergence leads to functionaldivergence in binding and catalytic domains of bacterialand fungal cellobiohydrolases. Journal of Biological Chemistry 295(43):14606-14617. Doi.org/10.1074/jbc.RA120.014792
Østby H, Hansen LD, Horn SJ (2020). Enzymatic processing of lignocellulosic biomass: principles, recent advances and perspectives. Journal of Industrial Microbiology and Biotechnology 47(9-10):623-657.
Parisutham V, Sung KL (2012). Heterologous Expression and Extracellular Secretion of Cellulases in Recombinant Microbes. Bioethanol. Intechopen, London pp. 239-252.
Robak K, Balcerek M (2020). Current state-of-the-art in ethanol production from lignocellulosic feedstocks, Microbiological Research 240:226534. doi: https://doi.org/10.1016/j.micres.2020.126534
Rosano GL, Ceccarelli EA (2014) Recombinant protein expression in microbial systems. Frontiers in Microbiology 5:341. DOI:10.3389/fmicb.2014.00341
Runajak R, Santi C, Wawat R, Malinee S, Prapakorn T, Somkiat P (2020). Analysis of Microbial Consortia with High Cellulolytic Activities for Cassava Pulp Degradation. E3S Web of Conferences 141, 03005, doi: 10.1051/e3sconf/202014103005 RI²C 2019.
Sambrook J, Green M (2012). Molecular cloning: a laboratory manual. In Molecular cloning: a laboratory manual (pp. 1890-1890).ISBN 978-1-936113-41-5 (cloth) – ISBN 978-1-936113-42-2 (pbk.)
Sandomenico A, Sivaccumar JP, Ruvo M (2020). Evolution of Escherichia coli expression system in producing antibody recombinant fragments, International Journal of Molecular Sciences 21(17):6324. DOI: 10.3390/ijms21176324
Virolle C, Goldlust K, Djermount S, Bigot S, Lasterlin C (2020). Plasmid Transfer by Conjugation in Gram-Negative Bacteria: From the Cellular to the Community Level. Genes 11(11):1239.
Wruck F, Katranidis A, Nierhaus K, Büldt G, Hegner M (2017). Translation and folding of single proteins in real time. Proceedings of the National Academy of Sciences 114(22):E4399-E4407.
Zhou Y, Lu Z, Wang X, Selvaraj J, Zhang G (2018). Genetic engineering modification and fermentation optimization for extracellular production of recombinant proteins using *Escherichia coli*. Applied Microbiology and Biotechnology 102(4):1545-1556.
Zoghlami A, Paës G (2019). Lignocellulosic Biomass: Understanding Recalcitrance and Predicting Hydrolysis. Frontiers in Chemistry 7(874):1-11.

Vol. 20(5), pp.194-201, May, 2021
DOI: 10.5897/AJB2021.17308
Article Number: 4BE8C8B66749
ISSN: 1684-5315

http://www.academicjournals.org/AJB

ACADEMIC JOURNALS
expand your knowledge

African Journal of Biotechnology

Full Length Research Paper

Quantification and characterization of faecal sludge produced in Kara

Piyabalo KODOM[1], Edem Komi KOLEDZI[2*], Nitale M'Balikine KROU[1], Kwamivi N. SEGBEAYA[1] and Bouwèdèo TOI BISSANG[1]

[1]Laboratory of Sanitation, Water Science and Environment (LASEE), Faculty of Science and Technology, University of Kara, P. O. BOX 404 Kara, Togo.
[2]Laboratory of Management, Treatment and valuation of Waste (GTVD), Department of Chemistry, University of Lomé, P. O. Box 1515 Lomé, Togo.

Received 8 January, 2021; Accepted 26 April, 2021

In Kara (Togo), as in most major sub-Saharan African cities, there is very little sewerage and autonomous systems are the most commonly used. These autonomous systems produce faecal sludge that must be drained and treated adequately in order to preserve the health of the population and protect the environment. Indeed, the risks are real, given the use of fresh faecal sludge in agriculture and the potential dangers of their raw rejection in nature. The purpose of this study was to quantify and characterize the faecal sludge derived from autonomous sanitation system and make available to the district of Kara. Sludge emptying trucks have been followed during a three months' period to quantify the faecal sludge produced. At the end, samples were taken to the laboratory for analysis. The chemical analysis conducted were suspended matter (SM), chemical oxygen demand (COD), a five-day biochemical oxygen demand (BOD_5), ammonium (NH_4^+), nitrates (NO_3^-), nitrites (NO_2^-) and orthophosphates (PO_4^{3-}). The result showed that 41347.2 m^3/year of faecal sludge are produced and 14616 m^3/year are collected. Also, the chemical analysis of total suspended solids, chemical oxygen demand, a five-day biochemical oxygen demand, ammonium, nitrates, nitrites and orthophosphates showed that the faecal sludge of the district of Kara is biodegradable. The data from this study will form scientific bases for a better feasibility of setting up a faecal sludge treatment plant in Kara.

Key words: Faecal sludge, specific ratio, quantity of faecal sludge, autonomous systems.

INTRODUCTION

Increasing urbanization is a phenomenon sweeping across the world especially in developing countries (Ahamada et al., 2016). This growth of population in urban areas in developing countries causes sanitation challenges for the urban authorities. The main challenges are related to the collection as well as treatment of excreta, solid waste and wastewater for the protection of human health and the environment (Tilley et al., 2010; Katukiza et al., 2012). The concern is serious, particularly in the area of sanitation as many African countries are

*Corresponding author. E-mail: edemledzi@yahoo.fr. Tel: 00228 90 19 85 35.

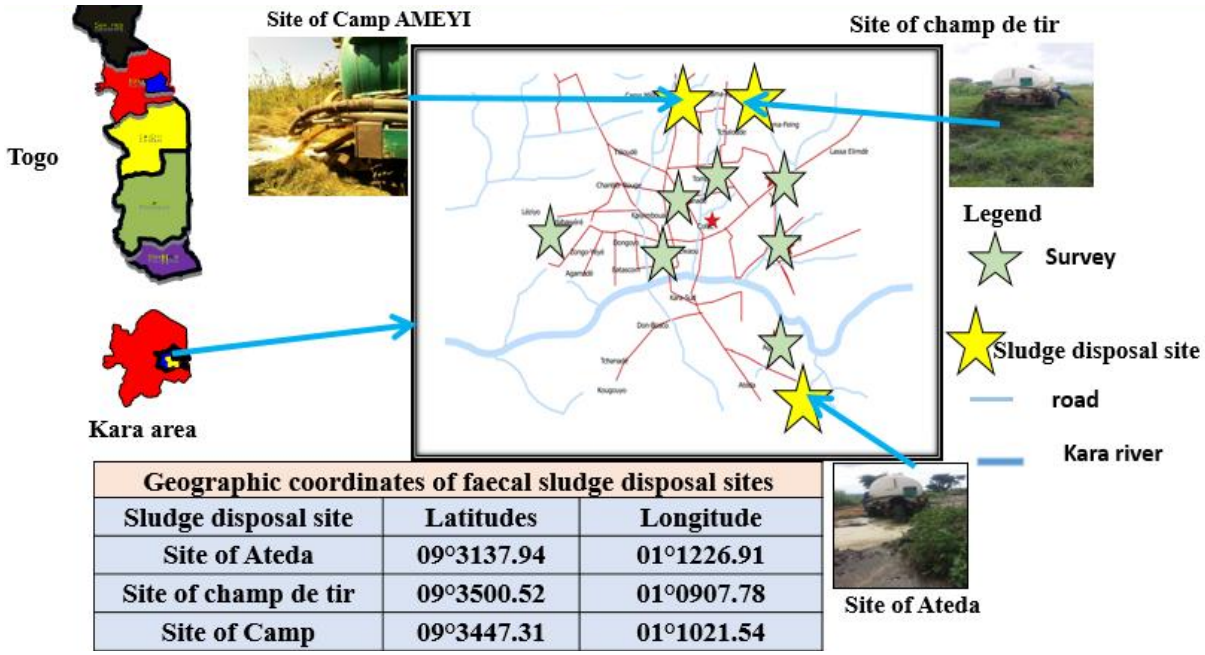

Geographic coordinates of faecal sludge disposal sites		
Sludge disposal site	Latitudes	Longitude
Site of Ateda	09°3137.94	01°1226.91
Site of champ de tir	09°3500.52	01°0907.78
Site of Camp	09°3447.31	01°1021.54

Figure 1. Study area.

unlikely to meet the Sustainable Development Goal (SDG) of halving the number of people without access to basic sanitation. The population of sub-Saharan African cities use autonomous sanitation (septic tanks) facilities for the management of wastewater and excreta (Bassan et al., 2013; Kajyibwami, 2018) which use self-sustaining wastewater treatment technology (Gnagne et al., 2019). This technology, although suitable for these cities, remains poorly implemented, suffering from the inadequacy of certain scientific database data (Gnagne et al., 2019). Usually, the sludge emptied in latrines and septic tanks is either dumped near the city or in the environment without treatment (Kouawa et al., 2015).

In Togo and most of the developing country, faecal sludge is openly dumped into the environment (Akpaki et al., 2016). These autonomous sanitations store large quantities of faecal sludge whose management is difficult (Ouédraogo, 2016). In Kara city, faecal sludge is emptied and most often dumped into the environment or reused without treatment in agriculture (Kodom, 2019). Some farmers are bribing septic tank truck drivers to dump faecal sludge into their field (Kodom, 2019). However, faecal sludge needs adequate treatment and disposal to safeguard public health and the environment (EAWAG, 2006). Recent studies in Sokodé (Togo) focused on economic potential show huge risks associated with sludge management in this city. However, there is limited or no information on the specific pollutant loads originating from the faecal sludge stream. Thus, the quantities of faecal sludge generated and the typical faecal sludge characteristics are difficult to determine due to the variety of onsite sanitation technologies in use, such as pit latrines, public tanks, septic tanks and dry latrines. The quantity and characteristic of faecal sludge also depends on the design and construction of the sanitation technology, how the technology is used, how the faecal sludge is collected and the frequency of collection. The objectives of this study are, therefore, to quantify and characterize the faecal sludge derived from autonomous sanitation system in district of Kara in order to propose an adequate treatment method. Decentralization has been effective in Togo since 2018; it is therefore up to each municipality to develop itself and development also takes into account issues related to sanitation and urban waste management. Moreover, autonomous sanitation is a credible choice for these districts for the decentralized treatment of faecal sludge waste in a very specific context. The results of this work will serve as scientific evidence to enable Kara Municipality authorities responsible for waste management to make informed decisions regarding municipal waste disposal and the establishment of a faecal sludge treatment plant.

MATERIALS AND METHODS

Study area

This study was carried out in the district of Kara located at 430 km from Lomé, the capital of Togo. The climate is of the Sudanese semi-humid tropical type, characterized by 2 distinct seasons: the dry and the rainy. The average annual temperature is around 37°C. Sludge is frequently dumped at the Atéda, AMEYI and shooting range sites located at 2, 3 and 4 km, respectively from the city of Kara where truck tracking and sampling were carried out (Figure 1).

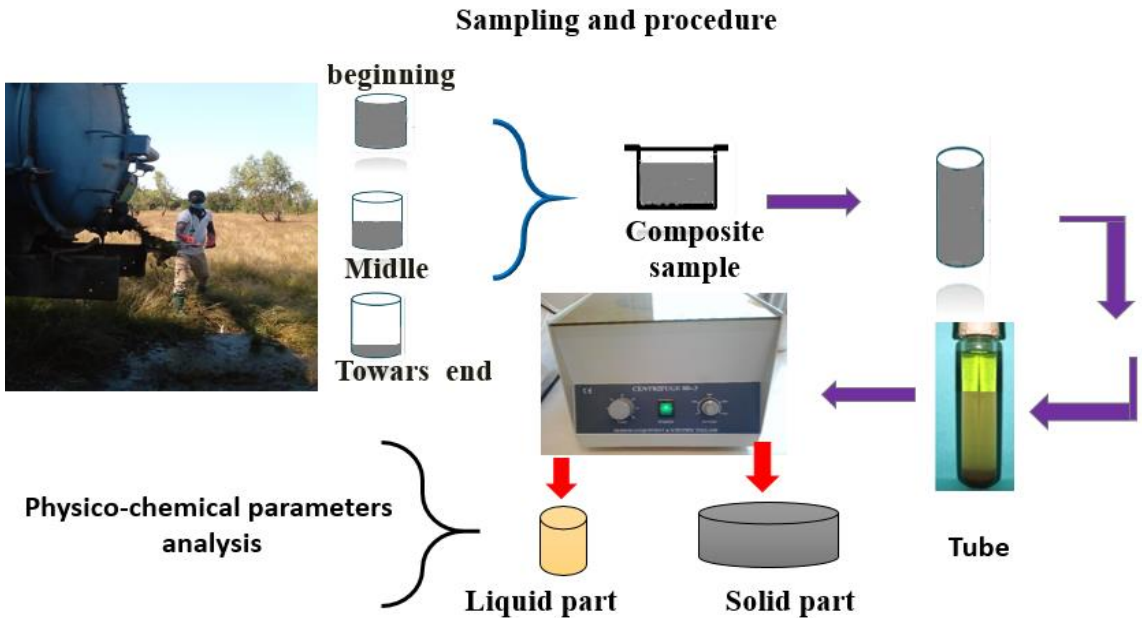

Figure 2. Sample methods and analyses.

Sludge samples are taken in a container at the start of unloading, when the tank is half empty and just before the end of unloading.

Surveys and observations

Field surveys use a questionnaire and observations made it possible knowing the existing emptying methods, the types of pits used, the emptying frequencies, the number of users, the number of trucks and the landfills.

Quantification methods of faecal sludge

In this study, two approaches were used to quantify faecal sludge. These methods were sludge production and sludge collection.

Method 1: Sludge collection

The study was conducted from June 24, 2020 to September 25th, 2020. During this period, the number of laps made and the quantity of sludge emptied by each truck was counted. The total quantity of drained sludge is obtained by cumulating the quantity of the two trucks according to Equation 1 (Talla et al., 2017; Koanda, 2006):

$$Q = \sum_{i} V_{ij} \cdot \eta_{ij} \quad (1)$$

where Q (m^3/month) is total volume of the sludge collected; Vij (m^3/rotation) is the useful volume of the i-truck for day j; ηij (rotations/truck) is the number of type i truck rotations for day j.

Method 2: specific production

The specific production of faecal sludge was obtained by Equation 2 (Koanda, 2006):

$$Q = 365 * \sum P_i * \frac{q_i}{1000} \quad (2)$$

where Q: total volume of the sludge; P_i: number of users for the tank I; and q_i: specific production of the tank i.

Sampling faecal sludge

In order to carry out some analysis on faecal sludge in Water Science and Environment Sanitation laboratory of University of Kara, the samples were prepared. For each sample, 1.5 L of sludge was measured at the beginning of the process of the truck, in the middle of the process and at the end of sampling. A total of, fifteen samples were collected. Five samples for each of the following type of septic tank were taken namely Domestic Septic Tank (DST), Public Septic Tank (PST) and Dry Latrines (DL). After mixing, 1.5 L which represents the composite sample is collected and sent to the Water Science and Environment Sanitation laboratory of University of Kara for analysis. For the chemical parameters, the liquid fraction was used (Klingel et al., 2002). The different phases of the sampling are schematized in Figure 2.

The physio-chemical analysis

The analysis method employed was adapted from the Standard Methods for the Examination of Water and Wastewater, as described by Rodier et al. (2009) and APHA (1998). The parameters analysed included: temperature, pH, electrical conductivity (EC), suspended matter (SM), chemical oxygen demand (COD), five-day biochemical oxygen demand (BOD_5), ammonium (NH_4^+), nitrates (NO_3^-), nitrites (NO_2^-) and orthophosphates (PO_4^{3-}).

Temperature, pH and electrical conductivity (EC) were measured *in situ* with the Multi HANNA HI 9811 parameters equipped with the different probes, following the same protocol by simply changing

Table 1. The amount of sludge produced during the companion.

Type of sanitation	Method 2: Specific production			Method 1: Sludge collection		
	specific production (L/day/pers)	Quantity (m^3/day)	Quantity (m^3/year)	Quantity (m^3/day)	Quantity (m^3/month)	Quantity (m^3/year)
DST	1	96	35040	42	840	10080
DL	0.2	2.88	1051.2	11.9	238	2856
PST	2	14.4	5256	7	140	1680
Total	-	113.28	41347.2	60.9	1218	14616

The results of this study show that the sludge produced is estimated to 113.28 m^3/day or 41347.2 m^3/year and that collected by truck to 60.9 m^3/day or 14616 m^3/year.

probes according to the parameter to be measured and the reading is done after stabilizing the display. The determination of the content of suspended matter (SM) was done using gravity after vacuum filtration with a microfilter of GF/C glass and drying in the oven at 105 ± 2°C. The evaluation of COD is based on open reflux colorimetric method. It was determined by oxidation with an excess of potassium dichromate in an acidic environment 150°C in the presence of silver sulphate as a catalyst. The value reading was made by a spectrophotometer of a mark GENESYS 10S UV-VIS. The five-day oxygen biochemical demand (BOD_5) was determined by the five-day incubation method in the dark and 20°C temperature using an OxiDirect (Lovibond). At the end of this incubation period, the value of BOD_5 was read directly on a BOD_5 scale on the bottle. Ammonia nitrogen (NH_4^+), nitrites (NO_2^-) nitrates (NO_3^-), and orthophosphates (PO_4^{3-}) were determined by using the colorimetric method with GENESYS 10S UV-VIS spectrophotometer reading at adequate wavelengths.

RESULTS

Management of faecal sludge in the district of Kara

Five trucks are involved in collecting of faecal sludge around Kara municipality. The dumping points are located at 2, 3 and 4 km from the center of Kara city.

Quantification of faecal sludge

Calculations of sludge produced considered the specific production to 1 L/person/day for domestic septic tanks, 0.2 L/person/day for dry latrines and 2 L/person/day for public tanks (Table 1).

The results of this study show that the sludge produced is estimated to 113.28 m^3/day or 41347.2 m^3/year and that collected by truck to 60.9 m^3/day or 14616 m^3/year.

Interpretation of physico-chemical parameters

The results of analysis of the physical and chemical parameters such as temperature, pH, electrical conductivity (EC), suspended matter (SM), chemical oxygen demand (COD), five-day biochemical oxygen demand (BOD_5), ammonium (NH_4^+), nitrates (NO_3^-), nitrites (NO_2^-) and orthophosphates (PO_4^{3-}) of the different types of sludge are recorded in Table 2.

Temperature, EC and pH

Temperature averages recorded for DL, DST and PST during the study period is respectively 26.2 ± 0.01, 27.8 ± 0.01 and 26.4 ± 0.01°C. Figure 3 shows the change in temperature between septic tanks.

Conductivity values show that the sludge is loaded into dissolved salts. Conductivity in the different sludge varied between 1641 and 16783 S/cm and the highest value is observed in the Public Septic Tanks (PST).

pH values obtained are 7.5, 7.3 and 8.4, respectively for DL, DST and PST, values consistent with the development of the bacterial that purify the sludge.

Suspended matter (SM)

The concentration of suspended matter (SM) is very high in sludge. As shown in Table 2, the concentration of materials suspensions at the different sludge varied for DL, DST and PST respectively 70 ± 20, 54 ± 2 and 75 ± 15 g/L.

Ammonium (NH_4^+), NO_3^-, NO_2^- and PO_4^{3-}

The degradation of organic nitrogen into ammonium is an integral part of the nitrogen cycle in nutrient production. High ammonium levels were found in the Public Septic Tank (Table 2).

The average nitrate concentration is 143 ± 7.54, 150 ± 0.4 and 406.3 ± 0.3 mg/L, respectively for Dry Latrine, Domestic Septic Tank and Public Septic Tank.

Carbon pollution: BOD_5 and COD

The results of analyses revealed that the ratio of the COD and BOD_5 average gives 2.35, 2.55 and 1.72 mg/L, respectively for Dry Latrine, Domestic Septic Tank and

Table 2. Physico-chemical parameters.

Parameter	DL		DST		PST	
	Average	SD	Average	SD	Average	SD
pH	7.5	0.01	7.3	0.01	8.4	0.01
EC (S/cm)	1641	0.2	2582	2	16783	3
SM (g/L)	70	20	54	2	75	15
Temperature (°C)	26.2	0.01	27.8	0.01	26.4	0.01
COD (mgO_2/L)	700	20	980	10	3400	264.57
BOD_5 (mgO_2/L)	297	36.055	384	4	1978	1
COD/BOD_5 (mgO_2/L)	2.35	0.97	2.55	0.51	1.72	1.4
NTK (mgN/L)	908	3	1610	15	4760	3
NH_4^+ (mgN/L)	337	1.73	347	22.5	850.94	0.1
NO_2^- (mgN/L)	14	1.02	13.4	2.69	17.7	1.71
NO_3^- (mgN/L)	143	7.54	150	0.4	406.3	0.3
PO_4^{3-} (mgP/L)	143	5.29	150	5	406.3	0.43

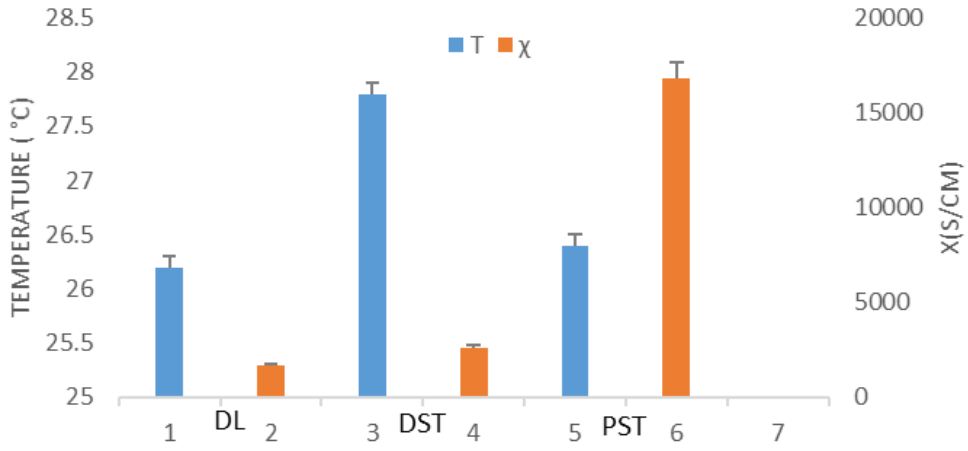

Figure 3. Electrical conductivity and temperature content.

Public Septic Tank. Figure 5 shows variations in BOD_5 and COD for different types of septic tanks.

DISCUSSION

Management of faecal sludge in the district of Kara

The study shows that mechanical emptying accounts for 92% versus 8% manual draining. This result proves that the predominant emptying mode is mechanical emptying and this is due to the permanent presence of trucks draining in the communality. The ideal would be to practice one 100% mechanical emptying to limit the risk of contamination of those who practice manual emptying. So the result obtained is more satisfactory compared to that of the city of Sokodé (Togo) where manual emptying is 24% and mechanical emptying 76%. The practice of manual emptying would be due to the fact that the populations lack financial means and also the difficulties of access to certain households by the emptying truck (Bissang, 2019).

Quantification of faecal sludge

The results of this study show that the sludge produced is estimated to be 113.28 m^3/day or 41347.2 m^3/year and that collected by truck to 60.9 m^3/day or 14616 m^3/year. The dumping activity is carried out without any control. The faecal sludge is spread into the environment sometimes anarchically. Some farmers living around the area use the sludge to irrigate their farms. The comparison of these two methods shows 26731.2 m^3/year or 65% of sludge is not drained. As in Kara, an average of 40.39 m^3/day of sludge is produced or 14

743.67 m^3/year in the city of Sokodé. The average quantity of faecal sludge collected is 8.68 m^3/day or 3168.20 m^3/year according to Water and Sanitation Project in Togo, Phase 2 (PEAT2, 2019). The quantity collected is very small compared to the quantity produced. Actions must be taken to strengthen the collection of faecal sludge in the town of Kara.

Interpretation of physico-chemical parameters

Figure 3 shows the change in temperature between septic tanks. It should be noted that the temperatures recorded in different tanks have a favourable microbial mineralization activity. Thus, it is noted that in hot period biological activity is more important than in winter, and it plays a major role on the kinetic reactions.

Conductivity values show that the sludge is loaded into dissolved salts. Conductivity in the different sludge varied between 1641 and 16783 S/cm and the highest value is observed in the Public Septic Tanks (PST). The conductivity values show that the effluent is loaded into dissolved salts. Indeed, anaerobic processes effectively mineralize organic matter and generate many dissolved salt, volatile fatty acids and hydrogen carbonates. This indicates that the sludge dumped in the district of Kara is highly mineralized, but still remains fermentable due to biodegradable organic pollutant levels. These average values are high than that found by Akpaki (2015) for Attidjin city (Lomé) and that found by Koné et al. (2016) at the Zagtouti (Burkina-Faso). These results confirm that there is a high mineral salt content in the environment leading to the risk of surface water contamination resulting in an excessive increase in conductivity and a balance of the aquatic ecosystem (Koné et al., 2016). Wetzel (1983) showed that low conductivity (0 to 200 µS/cm) is an indicator of pristine or background conditions. Mid-range conductivity (200 to 1000 µS/cm) is the normal background for most major rivers. Conductivity outside this range could indicate that the water is not suitable for certain species of fish or bugs. The results obtained in this study confirm that there is a strong presence of mineral salt in the medium. Taking into account the risks of contamination of surface water, an excessive increase in the conductivity of aquatic environments causes changes in the bacterial ecosystem and also has an influence on the survival of aquatic fauna and flora. In addition, too much salinity causes clogging of the soil (Koné et al., 2012), and negatively impacts the development of a large number of agricultural crops. For example, the excessive presence of salts causes a malfunction of the ion pumps allowing the plant, in normal times, to absorb this ion.

pH values obtained were 7.5, 7.3 and 8.4, respectively for DL, DST and PST, values consistent with the development of the bacterial that purify the sludge. The bacterial usually develop at pH between 5 and 9. The pH values obtained show that this faecal sludge are alkaline and their discharge into surface water could be dangerous for the survival of certain aquatic species such as fish, for example.

EC, pH and temperature can be limiting factors for the development of purifying bacterial.

Suspended matter (SM)

The concentration of suspended matter (SM) is very high in the sludge. These values greatly exceed the indicated standard which is 150 mg/L. Some authors have noted higher contents during similar work. Indeed, Mahamane (2011) reports an average SM value of 11,084 mg/L in Ouagadougou. This confirms the great variability in the characteristics of sludge with regard to its origin.

NH_4^+, NO_3^-, NO_2^- and PO_4^{3-}

The degradation of organic nitrogen into ammonium is an integral part of the nitrogen cycle in nutrient production. High ammonium levels were found in the Public Septic Tank (Table 2). This phenomenon is all more pronounced that the environment is alkaline and these values could be explained by the quality of the structure of the septic tank or latrine. Indeed, in these septic tanks, the anaerobic conditions favour the production of ammonium, which will oxidize in the aerobic conditions of the drying beds. Moreover, the longer sludge stays in the pit, the greater the mineralization. Nitrites an oxidized form on nitrogen is not stable; they evolve into nitrate in aerobic environment. The concentration of nitrite (15 mg/L) in this study is very high than (0.09 mg/L) from the study conducted in Zagtouti (Ouagadougou) by Koné et al. (2016) evaluating samples taken directly in the different basin. Figure 4 shows variations in nitrates and orthophosphates in different septic tanks.

The average nitrate concentration is 54, 56 and 85 mg/L, respectively for Dry Latrine, Domestic Septic Tank and Public Septic Tank. This indicates a good nitrification process when the sludge is dehydrated. Orthophosphates are undesirable when their levels become too high, although these are nutrients that can be used in agriculture. Nitrogen and orthophosphates contribute to the eutrophication of surface waters. Phosphorus in sludge in various forms (organic phosphorus, orthophosphates, etc.) can come from food but also from natural sources or from anthropogenic activities.

Carbon pollution: BOD_5 and COD

The results of the analyses revealed that the ratio of the COD and BOD_5 average was 2.35, 2.55 and 1.72 mg/L, respectively for Dry Latrine, Domestic Septic Tank and

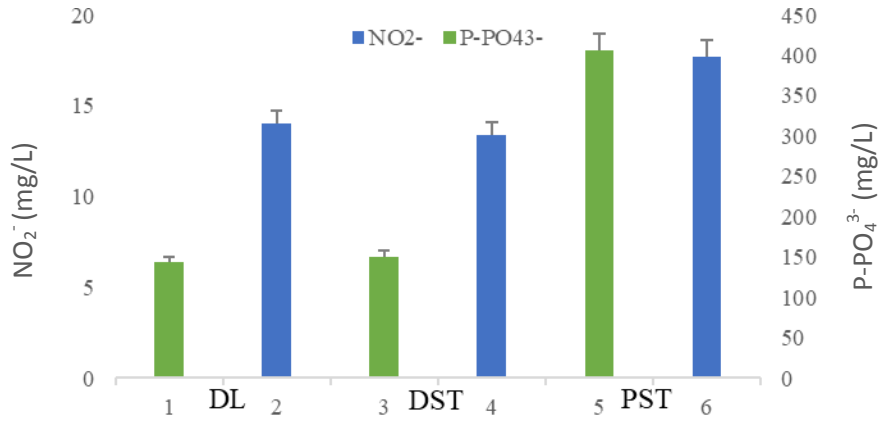

Figure 4. Nitrates and orthophosphate levels.

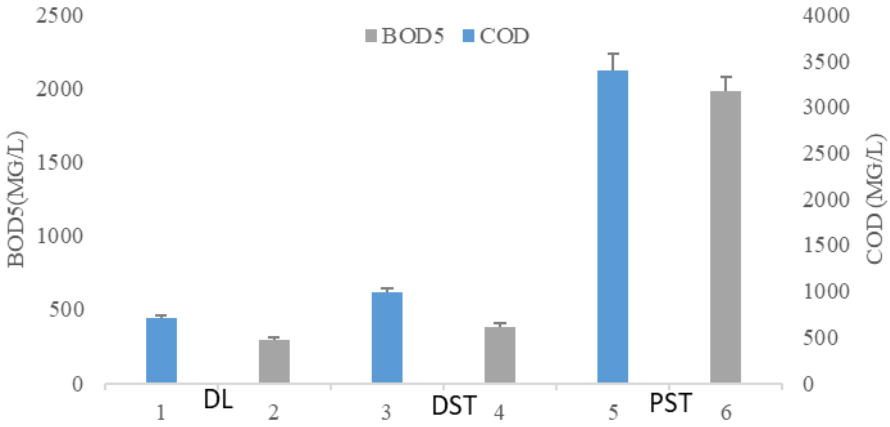

Figure 5. Values of COD and BOD_5.

Public Septic Tank, thus indicating the biodegradable nature of the sludge and the choice of biological applied treatment technology. These values obtained show that Kara district sludge is still biodegradable and undergoes mineralization. Figure 5 shows variations in BOD_5 and COD for different types of septic tanks.

Conclusion

The objective of this study was to know the characteristics and to estimate the quantity of the deposits of sludge produced in the city of Kara. To do so, it was necessary to carry out a sociological survey in the concessions and in the structures with high frequency, then to determine the physicochemical characteristics of the faecal sludge produced in the city of Kara. Two methods were used to assess the amount of sludge produced. The first method, based on specific production, shows that the estimated volume of sludge produced is 113.28 m^3/day or 41347.2 m^3/year. The second method based on the counting of trucks reveals that only 60.9 m^3 of sludge are emptied per month, that is, 14,616 m^3/year are emptied. The physico-chemical analyses focused on three types of septic tanks. The results of the parameters analyzed reveal that public septic tank latrines (PST) are more biodegradable than DL and DST justified by the fact that sludge from PST has a short residence time. This information is essential in the processing and sizing of structures. This work will be used by decision makers as an aid tool for decision making at the specific scale of the city of Kara.

CONFLICT OF INTERESTS

The authors have not declared any conflict of interests.

ACKNOWLEDGEMENT

The author thanks the various chemistry laboratories which served as a framework for carrying out the various

elemental analyses: Laboratory of Sanitation, Water Science and Environment (LASEE), University of Kara; Laboratory of Management, Treatment and valuation of Waste (GTVD), University of Lomé; and Center of Excellence "Sustainable Cities" (CERViDA) of University of Lomé.

REFERENCES

Ahamada Z, Kimuli D, Banadda N, Kabenge I, Kiggundu N, Kambugu R, Wanyama J, Kigozi J (2016). Quantification of Physico-Chemical Characteristics and Modeling Faecal Sludge Nutrients from Kampala City Slum Pit Latrines. International Journal of Research in Engineering and Advanced Technology 3(6):129-141.

Akpaki (2015). Physico-chemical characterization of Attidjin faecal sludge (prefecture of the gulf-togo). Doctoral thesis, Chemistry of Water and the Environment, University of Lomé P 167.

Akpaki O, Baba G, Segbeaya KN, Koledzi KE (2016). Quantification and Biogas Valorization of Attidjin Lomé-Togo Sewage Sludge (Togo). Journal de la Société Ouest-Africaine de Chimie 042:30-35 ISSN 0796-6687.

American Public Health Association (APHA) (1998), Standard Methods for the Examination of Water and Wastewater. 20th Ed., American Public Health Association, American Water Works Association and Water Environmental Federation, Washington DC.

Bassan M, Tchonda T, Yiougo L, Zoellig H, Mahamane I, Mbéguéré M, Strande L (2013). Characterization of faecal sludge during dry and rainy seasons in Ouagadougou, Burkina Faso. 36th WEDC Int. Conf., Nakuru. Kenya pp. 1-7. https://www.researchgate.net/publication/255710132.

Bissang (2019). Characterization and quantification of faecal sludge deposits in the city of Sokodé. M.SC. Thesis, University of Kara, p.65.

Federal Institute for Water Supply, Wastewater Treatment and Water Protection (EAWAG) (2006). Towards an improved management of faecal sludge P 32.

Gnagne T, Kouame YF, Tenena M (2019). Sizing, operation and operation of Unsaturated Flow Drying Beds (LSENS) for the treatment of faecal sludge from septic tanks. International Journal of Biological and Chemical Sciences 13(5):114-121. DOI: http://dx.doi.org/10.4314:ijbcs.v13i.9S .

Kajyibwami (2018). Sustainable management of faecal sludge in Bobo-dioulasso (Burkina-Faso) P 99.

Katukiza AY, Ronteltap M, Niwagaba CB, Foppen JWA, Kansiime F, Lens PNL (2012). Sustainable sanitation technology options for urban slums. Biotechnology Advances 30(5):964-978.

Klingel F, Montangero A, Koné D, Strauss M (2002). Fecal Sludge Management in Developing Countries: A Planning Manual, https://sswm.info/sites/default/files/reference_attachments/KLINGEL%202002%20Fecal%20Sludge%20Management%20in%20Developing%20Countries%20A%20planning%20manual.pdf

Koanda (2006). Towards sustainable urban sanitation in sub-Saharan Africa : An innovative approach to planning faecal sludge management. Federal Institute of Technology in Lausanne. Ph.D. Thesis P 360.

Kodom (2019), Characterization and quantification of faecal sludge deposits produced in the city of Kara: specific ratio per household and per sector of activity, master's thesis, University of Kara P 61.

Koné M, Bonou L, Koulidiati J, Joly P, Sodré S, Bouvet Y (2012). Treatment of urban wastewater by infiltration percolation on sand and on a coconut substrate after an anaerobic lagoon basin in a tropical climate. Journal of Water Sciences 25(2):139-151.

Koné M, Ouattara Y, Service E, Ouattara P, Bonou L, Joly P (2016). Characterization of faecal sludge deposited on the zagtouli drying beds (Ouagadougou). International Journal of Biological and Chemical Sciences 10(6):2781-2795. DOI: http://dx.doi.org/10.4314/ijbcs.v10i6.30.

Kouawa T, Wanko A, Beck C, Mose R, Maïga A (2015). Feasibility study of faecal sludge treatment by constructed wetlands in Sahelian context: Experiments with *Oryza longistaminata and Sporobolus pyramidalis* species in Ouagadougou. Ecological Engineering 84:390-397, DOI: http://dx.doi.org10.1016/j.ecleng.2015.09.021.

Mahamane (2011). Contribution to the sustainable management of faecal sludge in the city of Ouagadougou: Characterization of sludge and evaluation of the sizing of STBVs in Kossodo and Zagtouli. Specialized M.Sc. Thesis 2iE, Ouagadougou P 68.

Ouédraogo (2016), Characterization of dried faecal sludge and treated percolate from the Zagtouli treatment plant with a view to agronomic valuation, master, Water and Sanitation Engineering Sciences, 2iE, Ouagadougou P 89.

Rodier J, Legube B, Merlet N (2009). « Water Analyzed ». 9th Ed.

Talla A, Sezawo R, Ngohe-Ekam PS (2017). Characterization of Depoted Faecal Sludge into the Environment and Design of a Suitable Treatment System: case of Nomayos Area in Yaoude City. Current Journal of Applied Science and Technology 21(2):1-12. DOI.10.9734/BJAST/2017/32755

Tilley E, Zurbrügg C, Lüthi C (2010). A Flow Stream Approach for Sustainable Sanitation Systems. Social Perspectives on the Sanitation Challenge, pp. 69-86. DOI: 10.1007/978-90-481-3721-3.5.

Water and Sanitation Project in Togo, phase 2 (PEAT-2) (2019). Quantification and characterization of faecal sludge deposits in the city of Sokodé: Specific production of faecal sludge per inhabitant. Report, University of Kara P 19.

Wetzel (1983). Limnology. 2nd Ed. Saunders College Publishing. 760 p.

Vol. 20(5), pp.202-209, May, 2021
DOI: 10.5897/AJB2021.17333
Article Number: 4F2111066752
ISSN: 1684-5315

http://www.academicjournals.org/AJB

ACADEMIC JOURNALS
expand your knowledge

African Journal of Biotechnology

Full Length Research Paper

A rapid detection method on-site for *Zygosaccharomyces* based on loop-mediated isothermal amplification (LAMP) combined with a lateral flow dipstick (LFD)

Yang Liu[1≠], Jun Wu[2≠], Li-Qing Chen[3], Ya Shi[1], Hong-Xia Zhao[1], Wei Chen[3], Hong Li[4] and Lu-Ping He[1,5*]

[1]Key laboratory of Microbiol technology and Bioinformatics of Zhejiang Province, Zhejiang Institute of Microbiology, Hangzhou 310012, China.
[2]Lin'an Center for Disease Control and Prevention, Lin'an, 311300, China.
[3]Hangzhou Huqingyu tang Traditional Chinese Medicine Mordernize Institute, Hangzhou 311100, China.
[4]China National Accreditation Institute for Conformity Assessment, Beijing 100062, China.
[5]Hangzhou Digital-Micro Biotech Co., Ltd., Zhejiang, Hangzhou 311215, China.

Received 23 February, 2021; Accepted 22 April, 2021.

The *Zygosaccharomyces* is notorious for its remarkable spoilage characteristics. In the present study, the visual and rapid identification of the genus *Zygosaccharomyces* was performed by a loop-mediated isothermal amplification (LAMP) assay using specific primers in Mini Dry Bath within 30 min at 65°C followed by a lateral flow dipstick (LFD) detection. The sensitivity evaluation revealed LAMP-LFD assay with 1.0×10^1 copies/μL of *Zygosaccharomyces* DNA as its detection limit, which was the same as the methods of real-time quantitative PCR (qPCR) and conventional polymerase chain reaction (PCR). However, qPCR or PCR methods not only need to be performed in a specialist analytical laboratory with expensive equipment but also with risk of aerosol pollution. The LAMP-LFD assay had no cross-reactivity against 10 other yeast species and its specificity was 100%. A total of 25 Qiangli loquat Dew samples (17 bottles bulged and eight normal-appearing) were detected within 40 min with 100 and 92.0% accurately and specifically, when compared with the qPCR assay and the microbiology culture method, respectively. Therefore, the simple, fast, sensitive and low-cost LAMP-LFD assay is an effective and useful tool for the on-site identification of the genus *Zygosaccharomyces*.

Key words: *Zygosaccharomyces*, on-site detection, loop-mediated isothermal amplification (LAMP), lateral flow dipstick (LFD).

INTRODUCTION

Based on The Yeasts Fifth Edition (Fleet, 2011) and the latest studies, the genus *Zygosaccharomyces* comprises 14 species, which are *Zygosaccharomyces rouxii*, *Zygosaccharomyces bailii*, *Zygosaccharomyces pseudobailii*, *Zygosaccharomyces parabailii*, *Zygosaccharomyces bisporus*, *Zygosaccharomyces lentus*, *Zygosaccharomyces kombuchaensis*, *Zygosaccharomyces mellis*, *Zygosaccharomyces sapae*, *Zygosaccharomyces machadoi*, *Zygosaccharomyces siamensis*, *Zygosaccharomyces gambellarensis*, *Zygosaccharomyces favi*, and *Zygosaccharomyces seidelii* (Hulin and Wheals, 2014; Brysch-Herzberg et al., 2020). To our knowledge, the spoilage potential of the genus *Zygosaccharomyces* has been widely recognized

within the food industry (James and Stratford, 2011; Hulin and Wheals, 2014). As fermenting microbes, and although the *Zygosaccharomyces* species consequent on products spoilage vary with the characteristics and product type involved (Harrison et al., 2011), the ability to survive under various stresses, such as resistance to extreme osmotolerance and high-level weak acid preservatives, make these problematic in food or medicine industry (Fugelsang and Edwards, 2007; Čadež et al., 2015; Wang et al., 2015; Karaman and Sagdic, 2019). In addition, the ability to ferment sugars to ethanol and CO_2 might cause containers, cans and glass bottles to deform, and even explode (Tournas et al., 2006; Frisón et al., 2015; Wang et al., 2017). Thus, an effective method is needed to promptly detect the genus *Zygosaccharomyces* for its effective control, thereby reducing potentially large economic losses, and protecting consumer safety.

Various detecting approaches for *Zygosaccharomyces* spp. have been developed (Rawsthorne and Phister, 2006; Harrison et al., 2011; Hulin and Wheals, 2014; Wang et al., 2016; Wang and Sun, 2019). As a standard method, the culture-dependent technique has several shortcomings, for example, it was a time-consuming process with poor repeatability and qualitative inaccuracy (Duarte et al., 2004; National Food Safety Standard of the People's Republic of China, GB 4789.15-2016). Molecular methods, such as PCR and qPCR assays, have been widely used with high sensitivity, specificity and accuracy (Casey and Dobson, 2004; Rawsthorne and Phister, 2006; Andorrà et al., 2010), and industry standards related to *Zygosaccharomyces* spp. have been issued (General Administration of Quality Supervision, Inspection and Quarantine of the People's Republic of China (AQSIQ), SN/T 4675.30-2017; SN/T 4780-2017). However, these involve steps with temperature increments and decrements, the normal presence of inhibitors, and the requirement of specialized laboratories, expensive equipment and highly trained laboratory staff (Rawsthorne and Phister, 2006; Andorrà et al., 2010; Zuehlke et al., 2013; Hulin and Wheals, 2014). Therefore, the establishment of a cost-effective, simple, fast and sensitive assay at the field level has become increasingly important to realize the early and successful detection of *Zygosaccharomyces*.

Compared to PCR and qPCR, loop-mediated isothermal amplification (LAMP) assay is an efficient and novel amplification technology with great specific and highly sensitive based on isothermal conditions (Zhang et al., 2019). Furthermore, it is simpler to perform, and merely use constant-temperature equipment, such as a water bath or Mini Dry Bath within 60 min. This can be potentially used for tests in the field (Punati et al., 2019; Joon et al., 2019; Tumino et al., 2020). In addition, LAMP has been extensively applied in food-borne pathogens, allergens, and genetically modified organisms in food analysis (Hara-Kudo et al., 2010; Rostamkhani et al., 2011; Saharan et al., 2015; Shi et al., 2017; Yuan et al., 2018; Li et al., 2019; Zhuo et al., 2019; Tumino et al., 2020). Furthermore, LAMP products traditionally observed by gel electrophoresis and hydroxynaphthol blue (HNB) or SYBR are either difficult to distinguish by fluorescent dyes, which need special equipment and the process is time-consuming, or easily exposed to aerosol pollution due to the opening of the lid (Shi et al., 2017; Punati et al., 2019; Zhang et al., 2019). Moreover, the amplified products are visualized directly on an LFD with one or two bands, which is more suitable for on-site detection (Shi et al., 2017).

To our knowledge, the detection of the genus *Zygosaccharomyces* by LAMP assay has not been reported to date. For rapid qualitative test of the genus *Zygosaccharomyces*, an accurate, sensitive and visualized LAMP-LFD assay was developed in this study. All strains of DNA were analyzed using LAMP-LFD, PCR and qPCR for comparison of the sensitivity. To validate the effectiveness and robustness of the LAMP-LFD assay, the specificity and sensitivity were evaluated and the Qiangli loquat Dew samples were performed. That the LAMP-LFD assay is a simple, fast, sensitive and low-cost tool for the genus *Zygosaccharomyces* on-site detection.

MATERIALS AND METHODS

Strains, media and DNA extraction

Table 1 presents the yeast strains assessed in the present study. The strains were cultivated in Sabouraud Dextrose Agar (SDA) (Hope Bio-Technology Co., Ltd, Qingdao, China) at 28°C for 48 h. All DNAs of the strains or Qiangli loquat Dew samples were extracted using the DNeasy PowerSoil Kit (QIAGEN, Germany), according to the manufacturer's protocol. The DNA was eluted in 100 µL of elution buffe followed by storing at -20°C.

LAMP-LFD, PCR and qPCR assays

Primer is crucial for amplification efficiency of LAMP assay. Based on the the internal transcribed spacer (ITS) regions ITS1 and ITS2 flanking the 26S ribosomal genes of *Zygosaccharomyces* DNA sequences obtained from the NCBI GenBank, the primers (Table 2)

*Corresponding author. E-mail: hlpjoke@163.com, 18601383260@163.com .

#These authors contributed equally to the article.

Table 1. Yeast strains used in the present study.

Species	Culture collection[a]
Zygosaccharomyces parabailii	ATCC MYA-4549
Canidia albicans	CMCC(F) 98001
Candida parapsilosis	ATCC 22019
Rhodotorulamucilaginosa	ATCC 66034
Pichia guilliermondii	CGMCC 2.1862
Trichosporonasahii	CGMCC 2.319
Cryptococcus albida	CGMCC 2.5512
Pichia kudriavzevii	CICC 33192
Candida metapsilosis	CICC 31269
Saccharomyces cerevisiae	ATCC 9763
Candida glabrata	ATCC MYA-2950
Zygosaccharomyces bailii isolate[b]	-
Zygosaccharomyces mellis isolate[b]	-
Zygosaccharomyces parabailii isolate[b]	-

[a]ATCC: American type culture collection, America; CMCC: National center for medical culture collections, China; CGMCC: China General Microbiological Culture Collection Center; CICC: China Center of Industrial Culture Collection. [b]Isolates were isolated from bottle bulged Qiangli loquat Dew by Key Laboratory of Microbial Technology and Bioinformatics of Zhejiang Province, Hangzhou, China.

Table 2. Primer sequence information.

Type	Primer	Sequence (5'-3')
Outer primers	*Zyg*-F3	TGAAGCGGCAARAGCTCAA
	Zyg-B3	GAGCTGCATTCCCAAACAAC
Inner primers	*Zyg*-FIP	AAGSRCCAGCCCCAGARTCRAAATCTGGTACCTTCGGTGC
	Zyg-BIP	CCTTGGAACAGGACGTCATRGATCGACTCTTCGAARGCRCT
Loop primers	*Zyg*-LF	CYTTCTACAAATTACAACTCGG
	Zyg-LB	CCGTATGGCGAGGATCCC

were designed by using the Primer Explorer version 5 software and synthesized from Shanghai Generay Biotech Co., Ltd. LAMP-LFD assay was carried out in a 25 µL reaction mixture, containing 1×*Bst* DNA polymerase buffer (New England Biolabs Ltd., Ipswich, MA, USA), 1.6 µM of *Zyg*-FIP and *Zyg*-BIP, 4.0 µM of *Zyg*-LF and *Zyg*-LB, 2.0 µM of *Zyg*-F3 and *Zyg*-B3, 1.4 µM of dNTP (TaKaRa Biotechnology Co., Ltd., Dalian, China), 0.32 U/µL of *Bst* 2.0 DNA polymerase (New England Biolabs Ltd., Ipswich, MA, USA), 8 mM of $MgSO_4$, 1×SYBY Green I, 2.0 µL of template DNA and nuclease-free water. The whole amplification procedure was performed at 65°C for 30 min and 80°C for 5 min in the Mini Dry Bath (Hangzhou Yooning Instrument, China). The amplified products were tested using LFD devices (Ustar Biotech Co., Ltd., Hangzhou, China), with colored lines at both the "C" and "T" lines, which denote positive samples, while the ones that only presented a signal at "C" were negative samples.

The PCR assay was conducted in the ProFlex PCR System (Thermo Fisher Scientific, Inc., Waltham, MA, USA) with 25 µL reaction system, which contained 2×Phanta® Max Master Mix (Vazyme biotech Co., Ltd., Nanjing, China), 0.2 µM of each primer: Forward primer (Zygogen F3) 5'-ACACACAGTGGAGTTTC-3', Reverse primer (Zygogen R1) 5'-CGGTAAAACCTAATACGAC-3' (Hulin and Wheals, 2014), 2.0 µL of template DNA and nuclease-free water. The reactions were run in triplicate for 5 min at 95°C, followed by 35 cycles for 30 s at 95, 55 and at 72°C, respectively. 3 µL of amplified products were analyzed by gel electrophoresis on 1.5% gel with 6×loading buffer and visualized on the Tanon-1600 Gel Image System (Tanon Science & Technology Co., Ltd., Shanghai, China). Furthermore, the qPCR reaction performed in the StepOne™ Plus Real-Time PCR System (Applied Biosystems, Inc., Carlsbad, CA, USA) containing 1×SYBR® Premix Ex*Taq*™ (Tli RNaseH Plus) (TaKaRa Biotechnology Co., Ltd., Dalian, China), 0.2 µM of Forward primer, 0.2 µM of Reverse primer (the same as the PCR assay previously), 2.0 µL of template DNA and nuclease-free water with running in triplicate for 30 s at 95°C, followed by 40 cycles at 95°C for 5 s, and at 60°C for 30 s as its amplification procedure.

Sensitivity and specificity evaluation of the LAMP-LFD assay

In order to determine the sensitivity of the LAMP-LFD assay, in terms of the detection limits compared with the PCR and qPCR assays, the amplification reactions were performed with the *Z. bailii* DNA. The DNA fragment was purified from the agarose gel using the AxyPre™ DNA Gel Extraction Kit (Axygen Scientific, USA), and cloned into the pMD™18-T vector using the *E.coli* DH5α competent

cell, followed by plasmid extraction. Each dry plasmid DNA was then suspended in nuclease-free water. The copies of gene were determined by multiplying the DNA concentration through Avogadro's number and divided by the product of the plasmid size (bp) and the average weight of the base pair (Ahmed et al., 2014). The 10-fold serial dilutions ranged from 10^6 to 10^0 gene copies per microliter of DNA were prepared with three replicates for the LAMP-LFD, PCR and qPCR assays. The limit of detection (LOD) was determined as the concentration of the lowest dilutions, in which all three replicates had positive signals.

In order to verify the LAMP-LFD specificity, the LAMP results were compared with the DNA of *Zygosaccharomyces* and 10 other yeasts: *Canidia albicans, Candida parapsilosis, Rhodotorula mucilaginosa, Pichia guilliermondii, Trichosporon asahii, Cryptococcus albida, Candida metapsilosis, Saccharomyces cerevisiae, Candida glabrata* and *Pichia kudriavzevii.* In particular, the LAMP assay was conducted at 65°C for 30 min, as previously described. All samples were determined in triplicate, and the experiment was performed three times.

Evaluation of the LAMP-LFD assay using Qiangli loquat Dew samples

In order to evaluate the efficiency and robustness of the LAMP-LFD assay, a total of 25 Qiangli loquat Dew samples were used in detecting *Zygosaccharomyces*, while 17 of the samples were bottle bulged Qiangli loquat Dew samples, and the other eight samples were normal-appearing Qiangli loquat Dew samples. The DNA extracted from the Qiangli loquat Dew samples were tested by the LAMP-LFD assay and compared with the qPCR with three replicates for each sample. Simultaneously, the microbiology culture method was also used in the trial. Strains collected from the 25 Qiangli loquat Dew samples were, respectively cultivated in SDA at 28°C for 48 h. Then, the DNAs of the strains were extracted and verified by sequencing the D1/D2 region of the 26S rRNA gene.

RESULTS AND DISCUSSION

Sensitivity of the LAMP-LFD, PCR and qPCR assays

To contrast between the LAMP, PCR and qPCR assays, the sensitivities of PCR and qPCR were tested with the same plasmid DNA (1.0×10^0 to 1.0×10^6 copies/μL). The LFD readouts with clear-colored line reaction at the control "C" and test "T" lines were positive (+), while those with only the control "C" were negative (-) (Figure 1a). In Table 3, the LFD readouts of the LAMP amplified products that corresponded to the different concentrations of the plasmid DNA are shown. The conventional PCR amplified products were detected by agarose gel electrophoresis with different diluents (Figure 1b). The cycle threshold (Ct) values were plotted against copies/μL to establish the sensitivity of the amplification in different diluents (Figure 1c). When the concentration of the plasmid DNA was 1.0×10^0 copies/μL, the LAMP-LFD assay displayed a signal only at "C". Furthermore, the PCR assay had no band, and qPCR assay (two in three parallel results) had no Ct values. These results revealed that the LAMP-LFD assay detection limits were as low as 1.0×10^1 copies/μL, which was consistent with both the PCR assay and qPCR assay (Table 3).

The low-copies result is not unexpected, because specific primers were the key players in these molecular methods. Although the detection of the genus *Zygosaccharomyces* by LAMP assay has not been reported to date, the sensitivity of the LAMP assay was in agreement with other microorganisms studies (Saharan et al., 2015; Yuan et al., 2018; Li et al., 2019; Wu et al., 2019; Zhang et al., 2019; Zhuo et al., 2019). Seveval PCR or qPCR methods have detected *Zygosaccharomyces* spp. in previous studies, while the limits of these molecular methods were not for comparison validly to the results in the present study because of the different unit (CFU/μL) (Rawsthorne and Phister, 2006; Jaramillo et al., 2015). Some studies have suggested that species or genus specific PCR primers can be used to identify the genus *Zygosaccharomyces* (Harrison et al., 2011; Hulin and Wheals, 2014), but missing LOD data. Moreover, there was very few paper detected *Z. rouxii* using the qPCR assay with LOD approximately 20 times more sensitive than the LAMP assay in the present study (Syromyatnikov et al., 2018). This may be attributed to the set of primers only applied to the specific *Zygosaccharomyces* spp.

However, the PCR assay and qPCR assay involved steps with temperature increments and decrements and required a specialized laboratory, an expensive PCR or qPCR system, UV illumination equipment, and highly trained laboratory staff (Rawsthorne and Phister, 2006; Andorrà et al., 2010; Zuehlke et al., 2013; Hulin and Wheals, 2014). In addition, the qPCR assay needs approximately 2 h to accomplish each DNA test, while the PCR assay needs approximately 3 h. Furthermore, the amplified products analyzed by gel electrophoresis require the opening of the lid of the tube, which could cause aerosols pollution (Shi et al., 2017; Zhang et al., 2019). Moreover, the LAMP-LFD assay for the detection of *Zygosaccharomyces* could be rapidly completed in the Mini Dry Bath within 30 min at 65°C and visualized on an LFD without opening the lid in the field level (Figure 1d).

The minimum equipment required to run the LAMP-LFD assay includes Eppendorf tubes with reagents, heat blocks, nuclease-free water, pipettes and tips and lateral flow dipsticks.

Specificity of the LAMP-LFD assay

A highly specific assay at the field level is important for the detection of the genus *Zygosaccharomyces*, which could avoid cross-reactions and false-positive data. The specificity of the LAMP-LFD assay was determined with the *Zygosaccharomyces* DNA and other yeasts DNA. Then, 10 ng each of the *Z. bailii, Z. parabailii*, *Z. mellis*, *C. albicans*, *C. parapsilosis, R. mucilaginosa*, *P. guilliermondii*, *T. asahii, C. albida*, *C. metapsilosis*, *S. cerevisiae*, *C. glabrata* and *P. kudriavzevii* DNA were used in the tests. The results revealed that the DNA from *Z. parabailii*, *Zygosaccharomyces mellis* and *Z. bailii*

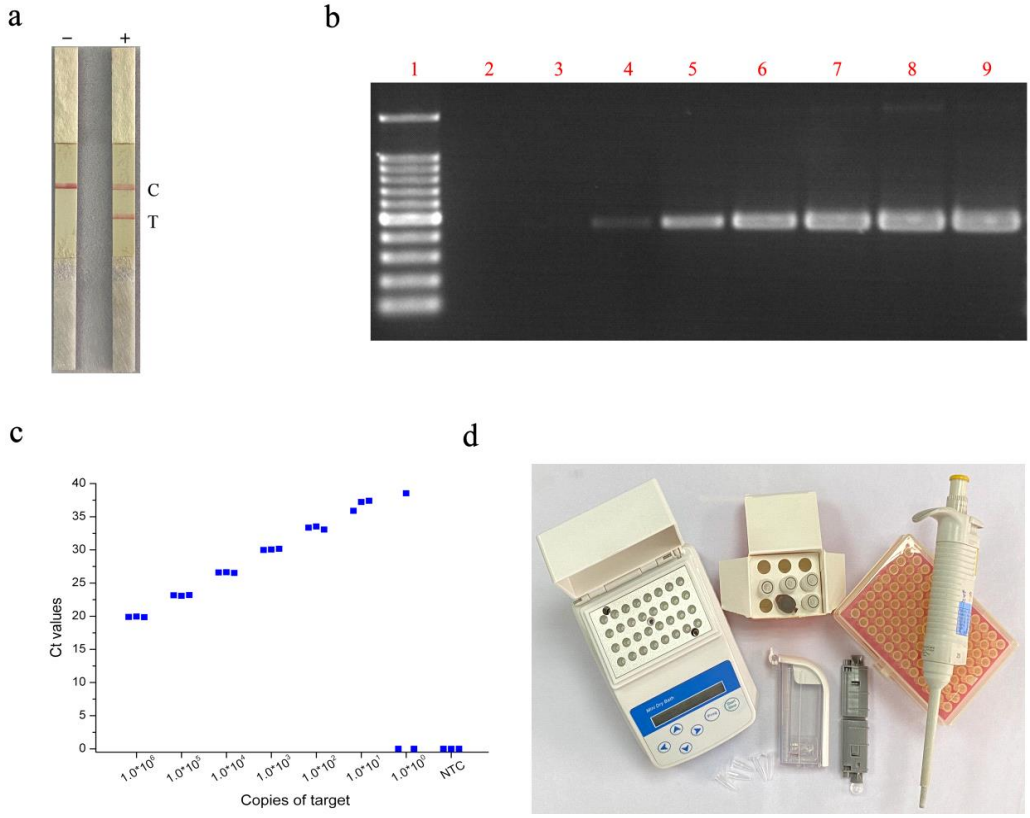

Figure 1. The sensitivity of the LAMP-LFD, PCR and qPCR assays for the detection of *Zygosaccharomyces*. a: Lateral flow dipstick readout. A positive result (+) with dual labels, both "C" and "T", negative result (-) with only "C". b: PCR assay; 1: 100 bp marker, 2: No template control, 3: 1.0×10^{0} copy/μL, 4: 1.0×10^{1} copies/μL, 5: 1.0×10^{2} copies/μL, 6: 1.0×10^{3} copies/μL, 7: 1.0×10^{4} copies/μL, 8: 1.0×10^{5} copies/μL, 9: 1.0×10^{6} copies/μL. c: The LOD of the qPCR assay (n=3). d: The minimum equipment needed for the LAMP-LFD assay.

Table 3. The LFD readouts of the LAMP amplified products in different concentrations.

Copies of target	LFD readouts
0	-
1.0×10^{0}	-
1.0×10^{1}	+
1.0×10^{2}	+
1.0×10^{3}	+
1.0×10^{4}	+
1.0×10^{5}	+
1.0×10^{6}	+

were detected as positive by the LAMP-LFD assay. The DNA samples that originated from the other 10 species of yeasts gave negative results. The data revealed no cross-reactions in the LAMP-LFD assay (Table 4). Therefore, the designed primers for the LAMP-LFD assay to detect *Zygosaccharomyces* had conservative property and specificity features. In other words, the specificity of the LAMP-LFD assay applied to the *Zygosaccharomyces* DNA was 100%. As expected, the results showed that the specificity of the primers play a crucial role in the LAMP-LFD assay, which was consistent with the specificity reported in other literatures (Wu et al., 2019; Zhuo et al., 2019).

The LAMP-LFD assay detection for Qiangli loquat Dew samples

In order to determine the efficacy and robustness of the LAMP-LFD assay for the detection of the genus *Zygosaccharomyces* in practical application, the DNA samples extracted from 25 Qiangli loquat Dew samples, respectively, were detected in contrast to the qPCR assay and microbiology culture method. As shown in Figure 2, the detected results for the 17 DNA samples (Nos. 1-4, 6, 8, 10-14, 17, 18, 20, 22, 23 and 25), which were obtained from the corresponding 17 bottles bulged Qiangli loquat Dew samples, were shown as positive (+) with blue color, and displayed two lines in the LFDs

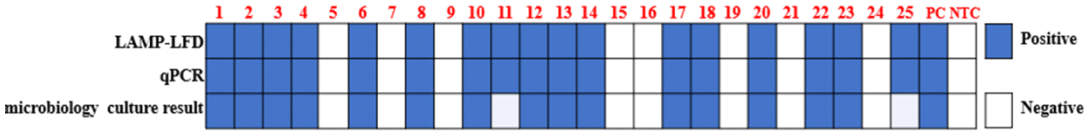

Figure 2. The LAMP-LFD, culture and qPCR assays for the detection of *Zygosaccharomyces* in the Qiangli loquat Dew samples. Nos. 1-4, 6, 8, 10~14, 17, 18, 20, 22, 23 and 25 were the bottles bulged Qiangli loquat Dew samples, while Nos. 5, 7, 9, 15, 16, 19, 21 and 24 were the normal-appearing Qiangli loquat Dew samples. PC: Positive control, NTC: No template control.

Table 4. Specificity test for the detection of *Zygosaccharomyces* by LAMP-LFD assay.

Species	LFD readout
Zygosaccharomyces parabailii ATCC MYA-4549(positive control)	+
Zygosaccharomyces parabailii isolate	+
Zygosaccharomyces mellis isolate	+
Zygosaccharomyces bailii isolate	+
Canidia albicans CMCC(F)98001	-
Candida parapsilosis ATCC 22019	-
Rhodotorula mucilaginosa ATCC 66034	-
Pichia guilliermondii CGMCC 2.1862	-
Trichosporon asahii CGMCC 2.319	-
Cryptococcus albida CGMCC 2.5512	-
Pichia kudriavzevii CICC 33192	-
Candida metapsilosis CICC 31269	-
Saccharomyces cerevisiae ATCC 9763	-
Candida glabrata ATCC MYA-2950	-
No template control	-

(Figure 1a). However, eight of these (Nos. 5, 7, 9, 15, 16, 19, 21 and 24) corresponded to the eight normal-appearing Qiangli loquat Dew samples, which displayed as negative (-), with the white color displaying only the "C" line (Figure 1a). It could also be observed that 17 qPCR-positive samples were positive and eight negative samples were negative in the LAMP-LFD assay (Figure 2). In another words, these LFD results were 100% consistent with the results of the qPCR assay. Nevertheless, all culture-positive samples (15 samples) were identified as *Z. parabailii* through the sequencing of the D1/D2 region of the 26S rRNA gene (data were not shown), and these were also positive in the LAMP-LFD and qPCR assays. In other words, compared to the microbiology culture result, the LAMP-LFD assay and qPCR for the detection of the genus *Zygosaccharomyces* in the Qiangli loquat Dew samples was 92.0% accurately and specifically, which is the gold standard method. Two samples (Nos. 11 and 25) with negative culture turned positive in the qPCR and LAMP-LFD assays. This was probably because the *Zygosaccharomyces* in these two samples were dead, and the LAMP-LFD and qPCR assays could not discriminate between live and dead cells (Cangelosi and Meschke, 2014).

Although there are no report related to direct identification of *Zygosaccharomyces* from Qiangli loquat Dew samples by using LAMP (Rawsthorne and Phister, 2006; Jaramillo et al., 2015; Wang et al., 2017), the LAMP-LFD was 100 and 92.0% accurately and specifically, when compared with the qPCR assay and the microbiology culture method, respectively in this study. But the qPCR assay takes approximately 2 h to accomplish each test, while the microbiology culture takes much more time. These indicate that the LAMP-LFD assay is an effective tool for the identification of the genus *Zygosaccharomyces* at the field level.

Conclusion

The present study is the first to develop the LAMP-LFD assay for the detection of the genus *Zygosaccharomyces*. The detection limit of the LAMP-LFD assay was the1.0×10^{1} copies/μL and 100% specificity to *Zygosaccharomyces* DNA. In addition, the LAMP-LFD assay can be performed under an isothermal condition without sophisticated equipment in only 40 min (in the present study), and the amplified products can be

directly and visually detected. Furthermore, the results could be easily understood by non-technical people. Based on the high specificity and sensitivity of the LAMP-LFD assay, the investigators detected 25 Qiangli loquat Dew samples with 100% and 92.0% positive agreement, respectively, and negative samples with no positive signal when compared with the qPCR assay and microbiology culture method. In conclusion, the LAMP-LFD assay is simple, fast, sensitive and low-cost, and is an effective tool for the identification of the genus *Zygosaccharomyces* at the field level.

CONFLICT OF INTERESTS

The authors have not declared any conflict of interests.

ACKNOWLEDGEMENT

This work was supported by the Science and Technology Department of Zhejiang Province, China (LGN20C050001).

REFERENCES

Ahmed W, Gyawali P, Sidhu JP, Toze S (2014). Relative inactivation of faecal indicator bacteria and sewage markers in freshwater and seawater microcosms. Letters in Applied Microbiology 59(3):348-354.

Andorrà I, Esteve-Zarzoso B, Guillamón JM, Mas A (2010). Determination of viable wine yeast using DNA binding dyes and quantitative PCR. International Journal of Food Microbiology 144(2):257-262.

Brysch-Herzberg M, Wohlmann E, Fischer R (2020). Zygosaccharomyces seidelii sp. nov. a new yeast species from the Maldives, and a revisit of the single-strain species debate. Antonie Van Leeuwenhoek 113:427-436.

Čadež N, Fülöp L, Dlauchy D, Péter G (2015). Zygosaccharomyces favi sp. nov., an obligate osmophilic yeast species from bee bread and honey. Antonie. Van Leeuwenhoek 107(3):645-654.

Cangelosi GA, Meschke JS (2014). Dead or alive: molecular assessment of microbial viability. Applied and Environmental Microbiology 80(19):5884-5891.

Casey GD, Dobson ADW (2004). Potential of using real-time PCR-based detection of spoilage yeast in fruit juice--a preliminary study. International Journal of Food Microbiology 91(3):327-335.

Duarte FL, Pais C, Spencer-Martins I, Leão C (2004). Isoenzyme patterns: avaluable molecular tool for the differentiation of Zygosaccharomyces species and detection of misidentified isolates. Systematic and Applied Microbiology 27(4):422-436.

Fleet GH (2011). Chapter 5-Yeast Spoilage of Foods and Beverages. The Yeasts (Fifth Edition). Elsevier pp. 53-63. https://doi.org/10.1016/B978-0-444-52149-1.00005-7.

Frisón LN, Chiericatti CA, Aríngoli EE, Basílico JC, Basílico MZ (2015). Effect of different sanitizers against *Zygosaccharomyces rouxii*. Journal of Food Science and Technology 52(7):4619-4624.

Fugelsang KC, Edwards CG (2007). Wine Microbiology: Practical Applications and Procedures (Second Edition). New York: Springer Science 393 p.

General Administration of Quality Supervision, Inspection and Quarantine of the People's Republic of China (2017). SN/T 4675.30-2017 Determination of Zygosaccharomyces bailli from wine for export—SYBR Green I PCR method. Standards Press of China.

General Administration of Quality Supervision, Inspection and Quarantine of the People's Republic of China (2017). SN/T 4780-2017 Detection of spoilage yeasts in food for export-Real-time PCR method. Standards Press of China.

Hara-Kudo Y, Yoshino M, Kojima T, Ikedo M (2010). Loop-mediated isothermal amplification for the rapid detection of Salmonella. FEMS Microbiology Letters 253(1):155-161.

Harrison E, Muir A, Stratford M, Wheals A (2011). Species-specific PCR primers for the rapid identification of yeasts of the genus Zygosaccharomyces. FEMS Yeast Research 11(4):356-365.

Hulin M, Wheals A (2014). Rapid identification of Zygosaccharomyces with genus-specific primers. International Journal of Food Microbiology 173:9-13.

James SA, Stratford M (2011). *Zygosaccharomyces* barker. Kurtzman CP, Fell JW, Boekhout T. The Yeasts, 5th ed. a Taxonomic Study. Elsevier Science. Amsterdam 2:937-948.

Jaramillo MC, Huttener M, Alvarez JM, Homs-Corbera A, Samitier J, Torrents E, Juárez A (2015). Dielectrophoresis chips improve PCR detection of the food-spoiling yeast *Zygosaccharomyces rouxii* in apple juice. Electrophoresis 36(13):1471-1478.

Joon D, Nimesh M, Gupta S, Kumar C, Varma-Basil M, Saluja D (2019). Development and evaluation of rapid and specific sdaA LAMP-LFD assay with Xpert MTB/RIF assay for diagnosis of tuberculosis. Journal of Microbiological Methods 4(159):161-166.

Karaman K, Sagdic O (2019). *Zygosaccharomyces bailii* and *Z. rouxii* induced ethanol formation in apple juice supplemented with different natural preservatives: A response surface methodology approach. Journal of Microbiological Methods 163:105659. doi: 10.1016/j.mimet.2019.105659.

Li L, Zhang SY, Zhang CQ (2019). Establishment of a Rapid Detection Method for Rice Blast Fungus Based on One-Step Loop-Mediated Isothermal Amplification (LAMP). Plant Disease 103(8):1967-1973.

National Food Safety Standard of the People's Republic of China (2016). GB 4789.15-2016 Food Microbiological Examination: Enumeration of Yeasts and Molds. Ministry of Health of P. R. China.

Punati RD, Mallepaddi PC, Poonati R, Maity SN, Sohal JS, Polavarapu KKB, Polavarapu R (2019). Development and evaluation of LAMP-coupled lateral flow device for the detection of MAP in livestock at point of care resource-limited areas. Brazilian Journal of Microbiology 50(4):1105-1114.

Rawsthorne H, Phister TG (2006). A real-time PCR assay for the enumeration and detection of Zygosaccharomyces bailii from wine and fruit juices. International Journal of Food Microbiology 112(1):1-7

Rostamkhani N, Haghnazari A, Tohidfar M, Moradi A (2011). Rapid identification of transgenic cotton (Gossypium hirsutum L.) plants by loop-mediated isothermal amplification. Czech Journal of Genetics and Plant Breeding 47(4):140-148.

Saharan P, Duhan JS, Gahlawat SK (2015). Detection of Pseudomonas fluorescens from broth, water and infected tissues by loop-mediated isothermal amplification (LAMP) method. African Journal of Biotechnology 14(14):1181-1185.

Shi Y, Feng Y, Xu CP, Cheng DQ (2017). Loop-Mediated Isothermal Amplification Assays for the Rapid Identification of Duck-Derived Ingredients in Adulterated Meat. Food Analytical Methods 10:2325-2331.

Syromyatnikov MY, Savinkova OV, Kiryanova SV, Frolov EN, Popov VN (2018). Taqman RT-PCR Analysis for the Identification of the Osmotolerant Yeast *Zygosaccharomyces rouxii*. Applied Biochemistry and Microbiology 54:682-688.

Tournas V, Heeres J, Burgess L (2006). Moulds and Yeasts in fruit salads and fruit juices. Food Microbiology 23(7):684-688.

Tumino S, Tolone M, Parco A, Puleio R, Arcoleo G, Manno C, Nicholas RAJ, Loria G.R (2020). Validation of Loop-Mediated Isothermal Amplification (LAMP) Field Tool for Rapid and Sensitive Diagnosis of Contagious Agalactia in Small Ruminants. Animals (Basel). 10(3):509. https://doi: 10.3390/ani10030509.

Wang H, Hu Z, Long F, Niu C, Yuan Y, Yue T (2015). Characterization of osmotolerant yeasts and yeast-like molds from apple orchards and apple juice processing plants in china and investigation of their spoilage potential. Journal of Food Science 80(8):M1850-860. https://doi: 10.1111/1750-3841.12946.

Wang HX, Hu ZQ, Long FY, Guo CF, Yuan YH, Yue TL (2016). Early detection of *Zygosaccharomyces rouxii*—spawned spoilage in apple

juice by electronic nose combined with chemometrics, International Journal of Food Microbiology 217:68-78.
Wang HX, Sun HM (2019). Potential use of electronic tongue coupled with chemometrics analysis for early detection of the spoilage of *Zygosaccharomyces rouxii* in apple juice. Food Chemistry 290:152-158.
Wang XJ, Min CL, Han PL, Qian RZ (2017). Selection, Identification of a Spoilage Microorganism from Bottle Bulged Qiangli Pipa Syrup and Preliminary Study on its control. Natural Product Research 29(4):635-640.
Wu X, Song ZX, Zhai XW, Zuo L, Mei XR, Xiang R, Kang ZZ, Zhou L, Wang HN (2019). Simultaneous and visual detection of infectious bronchitis virus and Newcastle disease virus by multiple LAMP and lateral flow dipstick. Poultry Science 98(11):5401-5411.
Yuan D, Kong J, Li X, Fang X, Chen Q (2018). Colorimetric LAMP microfluidic chip for detecting three allergens: peanut, sesame and soybean. Scientific Reports 8(1):1-8.
Zhang J, Cao J, Zhu M (2019). Loop-mediated isothermal amplification-lateral-flow dipstick (LAMP-LFD) to detect Mycoplasma ovipneumoniae. World Journal of Microbiology and Biotechnology 35(2):31.
Zhuo XH, Kong QM, Tong QB, Ding HJ, Zhang LS, Lou D, Ding JZ, Zheng B, Chen R, Wang TP, Lu SH (2019). DNA detection of Paragonimus westermani: Diagnostic validity of a new assay based on loop-mediated isothermal amplification (LAMP) combined with a lateral flow dipstick. Acta Tropica 200:105185. https://doi: 10.1016/j.actatropica.2019.105185.
Zuehlke JM, Petrova B, Edwards CG (2013). Advances in the Control of Wine Spoilage by Zygosaccharomyces and Dekkera/Brettanomyces, Annual Review of Food Science and Technology 4:57-78.

Vol. 20(5), pp. 210-215, May, 2021
DOI: 10.5897/AJB2020.17292
Article Number: 6EAF6E166849
ISSN: 1684-5315

http://www.academicjournals.org/AJB

ACADEMIC JOURNALS
expand your knowledge

African Journal of Plant Science

Full Length Research Paper

Synthesis, characterization and antibacterial activity of AgNPS mediated by *Ocimum sanctum*

A. V. Narasimha Swamy[1]* and R. Srinu Venkat Rao[2]

[1]Chemical Engineering Department, Faculty of Engineering, Jawaharlal Nehru Technological University (JNTU), Anantapur, India.
[2]Chemical Engineering Department, Faculty of Engineering, Bule Hora University, Ethiopia.

Received 5 December, 2020; Accepted 29 January, 2021

This research focused on isolation of Silver Nano Particles (AgNPs) using leaf filtrate of *Ocimum sanctum* and evaluation of their antibacterial action against *Bacillus aureus, Staphylococcus aureus and Escherichia coli*. It is known that plant extracts act as reducing agents, stabilizers and as capping agents. The *O. sanctum* plant was specifically selected due to its medicinal properties and abundant availability. The change in color of leaf extract was imminent when the silver nitrate was added to the basil leaf filtrates, indicating the formation of AgNPs. The UV-visible spectroscopy and SEM analysis confirmed the formation of AgNPs. Silver ions and nanoparticles are severely toxic to microorganisms; hence they are used predominantly as antimicrobial agents. The silver nanoparticles that were synthesized from *O. sanctum* leaf extract have exhibited antibacterial activity against *Klebsiella*, *B. aureus*, *S. aureus* and *E. coli* and the activity varied significantly with the different concentrations of silver nitrate used. The nano particles thus developed have been confirmed by UV along with SEM reports. AgNPs sizes varied from 53.3 to 121 nm. It has been observed that most of the plant extracts yielded silver nano particles of size less than 100 nm. However, the present experimental work yielded particle size of about 121 nm from *O. sanctum* leaf extract.

Key words: Silver nano particles (AgNPs), *Ocimum sanctum*, antibacterial activity.

INTRODUCTION

Nano technology is an interesting area of recent investigations with design, formation and structuring of particle in the range of 1-100 nm. Nano particle may be described as a minute matter that configures as a complete segment in relation to its momentum and character. AgNPs were used by professionals earlier in the fourth century in the well-known Roman Lycurgus cup made of dichroic glass, and also in the ninth century in Mesopotamia for developing sparking effect on pot surfaces. The luster comes along with thin layer that encompasses silver and copper NPs cover consistently in the glassy matrix of the ceramic glaze. These NPs were made by skilled people by pouring salts of Cu and Ag and oxides along with vinegar, ochre, and clay on the exterior of pottery that were sparkled previously.

The substance temperature was increased to 600°C in

*Corresponding author. E-mail: swamyn297@gmail.com.

a reducing environment in a kiln. The glaze softens during hot condition, resulting in migration of Cu and Ag ions to outer layers of the glaze surface. The ions migrate back to metals in reduced environment, which congruently form as the nanoparticles resulting in color and light effects. Sheen technique manifest that the previous skilled people had sufficient information of substances. Taniguchi (1974), Kodali and Klabunde (2012), Maynard et al., 2010 of Tokyo University of Science introduced the term “nano-technology” during a conference in 1974. According to his definition, “Nanotechnology comprises, partition, coalition, and deformation process of substances by one atom or one molecule.” It would be appropriate to mention here that Drexler’s (1991) Ph.D. work at the MIT was the first doctoral degree in the area of molecular nanotechnology. The size of nanoparticles would be about 10^{-9}. AgNPs turn out to be significant in research domain because of its innumerable applications. Anti-bacterial activities of silver and silver compounds have been applied in dentil, catheters and burns to mention a few. AgNPs may be made by reducing $AgNO_3$ to Ag ions in the presence of plant isolate. AgNPs production by plant extract is a promising field since plant portion works as reducing and capping agent which is devoid of toxic compounds. The benefits of incorporating plant extract for AgNPs production includes power conservation, profitability and usefulness in safeguarding health. The applications of silver nano particles are many and a few are represented here. Gajendra et al., (2020) studied generation of AgNPS using silver nitrate and stem of *Andrographis paniculata*. The Ag-NPs showed antibacterial activity against *Streptococcus pneumonia*. Bilal et al. (2019) worked on AgNPs using callus extract of basil, and observed their anti- proliferative potential against liver carcinoma cells. Dakshayania et al. (2019) performed studies on synthesis and characterization of AgNPs with *Selaginella bryopteris* plant extract and Ag-NPs are expected to treat thrombotic disorders. Shahnaz and Mussarat (2016) conducted studies on AgNPS using *Salix alba* bark extract and antibacterial activity of these AgNPs was evaluated by disc diffusion, against bacteria isolated from dental plaque. Junwen et al. (2019) generated AgNPs along with an aqueous extract of *Coptis chinensis*, using ecofriendly green-synthesis and found that CC-AgNPs regulated apoptos is using the intrinsic pathway to inhibit A549-cell multiplication. Azam et al. (2017) studied generation of AgNPs from aqueous solution of $AgNO_3$ by using *Nigella arvensis* L. seed extract and generated NPs were also found to exhibit good cytotoxic effect on human breast cancer cells. Le Ouay and Stellacci (2015) worked on the antibacterial activity of AgNPS. Ibrahim (2015) studied about an ecofriendly, profitable, quick and simple method for synthesis of AgNPS using banana peel extract. Vijaya et al., (2013) studied the antigenotoxic effect of generated AgNPS of *Ocimum sanctum* leaf extract against cyclophosphamide. Diptendu and Goutam (2017) studied the generation of AgNPS by using mint leaves extracts and also evaluated their antimicrobial activity. The aim of the studies is to evaluate the antibacterial activity of the AgNPS against *Klebsiella pneumonia, Staphylococcus aureus, Enterobacter aerogenes, Escherichia coli and Pseudomonas aeruginosa*.

MATERIALS AND METHODS

Production of leaf extract

O. sanctum (Basil) leaves were taken and cleaned once with tap water, twice with DW, for removing dirt and dust. 10 g of cleaned leaves were made into small parts and boiled in 100 ml of DW with continuous mixing for 5 min. 10 ml of the filtrate was collected and stored for further use.

Synthesis of AgNPs

AgNPs were prepared by treating 90 ml of 2.0 mM $AgNO_3$ with 10 ml of filtrate. The reaction mixture was maintained at room temperature for 10 min, giving rise to the formation of dark brown color indicating the formation of silver nano particles. This blend was incubated at room temperature in dark conditions. About 1 ml of silver nanoparticle solution was taken (dilution with 1:2 V/V double distilled water) and observed in a UV-Vis Spectrophotometer (BIO SPECTROPHOTOMETER (BL 198) at different time intervals (20, 40, 60 and 80 min). The effect of $AgNO_3$ was monitored by varying its concentration as: 1, 2, 3, and 4 mM, respectively).

Characterization of silver nanoparticles

Silver nanoparticles exhibit unique optical properties. Preparation of AgNPs was ensured by studying the UV-Vis spectra. UV-Vis spectroscopy analysis was carried out on ELICO BIO SPECTROPHOTOMETER (BL 198) at 500 - 600 nm. The double distilled water was used as blank observation and the characteristics of AgNPS were determined by scanning electron microscopy.

Protocol of scanning electron microscope

The exterior pattern of the specimen was tested by employing scanning electron microscope (JEOL Ltd., Japan). A little quantity of powder was disseminated by hand onto a carbon tab attached to an aluminum stub and were smeared with a fine layer (300A) of gold by using POLARON-E 3000 sputter coater. The specimens were inspected by scanning microscope while direct data seized the picture.

Antimicrobial activity of formed AgNPS

The antibacterial work of AgNPs obtained at various $AgNO_3$ concentrations and plant extract was evaluated against *K. pneumonia, S. aureus, E. aerogenes, and P. aeruginosa.* Single cultures of bacteria were sub-cultured in Nutrient Agar. Wells of 5-mm diameter were made using gel puncture. Using a micro pipette, nanoparticle solution was poured into every well of all plates. The diameter of zone inhibition was measured in centimeter subsequent to incubation at 37°C for 24 h.

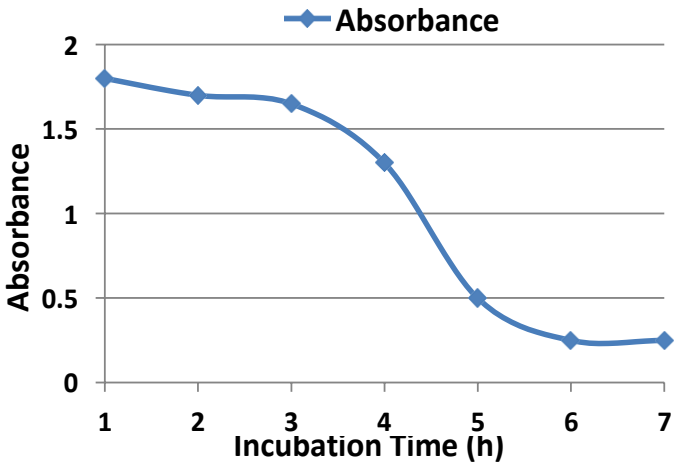

Figure 1. Incubation time.

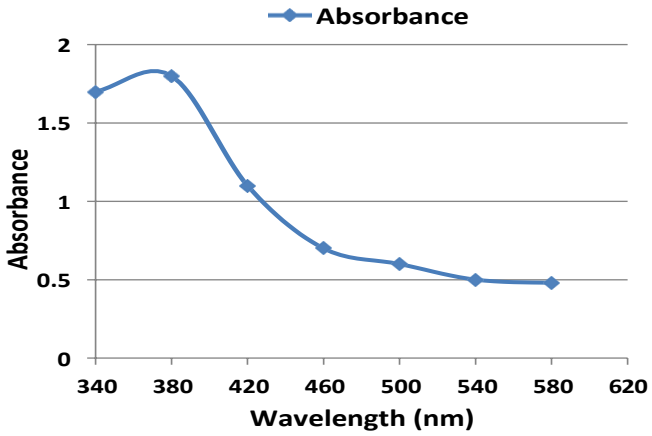

Figure 2. Spectra of leaf extract in 340 to 620 nm.

RESULTS

UV-Visible spectra analysis

The formed AgNPs were confirmed during visual observation by UV-Vis spectrometer. Absorption spectra of AgNPS formed in the solution at various nanometers. The *O. sanctum* isolates work as capping and stabilizing agents with *O. sanctum* having medicinal importance and is widely used in Ayurvedic medicine.

DISCUSSION

Reddish brown color indicates formation of AgNPs which exhibit reddish brown color in aqueous solution because of excitation of surface plasmon-vibrations. The dark brown color is formed in plant extract after addition of silver nitrate indicating the formation of silver nanoparticles as the reaction completes after 24 h (Shahnaz and Mussarat, 2016).

Absorption spectra of AgNPS formed in the solution at 380 nm showed the particle has increasingly sharp peak between 2nd and 3rd h and gradually decreasing with time (Figure 1). The synthesized silver nano particle using *O. sanctum* plant extracts were detected by UV-Vis spectrophotometer at various wavelengths (340, 380, 420, 460, 500, 540, 580 and 620 nm) with increasingly sharp absorbance maximum at 380 nm and gradually decreasing (Figure 2). Graph of time (x-axis) and optical density at 500 nm (y-axis) for various concentrations of $AgNO_3$ are thus plotted (Figure 3).

Antimicrobial analysis

The antibacterial activity of various plant extracts and the silver nanoparticle attained at various $AgNO_3$

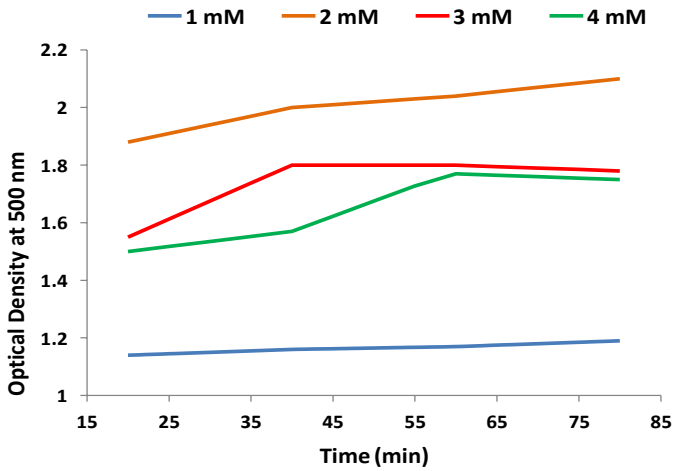

Figure 3. UV-VIS absorption spectroscopy of AgNPS.

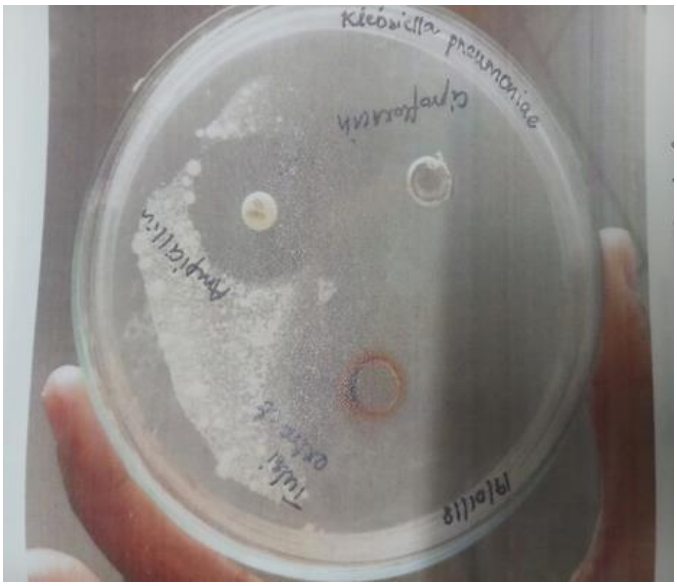

Figure 4. Zone of inhibition values for *Klebsiella pneumonia.*

concentration was evaluated against *K. pneumoniae*. After incubation at 37°C for 24 h, the zone of Inhibition diameter was measured.

The zone inhibitions are shown in Figures 4 to 8 and the corresponding values for different organisms with pertaining antibiotics are shown in Table 1.

SEM analysis

The scanning electron microscopic (SEM) image shows that high density AgNPS produced by *O. sanctum* plant extracts ultimately confirmed the presence of AgNPS (Figure 9). The picture shows consistently spherical silver nano particles having diameter of 53.3 to 121 nm. The nanoparticles stayed apart in the aggregates, showing the stabilization of the NP by a capping agent.

Conclusion

AgNPS prepared from leaf extract showed antibacterial activity against various pathogenic microorganisms and this activity varied with different concentrations of $AgNO_3$ used. The average particle size using *O. sanctum* is in the range of 53.3 to 121 cm. The inhibition zones found in these experiments by the authors are reported here. There is a good scope for these AgNPS in medicinal

Table 1. Zone of inhibition values for different organisms with antibiotics.

S/N	Organism	Disease caused	Antibiotic	Inhibition value CM
1	*Klebsiella pneumonia*	Pneumonia	Ciprofloxacin Ampicillin	50 2.6
2	*Staphylococcus aureus*	Endocarditis	Oxacillin Fluconazole	0.70 0.10
3	*Enterobacter aerogenes*	Infectious and opportunistic bacteria	Erythromycin Clindamycin	0.10 1.90
4.	*Escherichia coli*	Gastero-enteritis	Amoxicillin Ciprofloxacin	1.75 3.50
5	*Pseudomonas aeruginosa*	Skin infections etc.	Gentamycin Ciprofloxacin	3.55 2.40

Figure 5. Zone of inhibition values for *Staphylococcus aureus.*

Figure 7. Zone of inhibition for *Escherichia coli.*

Figure 6. Zone of inhibition values for *Enterobacter aerogenes.*

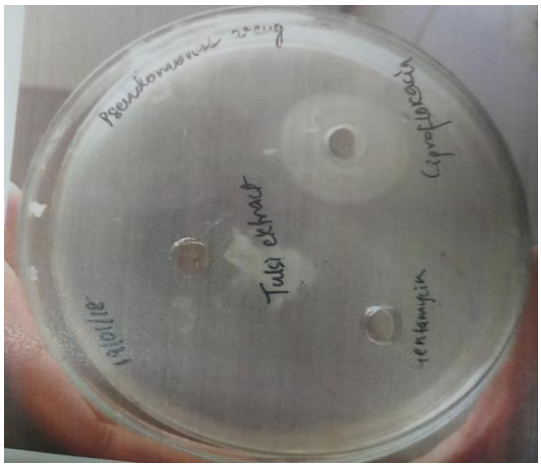

Figure 8. Zone inhibition of values for *Pseudomonas aerureginosa.*

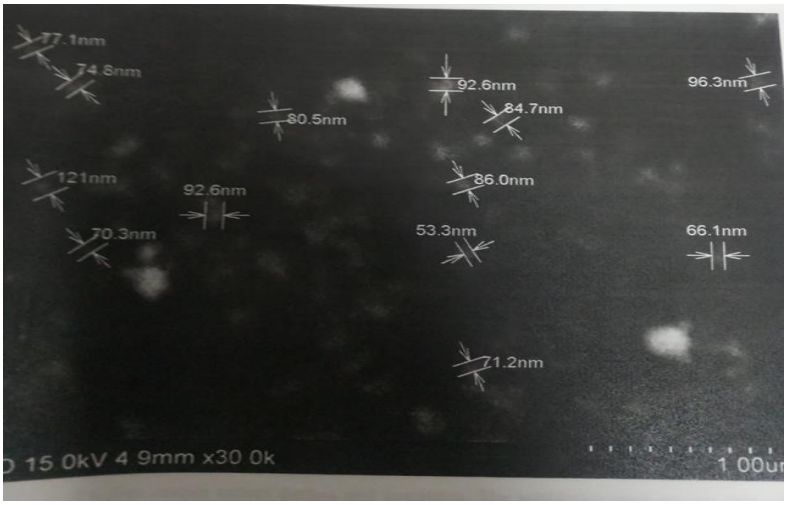

Figure 9. Scanning electron microscope analysis of silver nano particles.

applications also. The antibacterial activities of AgNPS on some pathogenic micro-organisms studied, thus reveals that the green synthesis method for the isolation of nano-particles provide rapid, stable, economic, simple and environmentally friendly mechanism.

CONFLICT OF INTERESTS

The authors have not declared any conflict of interests.

ACKNOWLEDGEMENTS

The authors gratefully appreciate the JNTUA, Anantapuramu, India for providing basic facilities for carrying out this research.

REFERENCES

Azam C, Naser K, Ali F (2017). Biosynthesis, Characterization, Antimicrobial and Cytotoxic Effects of Silver Nanoparticles Using *Nigella arvensis* L. seed extract. Iranian Journal of Pharmaceutical Research 16(3):1167-1175.

Bilal HA, Munazza N, Wali M, Syed SH, Rashda A, Lubna R, Christophe H (2019). A Comparative Evaluation of the Antiproliferative Activity against HepG2 Liver Carcinoma Cells of Plant-Derived Silver Nanoparticles from Basil Extracts with Contrasting Anthocyanin Contents. Biomolecules 9(8):320.

Dakshayani SS, Marulasiddeshwara MB, Sharath Kumar MN, Ramesh G, Raghavendra KP, Devaraja S, Rashmi H (2019). Antimicrobial, anticoagulant and antiplatelet activities of green synthesized silver nanoparticles using Selaginella (Sanjeevini) plant extract. International Journal of Biological Macromolecules 131(6):787-797.

Diptendu S, Goutam P (2017). Green synthesis of silver nano particles using *Mentha asiatica* (mint) Extract and Evaluation of their antimicrobial potential. International Journal of Current Research in Biosciences and Plant Biology 4(1):77-82.

Drexler (1991). Molecular Machinery and Manufacturing with Applications to Computation (PDF) (Ph.D. thesis). Massachusetts Institute of Technology.

Gajendra NM, Prasenjit M,Indranil C, Ganesh CS, Nirmal M, Kaushik G, Nandan B, Sudipta D, Soumitra M (2020). Green synthesis, characterization, antimicrobial and cytotoxic effect of silver nanoparticles using arabinoxylan isolated from Kalmegh. International Journal of Biological Macromolecules 162(11):1025-1034.

Ibrahim HMM (2015) Green Synthesis and Characterization of Silver Nanoparticles Using Banana Peel Extract and Their Antimicrobial Activity against Representative Microorganisms. Journal of Radiation Research and Applied Sciences 8:265-275.

Junwen P, Binfan F, Lifeng J, Taizhen S (2019). Biosynthesis, characterization, and anticancer effect of plant-mediated silver nanoparticles using Coptis chinensis. International Journal of Nanomedicine 14:1969-1978.

Le Ouay B, Stellacci F (2015). Antibacterial activity of silver nanoparticles: A surface science insight. Nano Today 10(3):339-354.

Maynard DA, Bowman DM, Hodge GA (2010). Tracing and disputing the story of nanotechnology. In Hodge, Graeme A, Bowman Diana M. Maynard Andrew D. International hand book on regulating nanotechnologies. Cheltenham, UK: Edward Elgar. p. 54. ISBN 9781849808125.

Shahnaz M,Mussarat K (2016). Green Synthesis of Silver Nanoparticles using Bark Extract of Salix Alba and Its Antimicrobial Effect Against Bacteria Isolated from Dental Plaque. Oriental Journal Chemistry 32(3):1611-1618.

Taniguchi N (1974). On the Basic Concept of 'Nano-Technology', Proceedings of the International Conference on Production Engineering, Part II, Japan Society of Precision Engineering.

Vijaya PP, Rekha B, Mathew AT, Syed MA, Yogananth N, Anuradha V, Kalitha PP (2014). Antigenotoxic effect of green-synthesised silver nanoparticles from sanctum leaf extract against cyclophosphamide induced genotoxicity in human lymphocytes-in vitro. Applied Nanoscience 4:415-420.

Vol. 20(5), pp. 216-229, May, 2021
DOI: 10.5897/AJB2021.17341
Article Number: 06FFF4166859
ISSN: 1684-5315

http://www.academicjournals.org/AJB

ACADEMIC JOURNALS
expand your knowledge

African Journal of Biotechnology

Full Length Research Paper

Optimization of growth media for maximal production of insecticidal vegetative protein (vip3A) from *Bacillus thuringiensis* and its activity against black cutworm (*Agrotis ipsilon*)

Fatimah Alshehrei[1], Doaa K. El-Ghareeb[1,2*], Ashraf El Baz[3], Sameer Qari[1], Hanafy Hamza[4], Hussein H. Abulreesh[5,6], Hesham A. Malak[5,6], Rehab Elmougy[7] and Gamal E. H. Osman[2,5,6]

[1]Biology Department, Al-Jumum University College, Umm Al-Qura University, Makkah, Saudi Arabia.
[2]Agricultural Genetic Engineering Research Institute (AGERI), ARC, Giza, Egypt.
[3]Department of Industrial Biotechnology, Genetic Engineering and Biotechnology Research Institute, University of Sadat City, Sadat City, Egypt.
[4]Microbial Biotechnology Department, Genetic Engineering and Biotechnology Research Institute, University of Sadat City, Sadat City, Egypt.
[5]Department of Biology, Faculty of Applied Science, Umm Al-Qura University, Makkah, Saudi Arabia.
[6]Research Laboratories Centre, Faculty of Applied Science, Umm Al-Qura University, Makkah, Saudi Arabia.
[7]Chemistry Department, Faculty of Science, Mansoura University, Mansoura, Egypt.

Received 15 March, 2021; Accepted 30 April, 2021

Bacillus thuringiensis **is a Gram-positive bacterium naturally found in soil, water and grain dust.** ***B. thuringiensis*** **has been used for decades as biological control for pests of economical and medical importance. The aim of this study was to test different growth media for the optimal production of vegetative insecticidal protein (Vip3) by** ***B. thuringiensis*** **recovered from the local environment. The local** ***B. thuringiensis*** **was grown under shaker conditions in commercially based media and commonly known growth based media to produce Vip3. The optimal C/N ratio for Vip3 production (3.88) was achieved with 20 g/l of glucose as carbon source and 15 g/l of soybean as nitrogen source. Different combinations of carbon and nitrogen sources were examined. Glucose and soybean were the best carbon and nitrogen source, respectively, for maximal Vip3 production. Terrific Broth supplemented with 20 g/l glucose was found to yield optimum growth significantly (*P* <0.01,** ***t*****-test) after 12, 14, 16, 18 and 20 h compared to a formulated medium with optimized C/N ratio of 3.88. The highest vegetative cell count was achieved after 22 h, thus indicating a higher production of Vip3 protein. The method described in this study will facilitate the production of biopesticides in a cost-effective manner.**

Key words: *Bacillus thuringiensis*, bioinsecticides, Vip3, culture media, vegetative protein.

INTRODUCTION

Resistance to inorganic insecticides by many insect species and the ecological damage caused by the toxic effects of insecticides has provided the impetus to seek alternative methods for insect control. This has led to the development of bioinsecticides, which are insecticides using living organisms or their extracts. Bioinsecticides

based on the insecticidal action of *Bacillus thuringiensis* are the most successful and environmental-harmless, commercial and natural alternative to inorganic insecticides (Osman et al., 2015; Siegwart et al., 2015) accounting for 90% of all biopesticides sold worldwide. *B. thuringiensis* is a Gram-positive spore-forming bacterium found naturally in soil, water, dead insects, and grain dust. This bacterium produces crystalline protein inclusions or crystals during sporulation and/or stationary growth phase. The insecticidal host range of *B. thuringiensis* includes Lepidoptera, Coleoptera, Diptera, Acarina, Hymenoptera, protozoa, trematodes, and nematodes (Osman et al., 2015; Nair et al., 2018). Intensive screening programs have yielded new genes that effectively produce vegetative insecticidal proteins (Vip). These are groups of insecticidal proteins that represent the second generation of insecticidal trans-genes, which will complement the novel δ-endotoxins in the future (Osman et al., 2015, 2018; Abulreesh et al., 2012). The Vip3 proteins have been reported to have broad-spectrum insecticidal properties (Osman et al., 2018; Wang et al., 2018).

Vip3 toxins exhibit broad-spectrum insecticidal activity against *Lepidoptera* despite that some of the insecticidal crystal proteins (ICPs) cannot display insecticidal activity against certain insects, such as *Agrotis ipsilon* (Abulreesh et al., 2012; Osman et al., 2018; Yu et al., 2012). Meanwhile, Vip3A transgenic crops have been developed, e.g., “corn MIR162” and cotton “COT102”, which should be valuable for resistance management (Burkness et al., 2010). It is possible for susceptible pests to develop resistance against *B. thuringiensis* due to its long-term use. The Vip3 proteins are suitable candidates in *B. thuringiensis* resistance management as these proteins recognize different receptors than those of Cry proteins (Osman et al., 2018). The homologs of the *vip3A* gene have been detected in approximately 15% of *Bacillus* strains analyzed (Estruch et al., 1996). The Vip3A proteins showed activity against lepidopteran insect larvae including black cutworm (*A. ipsilon*), fall armyworm (*Spodoptera frugiperda*), beet armyworm (*Spodoptera exigua*), tobacco budworm (*Heliothis virescens*) and corn earworm (*Helicoverpa zea*) (Osman et al., 2018, 2019).

It is believed that the higher production costs of commercial bioinsecticidal products of *B. thuringiensis* may, in part, hinder these products from being readily available for consumers at a cheaper price. Researchers worldwide have been developing culture media from cheap source material and optimizing growth conditions for cost-effective large scale growth of *B. thuringiensis* that subsequently yields large scale quantities of insecticidal proteins. The use of coconut cake with mineral salt showed higher production of Cry toxin by *B. thuringiensis* subsp. *israelensis* (Poopathi and Archana, 2012a). The use of corn steep liquor and glucose gave higher spore production of *B. thuringiensis*, thus higher delta endotoxin production (Ernandes et al., 2013). Zou et al. (2016), found that the use of food waste in 75% water content, 2% salt content, less than 5% oil content and pH 7, increased the production of delta endotoxin by *B. thuringiensis* chicken feather with coconut cake (Poopathi and Archana, 2012b), cactus extract in seawater (Hasanain, 2017) and wheat bran (Marzban, 2012) gave promising results in higher delta endotoxin production. Other researcher optimized currently available culture media such as Luria-Bertani broth for increased production of *B. thuringiensis* delta endotoxin (Valicente et al., 2010). Other studies evaluated specific nutrient sources such as soybean (Zribi et al., 2018; Navarro-Mtz et al., 2018) and common sugars (Poopathi and Kumar, 2003) as potential nitrogen and carbon sources for optimal growth of *B. thuringiensis* and subsequently maximal production of insecticidal proteins. The majority of the studies of developing an optimizing growth media for *B. thuringiensis* production were tested by examining the delta endotoxin production. However, studies concerning the optimization of culture media for the production of Vip toxins are sparse.

In this study, we attempted to evaluate the best carbon and nitrogen sources for optimal growth of *B. thuringiensis*, as well as the optimal C/N ratio for maximal production of insecticidal Vip3 protein. An attempt was also made to evaluate and optimize different culture media and growth conditions for the optimal growth and subsequent maximal production of Vip3 toxin. Thus the aim of this study was to evaluate different growth media and condition for the cost-effective, optimal production of vegetative insecticidal protein (Vip3) by *B. thuringiensis* recovered from the local environment.

MATERIALS AND METHODS

Isolation of *B. thuringiensis* from soil and dead larvae

A total of 25 soil samples were collected from different geographical locations of Egypt; Al-Ayat at Giza province, Assiut and Tanta cities. Soil samples were collected from 2 to 5 cm below the ground surface using a shovel. Each soil sample was placed in a plastic bag at ambient temperature. A total of 5 dead larvae of the Egyptian cotton leaf worm *Spodoptera littoralis* (Boisd.) (Lepidoptera: Noctuidae) was collected from the Giza province. Each dead larva was picked using sterile forceps and placed in a sterile plastic screw-cap bottle. All samples were transferred to the laboratory in an ice box and away from direct sunlight, microbiological

*Corresponding author. E-mail: dekeshek@uqu.edu.sa.

Table 1. Media composition for optimum C.N ratio for Vip3 maximal production.

Media composition (g/l)	Media number				
	I	II	III	IV	V
Soybean meal	15	15	15	10	10
Glucose	10	15	20	5	3
K_2HPO_4	1	1	1	1	1
$MgSO_4.7H_2O$	0.05	0.05	0.05	0.05	0.05
$MnSO_4.4H_2O$	0.04	0.04	0.04	0.04	0.04
$FeSO_4.7H_2O$	0.001	0.001	0.001	0.001	0.001
$CaCL_2.9H_2O$	0.2	0.2	0.2	0.2	0.2
$CaCO_3$	1	1	1	1	1
C/N ratio	3.16	4.75	3.8	2.4	1.45
pH adjusted to			7.2		

examinations begun on the same day of sampling. *B. thuringiensis* isolates were recovered from soil and insect samples following the method described by Assaeedi et al. (2011).

Identification of *B. thuringiensis* isolates

B. thuringiensis presumptive isolates were preserved at the Department of Microbial Molecular Biology, Agricultural and Genetic Engineering Research Institute (AGERI), Egypt. The isolates were identified using biochemical methods and 16S rRNA gene sequencing as previously described (EL-Ghareeb et al., 2012; Osman et al., 2013). One isolate was used throughout this study which is registered in the GenBank as *B. thuringiensis entomocidus HD110* (accession number JF811911).

Inoculum preparation

Inocula were prepared by growing *B. thuringiensis* in Luria-Bertani Broth (LB) medium at 28 to 30°C for 24 h. The growth was measured at OD_{600} and the absorbance was adjusted to a value of 0.9.

Vegetative cell count

Briefly, 100 µl of an overnight grown culture of *B. thuringiensis* was added to 900 µl of sterile water and mixed thoroughly. Then, l00 µl of this suspension was transferred to 900 µl of sterile water and mix thoroughly. The serial dilution was repeated until a dilution of 10^{10} was obtained. This is called the dilution factor. Each dilution was plated on LB agar medium and all the plates were incubated at 30°C for 48 h. The plates that showed 30 to 300 colonies are ideal for counting. Five plates were selected and the average CFUs per plate were counted. The number of viable cells per milliliter of the sample was calculated by multiplying the average number of colonies counted per plate by the reciprocal of the dilution factor (Bapat et al., 2006).

Determination of the optimum C/N ratio for the vegetative insecticidal protein (Vip3) production by *B. thuringiensis*

Five different media containing glucose (carbon source) and soybean meal (nitrogen source) were tested to select the optimum C/N ratio for Vip3 production media composition (Table 1). Other components such as K_2HPO_4, $MgSO_4.7H_2O$, $MnSO_4.4H_2O$, $FeSO_4.7H_2O$, $CaCl_2.9\ H_2O$ and $CaCO_3$ were added to the growth media and finally, the pH was adjusted to 7.2 before sterilization. Flasks with 50 ml of each medium were inoculated with 1.0 ml of inoculum, incubated at 30°C, and agitated at 200 rpm for 12, 14, 18, and 24 h.

Determination of the optimum carbon source for the vegetative insecticidal protein (Vip3) production by *Bt*

Five different media containing different carbon sources (glucose, fructose, sucrose, lactose, and corn starch) were examined for the optimum carbon source for Vip3 production (Table 2). Soybean meal was used as the nitrogen source and other components such as K_2HPO_4, $MgSO_4.7H_2O$, $MnSO_4.4H_2O$, $FeSO_4.7H_2O$, $CaCl_2.9\ H_2O$ and $CaCO_3$ were added to the medium. Finally, the pH of the medium was adjusted to 7.2 before sterilization. Flasks with 50 ml of each medium were inoculated with 1.0 ml of inoculum, incubated at 30°C, and agitated at 200 rpm for 12, 14, 18 and 24 h.

Determination of the optimum nitrogen source for the vegetative insecticidal protein (Vip3) production by *B. thuringiensis*

Three different media with different nitrogen sources (soybean meal, ammonium sulfate, and urea) were evaluated for the optimum nitrogen source for Vip3 production (Table 3). Glucose was used as the carbon source and other components such as K_2HPO_4, $MgSO_4.7H_2O$, $MnSO_4.4H_2O$, $FeSO_4.7H_2O$, $CaCl_2.9H_2O$, and $CaCO_3$ were added to the growth media and finally, the pH was adjusted to 7.2 before sterilization. Flasks with 50 ml of each medium were inoculated with 1.0 ml of inoculum, incubated at 30°C, and agitated at 200 rpm for 12, 14, 18 and 24 h.

Evaluation of common growth media for optimal production of (Vip3) protein

Luria-Bertani Broth

Luria-Bertani (LB) medium (Estruch et al., 1996) was prepared by dissolving tryptone 10.0 g, yeast extract 5.0 g, sodium chloride 5.0 g in 1 L of deionized water. The final pH of the medium was

Table 2. Media composition for optimal carbon source for the maximal production of Vip3 protein.

Media composition (g/l)	Media number				
	VI	VII	VIII	IX	X
Soybean meal	15	15	15	15	15
Glucose	20	-	-	-	-
Fructose	-	20	-	-	-
Sucrose	-	-	20	-	-
Lactose	-	-	-	20	-
Cornstarch	-	-	-	-	20
K_2HPO_4	1	1	1	1	1
$MgSO_4.7H_2O$	0.05	0.05	0.05	0.05	0.05
$MnSO_4.4H_2O$	0.04	0.04	0.04	0.04	0.04
$FeSO_4.7H_2O$	0.001	0.001	0.001	0.001	0.001
$CaCL_2.9H_2O$	0.2	0.2	0.2	0.2	0.2
$CaCO_3$	1	1	1	1	1
C/N ratio	3.16	4.75	3.8	2.4	1.45
pH adjusted to			7.2		

Table 3. Media composition for optimum nitrogen source for maximal production of Vip3 protein.

Media composition (g/l)	Media number		
	XI	XII	XIII
Soybean meal	15	-	-
Ammonium sulfate	-	15	-
Urea	-	-	15
Glucose	20	20	20
K_2HPO_4	1	1	1
$MgSO_4.7H_2O$	0.05	0.05	0.05
$MnSO_4.4H_2O$	0.04	0.04	0.04
$FeSO_4.7H_2O$	0.001	0.001	0.001
$CaCL_2.9H_2O$	0.2	0.2	0.2
$CaCO_3$	1	1	1
C/N ratio	3.16	4.75	3.8
pH adjusted to		7.2	

adjusted to 7.0. Flasks with 50 ml of the medium were inoculated with 1.0 ml of inoculum, incubated at 30°C, and agitated at 200 rpm for 12, 14, 18 and 24 h.

Terrific Broth

Terrific Broth (TB) medium (Estruch et al., 1996), was prepared by dissolving tryptone (12.0 g), yeast extract (24.0 g) and glycerol (4 ml) in 1 L of deionized water. After autoclaving, 100 ml of the filter-sterilized solution of 0.17 M KH_2PO_4 and 0.72 M K_2HPO_4 was added. Flasks with 50 ml of the medium were inoculated with 1.0 ml of inoculum, incubated at 30°C, and agitated at 200 rpm for 12, 14, 18 and 24 h.

Evaluating the effect of Terrific Broth supplemented with various concentrations of glucose on the production of Vip3 protein

This medium was prepared by adding different concentrations of glucose (5, 10, 20, 25 and 30 g/l) to the earlier-described formula of terrific broth. Flasks with 50 ml of each medium were inoculated with 1.0 ml of inoculum, incubated at 30°C, and agitated at 200 rpm for 12, 14, 18 and 24 h.

Comparison between formulated and common growth media for the Vip3 production by *B. thuringiensis*

Terrific Broth supplemented with 20 g/l glucose as the common

growth medium (medium 3) and the formulated medium (No. III) were compared to select the optimum medium for Vip3 production by *B. thuringiensis.* Flasks were filled with 50 ml of each medium and sterilized by autoclaving at 120°C for 20 min. Each flask was inoculated with 1.0 ml of inoculum, incubated at 30°C, and agitated at 200 rpm for 24 h.

Glucose analysis

Glucose was analyzed using the Glucose (GOD-PAP) Vitro Scient kit (Vitro Scient, Cairo, Egypt). Each sample was mixed with the R_2 buffer (phosphate buffer 100 mmol l^{-1}, phenol 10 mmol l^{-1}, 4-aminoantipyrine 0.3 mmol l^{-1}, glucose oxidase 1000 U l^{-1} and peroxidase 700 U l^{-1}) incubation was at 37°C for 10 min or 15 min at 20 to 25°C. The absorption spectrum was measured from 500 to 550 nm.

Bioassay

The bioassay was performed by growing the bacteria overnight in LB broth at 30°C, the growth was measured at OD_{600} and the absorbance was adjusted to a value of 0.9, to ensure that the bacteria do not enter the sporulation phase whereby delta endotoxin is produced, an OD equal to 0.9 ensures that the bacteria are in the vegetative growth stage by which Vip proteins are produced (Osman et al., 2015). The bioassay was performed by applying each inoculated medium samples on the top of a semi-artificial insect diet. Ten larvae (3 replicates) of the first instars of *A. ipsilon* were placed on each cup (5.5 cm in diameter and 3.3 cm in height), and a 100-µl aliquot of the toxin was tested. Incubation was performed at 26°C for 3 days as described earlier by Levinson and Navon (1969) and mortality was scored daily.

Statistical analysis

A nonparametric t-test was used to compare the vegetative cell counts between Luria-Bertani Broth and Terrific Broth, the same test was used to compare the vegetative cell counts between formulated medium no. III and Terrific Broth.

RESULTS

Determination of the optimum C/N ratio for the vegetative insecticidal protein (Vip3) production by *B. thuringiensis*

The final pH values of all 5-tested media ranged from 5.9 up to 6.6 after 18 h. After 24 h, the pH was decreased to 5.4 in medium II, 5.9 in medium I, and to 5.7 in medium III (Figure 1A). The highest vegetative cell count was observed in medium III (9.5×10^{10} CFU) and it became decreased to 4×10^{10} CFU in medium V after 24 h (Figure 1B). The highest mortality (100%) was recorded after 24 h in medium III, while medium V gave the lowest mortality (40%) and the lowest vegetative cell count 4×10^{10} CFU after 24 h (Figure 1C). In this respect, medium III that contained 20 g/l glucose and 15 g/l soybean (C/N ratio = 3.88) seemed to be the choice for optimum production of Vip3 proteins.

Determination of the optimum carbon source for the vegetative insecticidal protein (Vip3) production by *B. thuringiensis*

The pH values ranged from 5.4 to 6.5 for all 5 tested media after 24 h (Figure 2A). Medium VI (containing glucose) gave the highest vegetative cell count of 9.2×10^{10} CFU after 24 h, while medium X, which contained corn starch as a carbon source, gave the lowest vegetative cell count 5.1×10^{10} CFU after 24 h (Figure 2B). Medium VI containing glucose as a carbon source gave the highest mortality rate (100%) after 24 h. While medium VII, which contained fructose, gave a mortality rate of 85% after 14 up to 24 h. Medium VIII and IX, which contained sucrose and lactose, gave 70% mortality rate after 24 h, while medium X, which contained cornstarch, gave 50% mortality rate after 24 h (Figure 2C). The results indicated that glucose is the optimum carbon source for maximal production of Vip3 proteins.

Determination of the optimum nitrogen source for the vegetative insecticidal protein (Vip3) production by *B. thuringiensis*

The pH values ranged from 5 to 6.6 at all the 3 media after 24h (Figure 3A). Medium XI which contained soybean meal as the nitrogen source gave the highest vegetative cell count of 9.4×10^{10} CFU after 24 h, while medium XIII containing urea as the nitrogen source gave the lowest vegetative cell count of 6.5×10^{10} CFU after 24 h (Figure 3B). Medium XI gave the highest mortality rate (100%) after 24 h at the medium containing soybean meal as the nitrogen source; whereas medium XII, which contained ammonium sulfate as the nitrogen source, gave the mortality rate of 70% after 18 h and decreased to 60% after 24 h. The medium XIII gave 70% mortality after 24 h (Figure 3C). In general, soybean gave optimum results for the production of Vip3 proteins.

Evaluation of common growth media for optimal production of (Vip3) protein

The effect of using Luria-Bertani Broth and Terrific Broth for the growth of *B. thuringiensis* was expressed by changes in pH, vegetative count, and mortality. Obtained results showed that the pH of the 2 media was within the range and showed no bacterial mortality (Figure 4A and B and Table 4). However, the vegetative cell count reached its maximum only after 14 h in Terrific Broth with a 100% mortality rate (Figure 4B and Table 4). While in LB, the vegetative cell count reached the maximum after 24 h with an 80% mortality rate (Figure 4A and Table 4). Figure 4A and B and Table 4 show that the Terrific Broth was significantly ($P < 0.01$, *t*-test) better than the LB medium, which may be due to the presence of a higher amount of glucose (5, 10, 20, 25 and 30 g/l) in the Terrific Broth.

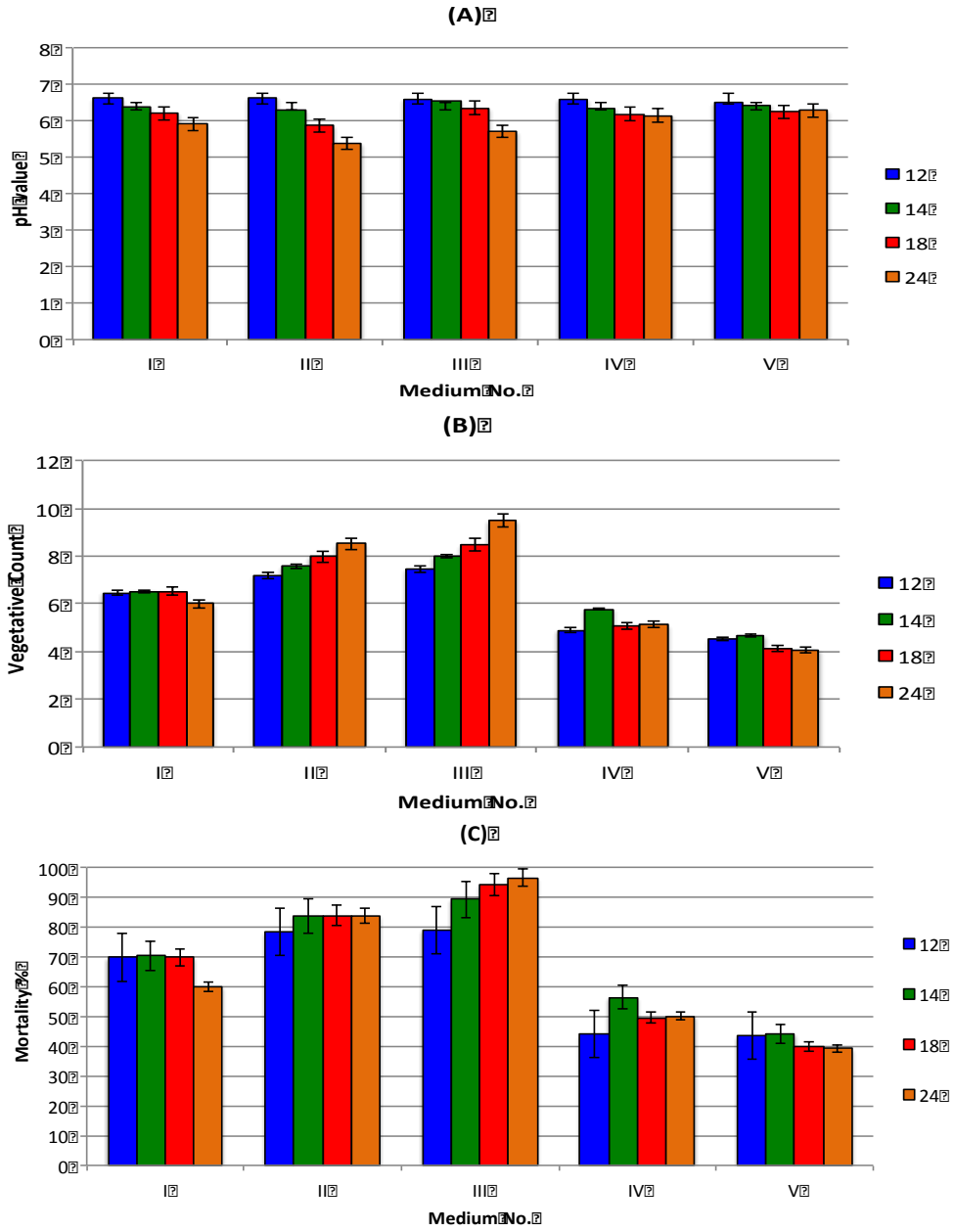

Figure 1. Determination of the optimum C/N ratio for maximal production of Vip3 protein, expressed in (**A**) pH changes; (**B**) vegetative count (x 10^{10}) and (**C**) mortality %, measured after 12, 14, 18 and 24 h of shaking incubation.

Effect of using terrific broth supplemented with different glucose concentrations on the growth of Vip3 toxin production by *B. thuringiensis*

The results showed that the vegetative cell count and mortality rate were increased and reached 8.0 ×10^{10} CFU and 100% mortality after 14 h in Terrific Broth supplemented with 20 g/l of glucose. It is interesting to note that when glucose was increased to more than 20 g/l in medium 4 and 5, the vegetative cell count decreased to 5.4×10^{4} CFU with 50% mortality rate (Figure 5A, B and C).

Comparison between the best formulated medium and common growth medium on the growth of Vip3 toxin production by *B. thuringiensis*

Obtained results showed that medium III (20 g/l glucose + 15 g/l soybean) was the best formulated medium; whereas medium 3 (Terrific Broth supplemented with 20 g/l glucose) was the best common growth medium. A

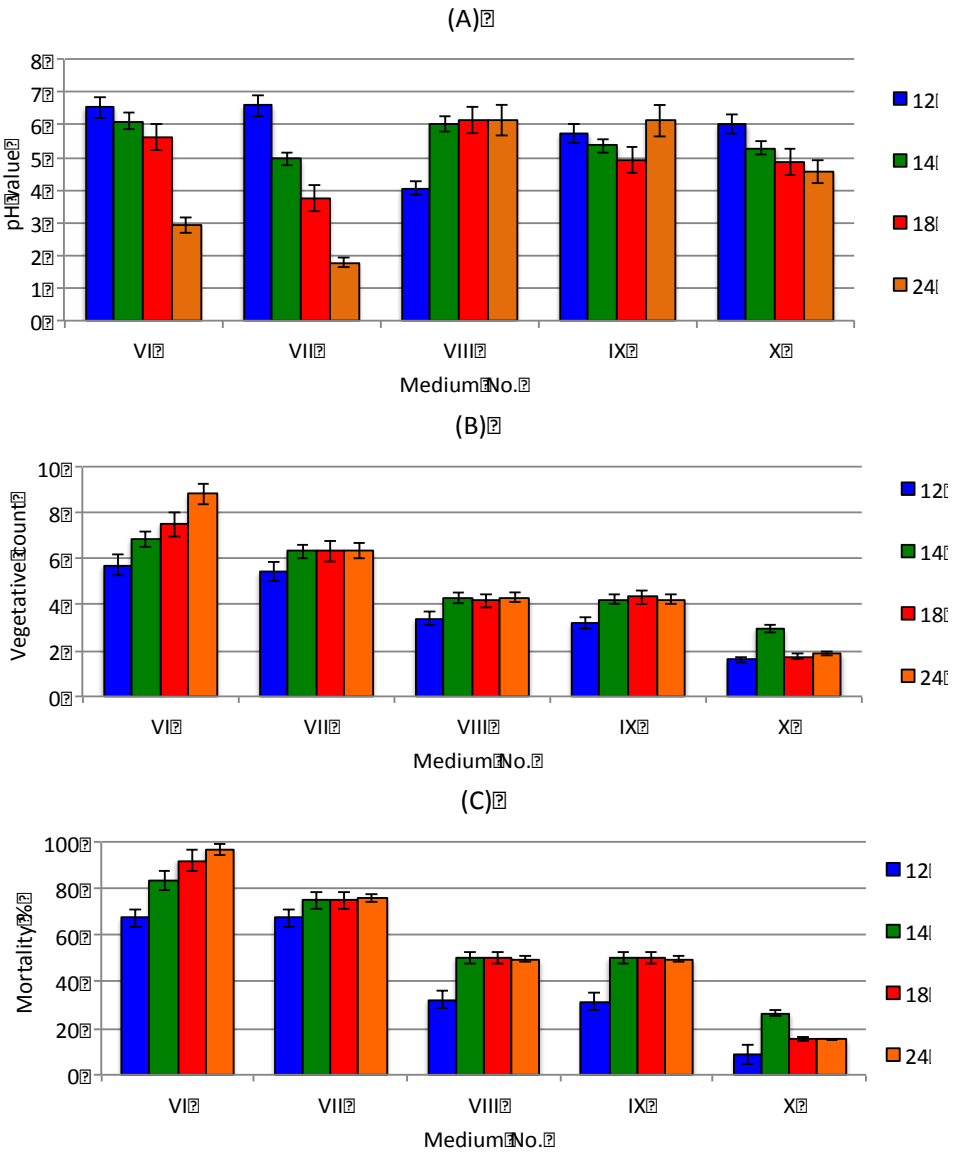

Figure 2. Determination of the optimum carbon source for maximal production of Vip3 protein, expressed in (**A**) pH changes; (**B**) vegetative count (x 10^{10}) and (**C**) mortality %, measured after 12, 14, 18 and 24 h of shaking incubation.

comparison between the 2 media was important to select the optimum growth media for Vip3 production expressed by changes in pH (Figure 6A and Table 5), vegetative cell count, residual glucose, and mortality rate. The highest vegetative cell count of 8.4 ×10^{10} CFU in medium III was only reached after 24 h; however, medium 3 gave its highest vegetative cell count of 10 ×10^{10} after 22 h (Figure 6B and Table 5). Overall, significant differences ($P < 0.01$, *t*-test) were noted in terms of vegetative cell count between the 2 media, where medium 3 was superior in yielding 10-folds higher vegetative cell count after 12, 14, 16, 18 and 20 h (Table 5). Bacterial mortality rate of 100% was reached in medium III after 24 h, while in medium 3, the mortality rated reached 100% after 14 h (Figure 6C and Table 5). The residual glucose decreased from 20 to 12 g/l in medium III. However, medium 3, residual glucose reduced to 1.833 after 24 h (Figure 6D and Table 5). Therefore, Terrific Broth supplemented with 20 g/l glucose showed more superiority than the formulated medium III (20 g/l glucose + 15 g/l soybean) for the maximal production of Vip3 proteins.

DISCUSSION

Recently the *B. thuringiensis* has been selected as the

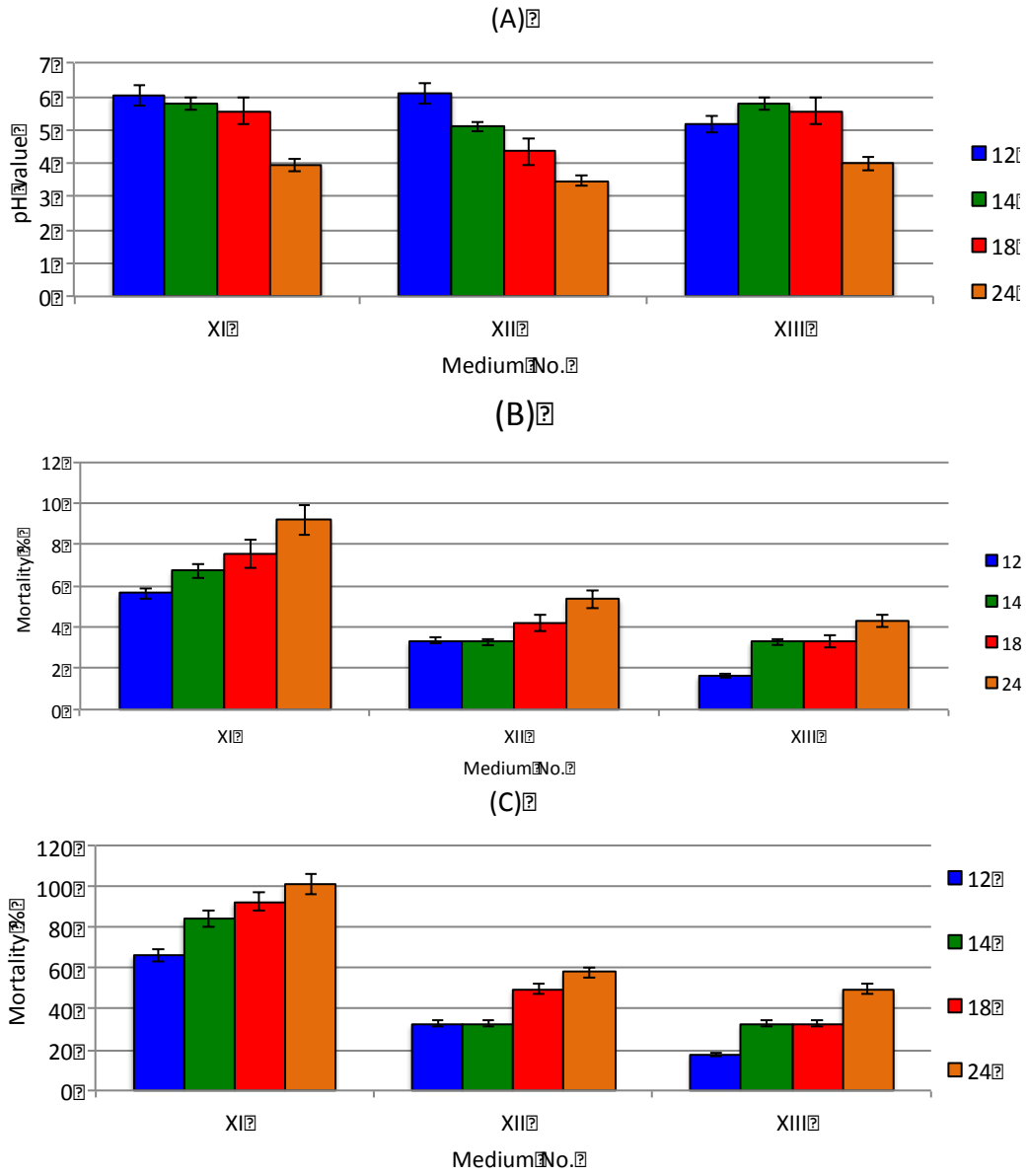

Figure 3. Determination of the optimum nitrogen source for maximal production of Vip3 protein, expressed in (A) pH changes; (B) vegetative count (x 10^{10}) and (C) mortality %, measured after 12, 14, 18 and 24 h of shaking incubation.

most successful commercial biopesticide used worldwide. It has been applied to protect crops and plants, and it is also expected to replace inorganic insecticides in several areas of application (Jouzani et al., 2017). Vip3A is a novel toxin with a broad spectrum of insecticidal activity and with a mode of action different from Cry1A toxins (Osman et al., 2015, 2018; Wang et al., 2018). Vip3 promises to be a new measure to kill insect pests.

Optimization of a cost-effective process of Vip3A production from *B. thuringiensis* necessitates the development of a fermentation method that allows the production of high amounts of Vip3a protein toxin. The aim of this study was to investigate the possibilities of supplying adequate amounts of glucose and other nutrients to maximize cell growth and Vip3 production using *B. thuringiensis.*

Previous studies (Dulmage, 1971; Gopinathan et al., 2016) showed that the C/N ratio was the key for *B. thuringiensis* vegetative toxins production. Thus, we optimized the C/N ratio to optimum level for maximal production of Vip3 proteins. The following ratios (1.45-4.75) were tested and the selection of the medium components was carried out based on the following considerations: (i) soybean meal was used as the

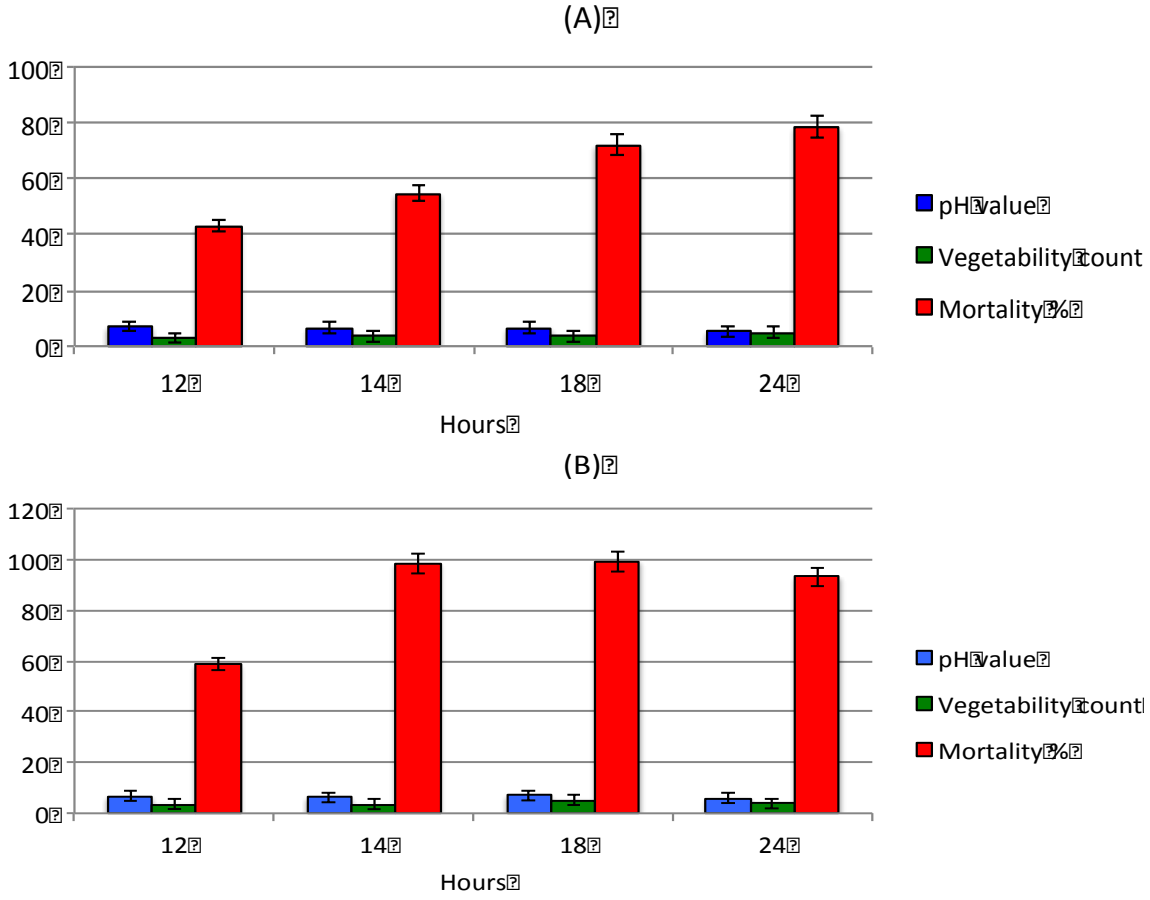

Figure 4. Comparison between LB (A) and Terrific broth (B) for the maximal production of Vip3 proteins expressed in pH changes, vegetative counts (x 10^{10}) and mortality percentage measured after 12, 14, 18 and 24 h of shaking incubation.

Table 4. Comparison between LB and TB for maximal production of Vip3 protein.

Incubation time (h)	pH		Vegetative cell count		Mortality %	
	LB	TB	LB	TB	LB	TB
12	5.68	6.82	2.2×10^4	3.2×10^9	44	60
14	5.67	6.5	2.8×10^4	4.6×10^{10}	56	100
18	5.58	6.2	3.5×10^4	4.1×10^{10}	72	100
24	5.2	5.9	4.6×10^4	3.5×10^{10}	80	95
P			<0.01			

LB = Luria-Bertani, TB = Terrific Broth. *P* = is the *t*- test, for testing the null hypothesis that the vegetative cell count of *Bt* is similar when using LB or TB. Significant difference is observed in the vegetative cell count at 0.01 level, thus rejecting the null hypothesis, and terrific broth proved to be a better medium for maximal growth of *Bt*, and subsequently, maximal production of Vip3 protein.

nitrogen source as it was cheap and locally available; (ii) glucose was used as the carbon source as it is easily metabolized and easily available; (iii) potassium phosphate was used as the phosphate source; (iv) calcium carbonate was used as the buffering agent; (v) magnesium sulfate, manganese sulfate, ferrous sulfate, and calcium chloride were used as sources of trace elements. By increasing time, the vegetative cell count was increased in medium III (that is, from 7.4×10^{10} CFU after 12 h to 9.5×10^{10} CFU after 24 h); whereas, in

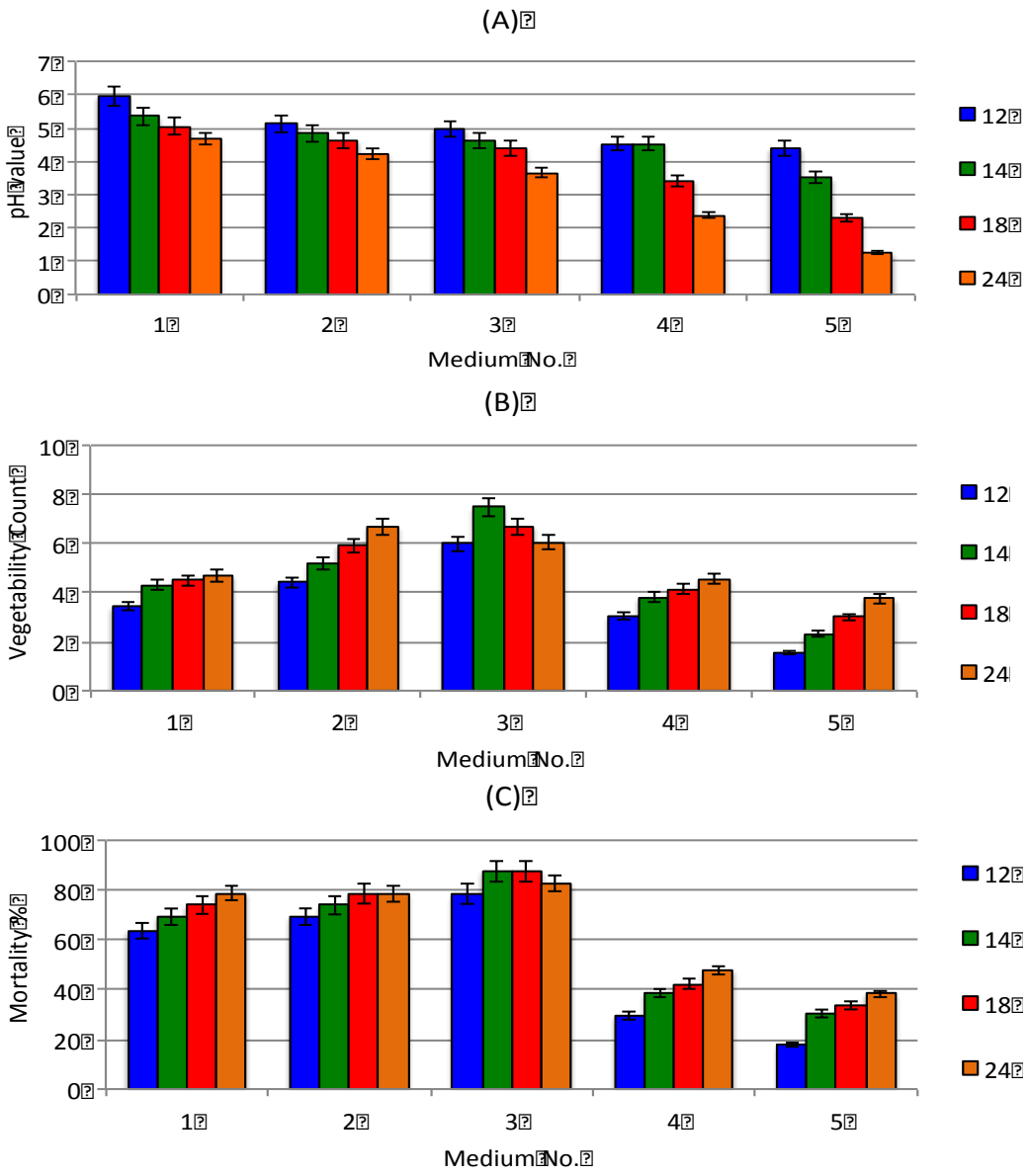

Figure 5. Evaluation of Terrific broth supplanted with various concentrations of glucose; 1 (5 g/l); 2 (10 g/l), 3 (20 g/l); 4 (25 g/l) and 5 (30 g/l) for the maximal production of Vip3 proteins, expressed in (A) pH changes, (B) vegetative counts (x 10^{10}) and (C) mortality percentages, measured after 12, 14, 18 and 24 h in shaking incubation.

medium II, the vegetative cell count increased from 7.2 × 10^{10} CFU after 12 h to 8.5× 10^{10} CFU after 24 h (Figure 1B). In medium I, IV, and V, the total cell count was constant during the growth period (Figure 1B), which means that the C/N ratios are not suitable for Vip3 production. These were also reflected in the results of mortality assay as these media (I, IV, and V) showed the lowest mortalities (Figure 1C). Based on the results obtained, we suggest that the C/N ratio of 3.88 was the best ratio for vegetative protein production. These results were also in agreement with the results reported by Dubois et al. (2019) who stated that the carbon content should be higher than the nitrogen content to obtain a higher vegetative count, delay sporulation, and crystal formation in *B. thuringiensis* cultures.

Different carbon sources, including complex sugars such as cornstarch and disaccharides (e.g. lactose and sucrose) were examined for optimum growth of *B. thuringiensis*. The highest vegetation cell count was obtained by glucose 7.8 × 10^{10} CFU with the highest mortality rate of 100%, while cornstarch showed the lowest vegetative count of 5.1 ×10^{10} CFU and a mortality rate of 50%. This may be due to the fact that glucose is rapidly metabolized and is known to repress the formation

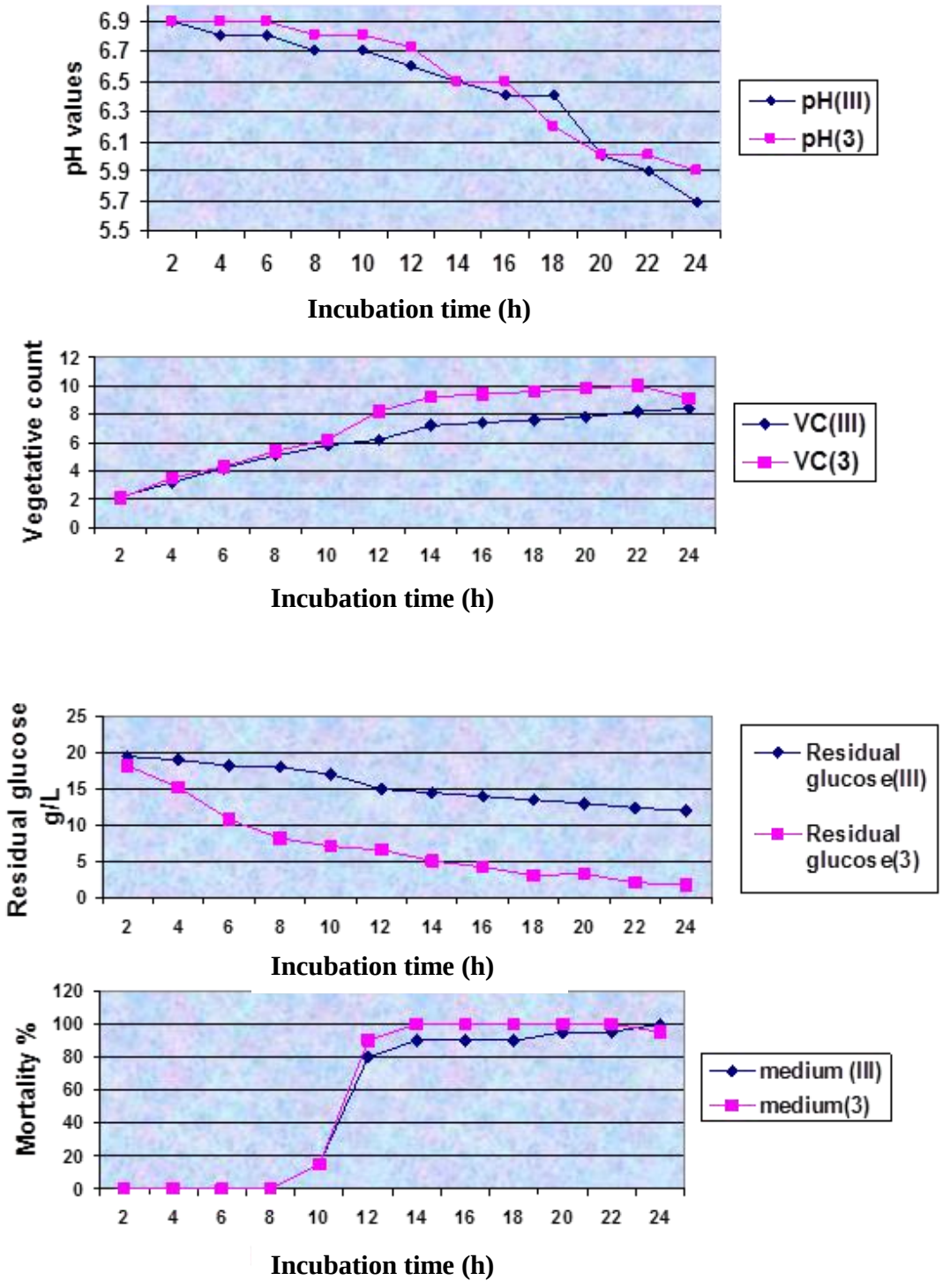

Figure 6. Comparison between formulated medium III (20 g/l glucose + 15 g/l soybean) and Terrific Broth supplemented with 20 g/l glucose (medium 3) for the maximal production of Vip3 proteins, expressed in (A) pH changes, (B) vegetative counts (x 10^{10}), (C) residual glucose and (D) mortality percentages, measured at different incubation hours in shaking cultures.

of proteolytic and Tri Carboxylic Acid (TCA) cycle enzymes in *Bacillus* (Doi, 1989), which supply precursor metabolites for the formation of sporulation-phase-associated protein (Berbert et al., 2008).

Different nitrogen sources were also examined including soybean, organic soluble source like urea, and inorganic

Table 5. Comparison between formulated media and TB with 20 g/l glucose for maximal production of Vip3 protein.

Media type	Formulated media (III)				Terrific Broth with 20 g/l glucose (3)			
Incubation time (h)	pH	Veg. count	Residual glucose (g/l)	Mortality %	pH	Veg. count	Residual glucose (g/l)	Mortality %
0	7.2	5.2×10^2	20	0	7.2	6.1×10^2	20	0
2	6.9	2.2×10^3	19.5	0	6.9	2.1×10^3	18.23	0
4	6.8	3.2×10^4	19	0	6.9	3.5×10^4	15.22	0
6	6.8	4.2×10^5	18.2	0	6.9	4.3×10^5	10.86	0
8	6.7	5.1×10^6	18	0	6.8	5.4×10^6	8.2	0
10	6.7	5.8×10^7	17	15	6.8	6.2×10^7	7.1	15
12	6.6	6.2×10^8	15	80	6.72	8.2×10^9	6.66	90
14	6.5	7.2×10^9	14.5	90	6.5	9.2×10^{10}	5.1	100
16	6.4	7.4×10^9	14	90	6.5	9.4×10^{10}	4.2	100
18	6.4	7.6×10^9	13.5	90	6.2	9.6×10^{10}	3.1	100
20	6.0	7.8×10^9	13	95	6.0	9.8×10^{10}	3.3	100
22	5.9	8.2×10^{10}	12.4	95	6.0	10×10^{10}	2.1	100
24	5.7	8.4×10^{10}	12	100	5.9	9×10^9	1.83	95
P		0.01				0.01		

P = is the *t*- test, for testing the null hypothesis that the vegetative cell count of *Bt* is similar when using formulated medium (III) or Terrific Broth supplemented with 20 g/l glucose (3). Significant difference is observed in the vegetative cell count at 0.01 level, thus rejecting the null hypothesis, and Terrific Broth supplemented with 20 g/l glucose (medium 3) proved to be a better medium for maximal growth of *Bt*, and subsequently, maximal production of Vip3 protein.

source (ammonium sulfate). The soybean meal gave the highest vegetative count when used as the nitrogen source; similar observation was made by Sadek (2000) and Smitha et al. (2019). The vegetative cell count was increased in medium I (that is from 7.4×10^{10} CFU after 12 h to 9.5×10^{10} CFU after 24 h). On the other hand, the vegetative cell counts in medium number XI and XII (Table 3) were very poor with high mortalities (Figure 3A, B and C). Morris et al. (1997) stated that among the legumes, soybean meal showed the highest relative economic yield of biomass and relative potency against bertha armyworm larvae.

The experimental pH was within 5 to 6.6 and did not show any negative effect on the growth, which is in agreement with the results by Morris et al. (1997) who suggested that the pH within 5 to 6 did not produce any recoverable spore-crystal complex. Also, Bernhard (1993) concluded that *Bt* was not particularly sensitive to pH and growth will occur between pH 5.5 and 8.5 with optimum growth between pH 6.5 and 7.5.

Luria-Bertani (LB) and Terrific Broth (TB) media are nutrient-rich media primarily used for the growth of bacteria. They are composed of the following ingredients: (i) peptides and casein peptones; (ii) vitamin (including B vitamin); (iii) trace elements (e.g., nitrogen, sulfur, magnesium); and (iv) minerals. Peptides and proteins are provided by tryptone. Vitamin and certain trace elements are provided by yeast extract. Sodium ions responsible for transport and osmotic balance are provided by sodium chloride. In addition, Terrific Broth contains glycerol, which is a cheap carbon source (Estruch et al., 1996).

A comparison between LB and TB media for the growth of *B. thuringiensis* was expressed by changes in pH, vegetative count, and mortality rates were included in this study. Obtained results showed that the pH of the two media was within the range and showed no bacterial mortality, this in agreement with the results of Bernhard (1993). However, the vegetative count reached its maximum only after 14 h in Terrific Broth with a 100% mortality rate. While in the LB, vegetative cell count reached the maximum after 24 h with 80% mortality rate. This is, probably, because the TB contained a higher amount of glucose than the LB medium, which helped TB to reach a high vegetative count within 14 h. Thus, *B. thuringiensis* growing in TB may produce Vip3 proteins faster than growing in LB medium.

Exploring the supplementation of TB with varied concentrations of glucose, showed that the vegetative cell count and mortality rates were increased and reached 8.0×10^{10} CFU and 100% mortality rate after 14 h in TB containing 20 g/l of glucose. It is interesting to note that when glucose was increased to more than 20 g/l in media 4 and 5 the vegetative cell count decreased to 5.4×10^4 CFU with 50% mortality rate. A similar result was also noted by Holmberg et al. (1980) who reported that a high concentration of nutrients inhibits the growth of *B. thuringiensis* var. *thuringiensis* by reducing sporulation and releasing of toxins. However, the opposite results were observed by Berbert-Molina et al. (2008) who stated that for the growth of *B. thuringiensis* var. *kurstaki,* a

maximum glucose concentration (56 g/l) can be utilized. Most of the studies state that the substrate concentration should not exceed 23 g/l. The main problem of adding higher glucose concentrations in the medium, however, is the formation of acetate, which in un-buffered media causes a substantial drop in pH. Phosphate buffer helps control the growth rate by gradual glucose feeding rather than just putting in all the glucose at once.

As Terrific Broth supplemented with 20 g/l glucose (medium 3) showed a promising optimum growth of *B. thuringiensis;* and C/N ratio for Vip3 production was shown to achieve increased growth of the bacteria (medium III), thus, a comparison between the two media on the basis of pH, vegetative cell count, residual glucose and mortality rates was performed every 2 h for 24 h. In medium III, the vegetative cell count increased from 2.2 $\times 10^3$ CFU (after 2 h) to 8.4 $\times 10^{10}$ CFU (after 24 h), while in medium 3 (terrific broth + 20 g/l glucose) vegetative cell counts were 2.1 $\times 10^3$ CFU initially but reached 10 $\times 10^{10}$ CFU within 22 h. Bacterial mortality rate was (100%) in medium III after 14 h. An interesting thing to note was the residual glucose in both the medium after 24 h. Medium III consumed only 6.5 g of glucose, while medium 3 consumed 18.2 g of glucose. Although both the media (medium 3 and medium III) exhibited similar bacterial growth, medium 3 showed 100% bacterial mortality rate after 14 h and consumed a high amount of glucose. Therefore, medium 3 (TB with 20 g/l glucose) was better than the formulated medium III (20 g/l glucose and 15 g/l soybean) and thus we suggest to consider it as the low-cost medium of choice for maximal production of Vip3.

Conclusion

An optimized C/N ratio of 3.88 as glucose and soybean that served as carbon and nitrogen source, respectively, was shown to provide optimum growth conditions for increased growth of *B. thuringiensis* and subsequently higher yield of Vip3 protein production. However, Terrific Broth supplemented with 20 g/l glucose yielded optimum growth significantly ($P < 0.01$, *t*-test) after 12, 14, 16, 18 and 20 h than the formulated medium with optimized C/N ratio of 3.8. Highest vegetative cell counts of *B. thuringiensis* in medium no. 3 was noted after 22 h; thus, indicating a higher production of Vip3 protein. The findings reported in this study should contribute to the low-cost production of *Bt* Vip3 proteins and encourage large scale production of the toxin. This is perhaps the first study to optimize the growth conditions of *B. thuringiensis* for the maximal production of Vip3A toxin.

CONFLICT OF INTERESTS

The authors have not declared any conflict of interests.

REFERENCES

Abulreesh HH, Osman GEH, Assaeedi ASA (2012). Characterization of insecticidal genes of *Bacillus thuringiensis* strains isolated from arid environments. Indian Journal of Microbiology 52(3):500-503.

Assaeedi ASA, Osman GEH, Abulreesh HH (2011). The occurrence and insecticidal activity of *Bacillus thuringiensis* in the arid environments. Australian Journal of Crop Science 5:1185-1190.

Bernhard K (1993). Development of *Bacillus thuringiensis* insecticides in Ciba-Geigy ad axemplified with CGA 237'218. In: *The Biopesticide Bacillus thuringiensis* and its Applications in Developing Countries. Salama HS, Morris ON, Rached E (Eds.), National Research Center, Cairo, Egypt., pp. 283-301.

Berbert-Molina MA, Prata AM, Pessanha LG, Silveira MM (2008). Kinetics of *Bacillus thuringiensis* var. *israelensis* growth on high glucose concentrations. Journal of Industrial Microbiology and Biotechnology 35(11):1397-1404.

Burkness EC, Dively G, Patton T, Morey AC, Hutchinson WD (2010). Novel Vip3A *Bacillus thuringiensis* (*Bt*) maize approaches high-dose efficacy against *Helicoverpa zea* (Lepidoptera: Noctuidae) under field conditions: implications for resistance management. GM Crops 1(5):337-343.

Doi RH (1989). Sporulation and germination. In: *Bacillus*. Harwood CR. (Ed.). Plenum, New York, USA, pp. 169-215.

Dubois T, Tremblay YDN, Hamiot A, Martin-verstraete I, Deschapms J, Monot M, Briandet R, Dupuy B (2019). A microbiota-generated bile salts induces biofilm formation in *Clostridium difficile*. NPJ Biofilms and Microbiomes 5:14.

Dulmage HT (1971). Production of-endotoxin by eighteen isolates of Bacillus thuringiensis, serotype 3, in 3 fermentation media. Journal of Invertebrate Pathology 18(3):353-358.

El-Ghareeb DK, Osman GH, El Baz AF (2012). Isolation, cloning and overexpression of vip3Aa gene isolated from a local *Bacillus thuringiensis*. Biocontrol Science and Technology 22(1):11-21.

Ernandes S, Del Bianchi VL, de Oliveria Moraes (2013). Evaluation of two different culture media for the development of biopesticides based on *Bacillus thuringiensis* and their application in larvae of *Aedes aegypti*. Acta Scientiarum-Technology 35:11-18.

Estruch JJ, Warren GW, Mullins MA, Nye GJ, Craig JA, Koziel MG (1996). Vip3A, a novel *Bacillus thuringiensis* vegetative insecticidal protein with a wide spectrum of activities against lepidopteran insects. Proceedings of the National Academy of Sciences of the United States of America 93:5389-5394.

Gopinathan C, Chaudhury A, Vivek AT (2016). Novel techniques for *Bacillus thuringiensis* subsp. *israelensis*. International Journal of Mosquito Research 3(4):17-29,

Hasanain AM (2017). Development of a cheap media for *Bacillus thuringiensis* growth. International Journal of Biotechnology and Bioengineering 3:221-229.

Holmberg A, Sievanen R, Carlberg G (1980). Fermentation of *Bacillus thuringiensis* for exotoxin production: process analysis study. Biotechnology and Bioengineering 22(8):1707-1724.

Jouzani GS, Valijanian E, Sharafi R (2017). *Bacillus thuringiensis*: a successful insecticide with new environmental features and tidings. Applied Microbiology and Biotechnology 101(7):2691-2711.

Levinson ZH, Navon A (1969). Ascorbic acid and unsaturated fatty acids in the nutrition of the Egyptian cotton leaf worm. Journal of Insect Physiology 15(4):591-595.

Marzban R (2012). Investigation on the suitable isolate and medium for production of *Bacillus thuringiensis*. Journal of Biopesticides 5(2):144-147.

Morris ON, Kanagaratnan P, Converse V (1997). Suitability of 30 agricultural products and by-products as nutrient sources for laboratory production of *Bacillus thuringiensis* subsp. *aizawai* (HD 133). Journal of Invertebrate Pathology 70(2):113-120.

Nair K, Al-Thani R, Al-Thani D, Al-Yafei F, Ahmad T, Jaoua S (2018). Diversity of *Bacillus thuringiensis* strains from Qatar as shown by crystal morphology, δ-endotoxins and cry gene content. Frontiers in Microbiology 9:708.

Navarro-Mtz AK, Martinez-Garcia R, Urazua-Valenzuela M, Roldan-Sabino C, Kakazey M, Juarez-Arellano EA (2018). High-energy ball millimg treatment of soybean for *Bacillus thuringiensis* culture media.

Journal of Bioscience and Bioengineering 128(3):296-301.
Osman G, Assaeedi ASA, Osman Y, El-Ghareeb D, Alreedy, R (2013). Purification and characterization of *Bacillus thuringiensis* vegetative insecticidal toxin protein(s). Letters in Applied Microbiology 57(4):310-6.
Osman GEH, Alreedy R, Assaeedi ASA, Organji SR, El-Ghareeb D, Abulreesh HH, Althubiani AS (2015). Bioinsecticide *Bacillus thuringiensis* a comprehensive review. Egyptian Journal of Biological Pest Control 25:271-288.
Osman GEH, Altaf WJ, Saleh IAS, Soltane R, Abulreesh HH, Arif IA, Ramadan AM, Osman YA (2018). First report of detection of the putative receptor of *Bacillus thuringiensis* toxin Vip3Aa from black cutworm (*Agrotis ipsilon*). Saudi Journal of Biological Sciences 25(3):441-445.
Osman GEH, Soltane R, Saleh, I. Abulreesh HH, Gazi KS, Arif IA, Ramadan AM, Alameldin HF, Osman YA, Idriss M (2019). Isolation, characterization, cloning and bioinformatics analysis of a novel receptor from black cutworm (*Agrotis ipsilon*) of *Bacillus thuringiensis* Vip3Aa toxins. Saudi Journal of Biological Sciences 26(5):1078-1083.
Poopathi S, Kumar AK (2003). Novel fermentation media for production of *Bacillus thuringiensis* subsp. *isrealensis*. Journal of Economic Entomology 96(4):1039-1044.
Poopathi S, Archana B (2012a). A novel cost-effective medium for the production of *Bacillus thuringiensis* subsp. *israelensis* for mosquito control. Tropical Biomedicine 29(1):81-91.
Poopathi S, Archana, B (2012b). Optimization of medium composition for the production of mosquitocidal toxins from *Bacillus thuringiensis* subsp. *israelensis*. Indian Journal of Experimental Biology 50(1):65-71.
Sadek KH (2000). Studies on some factors affecting growth and sporulation of *Bacillus thuringiensis*. M.Sc. thesis, Faculty of Science, Cairo University, Cairo, Egypt.
Siegwart M, Graillot B, Blachere Lopez C, Besse S, Bardin M, Nicot PC, Lopez-Ferber M (2015). Resistance to bio-insecticides or how to enhance their sustainability: a review. Frontiers in Plant Science 6:381.
Smitha RB, Sailas B, Prakashkumar R (2019). Fermentation strategies for the production of α-amylase and δ-endotoxin from *Bacillus thuringiensis* subsp. *kurstaki*. Avid Science Monograph Series.2019.
Valicente FH, de Souza Tuelher E, Leite MIS, Freire FL, Vieira CM (2010). Production of *Bacillus thuringiensis* biopesticide using commercial lab medium and agricultural by-products as nutrient sources. Revista Brasileira de Milho e Sorgo 9(1):1-11.
Wang Z., Fang L, Zhou Z, Pacheco S, Gomez I, Song F, Soberon M, Zhang J, Bravo A (2018). Specific binding between *Bacillus thuringiensis* Cry9Aa and Vip3Aa toxins synergizes their toxicity against Asiatic rice borer (*Chilo supperralis*). Journal of Biological Chemistry 293(29):11447-11458.
Yu X, Liu T, Sun Z, Guan P, Zhu J, Wang S, Li S, Deng Q, Wang L, Zhrng A, Li P (2012). Co-expression and synergism analysis of Vip3Aa29 and Cyt2Aa3 insecticidal proteins from *Bacillus thuringiensis*. Current Microbiology 64(4):326-331.
Zou H, Ding S, Zhang W, Yao J, Jiang L, Liang J (2016). Study on influence factors in *Bacillus thuringiensis* production by semi-solid state fermentation using food waste. Procedia Environmental Sciences 31:127-135.
Zribi Zghal R, Kharrat M, Rebai A, Ben Khedher S, Jallouli W, Elleuch J, Ginibre C, Chandre F, Tounsi S (2018). Optimization of bio-insecticide production by Tunisian *Bacillus thuringiensis israelensis* and its application in the field. Biological Control 124:46-52.

Related Journals: